

**Aus der Medizinischen Klinik und Poliklinik IV der Ludwig-Maximilians-Universität
München**

Direktor: Prof. Dr. med. Martin Reincke

**Modulation of the renal homeostatic milieu by
mononuclear phagocytes in diabetic nephropathy**

Dissertation

zum Erwerb des Doktorgrades der Naturwissenschaften

an der Medizinischen Fakultät

der Ludwig-Maximilians-Universität München



vorgelegt von

Carsten Jäckel

aus Fulda

2017

**Mit Genehmigung der Medizinischen Fakultät
der Universität München**

Betreuer: Prof. Dr. Peter Jon Nelson
Zweitgutachter: Prof. Dr. Heiko Hermeking

Dekan: Prof. Dr. med. dent. Reinhard Hickel

Tag der mündlichen Prüfung: 15.11.2017

Table of Contents

Abstract	I
Zusammenfassung	III
1 Introduction	1
1.1 Chronic Kidney disease	1
1.1.1 Diabetic nephropathy	2
1.1.2 Alterations in signaling pathways during progressive DN	3
1.1.3 Homeostatic signal transduction pathways	4
1.1.4 Hedgehog signaling	5
1.1.5 TGF β /SMAD and BMP/SMAD signaling	6
1.1.6 WNT signaling	8
1.1.7 Hippo signaling	10
1.1.8 MAPK, JAK/STAT and JNK/SAPK pathways.....	12
1.1.9 Interactions between signaling pathways	14
1.1.10 The human immune system.....	15
1.1.11 Immune system in the kidney and the myeloid phenotype ercDC/2 ⁺ MoPh.....	17
1.1.12 Renal damage, inflammation and fibrosis	18
1.2 Rationale of this study.....	19
1.3 Specific Aims of this study.....	20
2 Materials.....	21
2.1 Cell culture	21
2.1.1 Cells and cell lines	21
2.1.2 Culture media and additives	21
2.1.3 Cell culture chemicals.....	22
2.2 Microbiology	22
2.2.1 Bacteria strains	22
2.2.2 Bacterial media	22
2.2.3 Microbiology solutions	23
2.3 Buffers and solutions for molecular biology.....	24
2.4 Enzymes	25
2.5 Size Standards for electrophoresis	26
2.6 Recombinant proteins and peptides.....	26
2.7 Small molecule agonists and antagonists	26
2.4 Primers.....	27
2.5 Plasmids and vectors	28
2.6 Kits.....	29
2.7 Other laboratory equipment	29
2.8 Chemicals	30
2.8 Disposables and other materials.....	30
2.9 Antibodies for flow cytometry	31
2.10 Software.....	32
3 Methods	33
3.1 Microarray analysis	33
3.1.1 Samples.....	33
3.1.2 Robust multichip average (RMA) analysis, batch correction and filtering .	33
3.1.3 GeneRanker analysis	33
3.1.3 Deconvolution analysis to selectively identify 2 ⁺ MoPh cells in complex data.....	33
3.1.4 Weighted Gene Correlation Network Analysis (WGCNA).....	34
3.2 Cell culture	34

Table of Contents

3.2.1	General cell culture	34
3.2.2	Freezing and thawing of cells	34
3.2.3	Counting cells	35
3.3	Molecular biology	35
3.3.1	Freezing and thawing of bacteria	35
3.3.2	Preparation of agar plates	35
3.3.3	Restriction digestion of DNA	35
3.3.4	Separation of DNA fragments by electrophoresis	36
3.3.5	Determination of DNA and RNA concentrations	36
3.3.6	Dephosphorylation of DNA ends	36
3.3.7	Assembly of short synthetic DNA elements for reporter constructs	37
3.3.8	Ligation of DNA fragments	37
3.3.9	Preparation and transformation of competent <i>E. coli</i> MACH-1	37
3.3.10	Isolation and analysis of plasmid DNA from transformed bacteria	38
3.3.11	Polymerase chain reaction (PCR)	38
3.3.12	Sequencing of DNA	38
3.4	Cloning Strategies	39
3.4.1	Adaptation of the pGL3-Promoter vector for <i>Gaussia</i> Luciferase	39
3.4.2	Modifications of pCDNA6/TR for Sleeping Beauty compatibility	40
3.4.3	Generation of pSBTET.Reporter by fusion of the modified pGL3 Promoter and pCDNA6/TR-ITR	41
3.4.4	Generation and insertion of transcription factor specific reporter elements	41
3.4.5	Generation of pSBDEST by Fusion of pCDNA6/TR-ITR and pcDNA6.2 V5 PL-DEST	43
3.4.6	Generation of Entry Clones	44
3.4.7	Generation of Expression vectors	45
3.5	<i>In vitro</i> experiments	46
3.5.1	Stable transfection of cells by electroporation	46
3.5.2	Antibiotic selection for transformants	47
3.5.3	Stimulation and validation of reporter cell lines	47
3.5.4	Overexpression methods	48
3.5.5	Co-culture assays	48
3.5.6	Luciferase Assays	48
3.5.7	Harvesting and concentration of serum-free supernatants	48
3.5.8	Exosome Preparation	49
3.5.9	Determination of protein content	49
3.6	Quantitative real-time PCR	49
3.6.1	RNA Purification	49
3.6.3	Quantification of RNA	50
3.6.4	Reverse Transcription	50
3.6.5	Quantitative PCR (qPCR)	51
3.6.6	Calculation of regulation	52
3.7	Microscopy of Kidney sections	52
3.7.1	Sample preparation	52
3.7.2	Immunohistochemistry	52
3.8	Generation of 2 ⁺ MoPh and imDC cells	53
3.8.1	Isolation of mononuclear cells from peripheral blood	53
3.8.2	Positive isolation of monocytes from PBMC	53
3.8.3	<i>In-vitro</i> -differentiation of myeloid cell types from monocytes	53

3.9	Fluorescence activated cell scanning (FACS) Analysis	54
3.10	Mass spectrometry	54
3.10.1	Sample preparation for mass spectrometry	54
3.10.2	LC-MS/MS analysis	54
3.10.3	Protein identification and label-free quantification.....	55
4	Results	56
4.1	Bioinformatic characterization of DN samples and calculation of 2 ⁺ MoPh presence	56
4.1.1	Dysregulation of developmental/regulatory pathways in the context of diabetic nephropathy	56
4.1.2	Detection of 2 ⁺ MoPh in complex tissues by deconvolution analysis	58
4.2	Cloning and Establishment of the Vector Platform.....	60
4.2.1	Cloning of pathway reporter vectors	61
4.2.2	Cloning of Gateway Destination vectors	63
4.2.3	Cloning of Entry Clones	64
4.2.5	Transfection of cell lines using Nucleofection techniques and the SB100 Transposase	66
4.2.6	Proof of principle stimulation experiments for validation of the vector platform.....	67
4.2.7	Proof of principle: induced overexpression of genes within the vector platform.....	68
4.3	<i>In-vitro</i> model for myeloid infiltrate driven signaling alterations in the kidney..	70
4.3.1	Flow cytometric characterization of myeloid cells	70
4.3.2	2 ⁺ MoPh and related myeloid cells can activate homeostatic pathways by co-incubation with reporter cells	72
4.3.3	The factor(s) responsible for the activation of these pathways are secreted by 2 ⁺ MoPh cells.....	74
4.3.4	Proteomics.....	79
4.3.5	Inhibitor studies were used to identify potential upstream signaling cascades	80
4.3.6	Can LXR activation modulate 2 ⁺ MoPh and imDC activation patterns?	82
4.4	Bioinformatic analysis of pathway alterations associated with 2 ⁺ MoPh in DN patient biopsies	84
4.4.1	Identification of co-regulated gene modules by weighted gene co-expression network analysis (WGCNA).....	84
4.4.2	Genetic composition of modules.....	86
4.4.3	Potential “high impact” pathway genes within modules	88
5	Discussion	92
5.1	Initial transcriptomic findings.....	93
5.2	Development of a next generation vector system.....	94
5.3	2 ⁺ MoPh <i>in-vitro</i> findings.....	94
5.3	Evidence implicating MAPK as pivotal for the homeostatic alterations caused by 2 ⁺ MoPh presence	95
5.4	Identification of transcriptomically altered pathway components using the WGCNA method strongly hints at MAPK.....	96
5.5	Working model.....	99

Table of Contents

6 Addendum	102
6.1 Supplemental tables	102
6.2 Proof of principle and validation of reporter tools.....	110
6.3 Flow cytometric characterization of myeloid cell lines.....	112
6.3.1 AP-1 reporter titration with Mono-Mac-6 cells	115
6.4 Additional characterization of LXR signaling.....	115
6.5 Additional characterization of Hippo signaling	123
7 References	129
8 Acknowledgements	141

Abstract

Diabetic nephropathy (DN) is the most prevalent type of chronic kidney disease (CKD) in the western world, and represents the leading cause of end stage renal disease. DN develops as a complication of diabetes mellitus, and thus the pathogenesis is defined by systemic changes in blood glucose and often increased blood pressure. Tubulointerstitial renal fibrosis is causal to the destruction of the kidney fine structure, but the specific mechanisms driving it are still poorly understood. DN is a sterile inflammatory process, since immune infiltrates increase with disease progression and tissue fibrosis, in the absence of external pathogens. Myeloid cell types are found to be increased in DN, and macrophages and dendritic cells (DC) have been proposed to act as drivers of fibrotic processes in CKD. The recently described kidney specific myeloid CD209 and CD14 positive phenotype of mononuclear phagocytes (2⁺MoPh) was reported to be enriched in CKD.

Using a set of cDNA microarrays and a bioinformatics deconvolution approach, 2⁺MoPh-associated gene signatures were shown to be significantly increased in human DN biopsy samples, as compared to healthy controls. The increase of 2⁺MoPh-related genes correlated with a decrease in renal function. Additionally, transcriptomic regulation of key homeostatic pathways was found to be altered in samples with enhanced 2⁺MoPh signals. To establish direct effects on these pathways, a reporter vector and cloning system specifically generated for this study was used for co-incubation experiments carried out using *in-vitro* polarized 2⁺MoPh and immature DC control cells. The results showed strong activation of the Hedgehog, WNT, TGFβ and MAPK pathways in model parenchymal cells by co-incubation with 2⁺MoPh cells. The nature of the signals exerted by 2⁺MoPh cells in co-culture was found to be protein/peptide based, not reliant on cell-cell contact, and not exosome mediated. Small molecule antagonist studies identified MAPK components as playing a central role in the activation seen. Using a compiled gene list derived from the four pathways identified in the *in-vitro* validation study, a weighted gene co-expression analysis (WGCNA) was then used to identify co-regulated gene modules across the four pathways, and associated with an increase in 2⁺MoPh gene signatures in the DN patient transcriptomic data. Further study of the individual genes correlated with 2⁺MoPh presence identified a pronounced MAPK-associated signature. Together,

these findings suggest a strong MAPK based component as a driving force of fibrosis in DN.

Zusammenfassung

Diabetische Nephropathie (DN) ist der prävalenteste Typus der chronischen Niereninsuffizienzen (CNI) in der westlichen Welt und die Hauptursache für Nierenversagen. Diabetische Nephropathie entsteht als Komplikation von Diabetes mellitus und die Pathogenese ist daher definiert durch systemische Änderung des Blutzuckerspiegels und häufig durch erhöhten Blutdruck. Tubulointerstitielle Fibrose ist dabei für die Zerstörung der Nierenfeinstruktur verantwortlich, über die Mechanismen die diesen Prozess vorantreiben ist allerdings kaum etwas bekannt. DN ist ein steriler Entzündungsprozess, da Immunzellinfiltrate mit voranschreitender Krankheit und Fibrose zunehmen, ohne dass externe Pathogene vorhanden sind. Myeloische Zelltypen treten im Verlauf der DN vermehrt auf und Makrophagen und Dendritische Zellen (DC) werden als treibende Kraft für die fibrotischen Prozesse in CNI diskutiert. Über den vor Kurzem beschriebenen nierenspezifischen myeloischen CD209 und CD14 positiven Phänotyp der Mononukleären Phagozyten (2^+ MoPh) wurde eine Anreicherung in CNI berichtet.

Mittels cDNA-Microarrays und einem bioinformatischen Dekonvolutionsansatz wurde gezeigt, dass 2^+ MoPh assoziierte Gensignaturen signifikant erhöht in menschlichen DN Biopsien, verglichen mit gesunden Kontrollen, vorliegen. Die Erhöhung korrelierte mit einer Reduktion der Nierenfunktion. Weiterhin wurden Veränderungen in der transkriptionellen Regulation homöostatischer Schlüsselsignalwege in Proben mit erhöhten 2^+ MoPh Signalen nachgewiesen. Mittels einem eigens für diese Studie generierten Reportervektor- und Klonierungssystem wurden Kokultur-Experimente mit *in-vitro* polarisierten 2^+ MoPh und unreifen DC als Kontrollen durchgeführt, um die direkten Auswirkungen auf diese Signalwege zu bestimmen. Als Ergebnis zeigte sich eine starke Aktivierung der Hedgehog, WNT, TGF β und MAPK Signalwege in parenchymalen Modellzellen bei Kokultur mit 2^+ MoPh. Die Signale mit denen 2^+ MoPh Zellen in Kokultur Einfluss nehmen wurden als Protein/Peptid basiert, unabhängig von Zell-Zell Kontakten und als nicht auf Exosomen basierend bestimmt. Eine zentrale Rolle für MAPK Komponenten konnte in Studien mit niedermolekularen Antagonisten belegt werden. Eine Gesamtgenliste bestehend aus den vier *in-vitro* identifizierten Signalwegen wurde als Basis für eine gewichtete Genkoexpressionsanalyse (WGCNA) verwendet um koregulierte Genmodule zu identifizieren. Dabei wurden gefundene Module auch mit der Gensignatur für 2^+ MoPh im transkriptionellen DN-

Patientendatensatz assoziiert. Weitere Analysen der mit der 2⁺MoPh Präsenz korrelierenden Einzelgene zeigten eine ausgeprägte MAPK-assoziierte Signatur. Zusammen deuten diese Ergebnisse auf eine starke MAPK basierte Komponente als treibende Kraft für fibrotische Prozesse in DN hin.

1 Introduction

1.1 Chronic Kidney disease

Chronic kidney disease (CKD) is defined by the gradual loss of kidney function which can eventually be reduced to life threateningly low levels [1]. While the kidney serves many functions, such as regulating blood pressure and bone formation, and control of red blood cell production, CKD is usually diagnosed by loss of the kidney's filtration and reabsorption functions via measurement of serum creatinine levels and albuminuria [2-4]. Clinically, CKD is stratified into three levels of severity based on albuminuria, and five based on serum creatinine, through the calculation of an estimated glomerular filtration rate (eGFR) value (volume of fluid filtered by the renal glomerular capillaries per unit time). These values are then used to gauge the amount of kidney damage present in a specific case [1, 5]. Since the kidney has many functions, the symptoms of kidney damage are also widespread. While early CKD stages are usually asymptomatic, later stages can lead to hypertension, anemia, uremia, fluid volume overload and a number of electrolytic imbalances, generally severely limiting quality-of-life [6, 7].

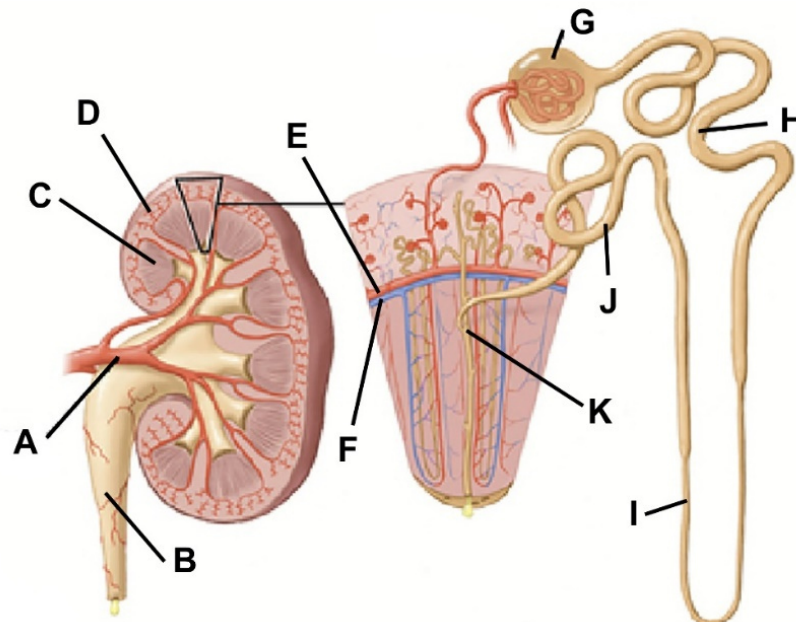


Figure 1. Overview of the kidney and its functional units, the nephrons. A) Renal arteries B) Ureter C) Medulla D) Cortex E) Arteriole F) Venule G) Glomerulus H) Proximal tubule I) Loop of Henle J) Distal tubule K) Collecting duct. Adapted from <http://my.clevelandclinic.org>

CKD is rarely diagnosed as an isolated disease, and thus, usually has causal comorbidities like hypertension, diabetes, and cardiovascular diseases [8]. Treatment of these comorbidities is the principal component of patient care, which is even more important since presence of CKD increases the risk of acute kidney injury (AKI), an abrupt loss of kidney function, which can be caused by exposure to nephrotoxic compounds, inflammatory processes in the kidney, or an obstruction of the urinary tract. Episodes of AKI can be life threatening, and if survived, often cause additional damage to the kidney already suffering from CKD [9, 10]. If CKD progresses to stage five, also known as end-stage renal disease (ESRD), kidney function is usually so impaired that renal replacement therapy by dialysis or kidney transplantation is required [11].

With an incidence of 500 million afflicted, CKD occurs in about 1 out of 10 individuals, especially in industrial nations with western life styles [12]. The most common cause for end stage renal disease and the required renal replacement therapy in Germany is type II diabetes, followed by nephrosclerosis caused by high blood pressure [13].

1.1.2 Diabetic nephropathy

Diabetic nephropathy (DN) is the leading cause of ESRD, accounting for 32% of all instances of renal replacement therapy. While DN is a serious complication of diabetes, only an estimated 20-40% of diabetics develop kidney complications, suggesting a genetic component to disease progression [14, 15].

A series of underlying causes of diabetic nephropathy are currently discussed [16, 17]: Hyperfiltration caused by increased pressure in nephrons leads to nephrosclerosis of the glomeruli. Increased blood glucose levels leading to accumulation of extra cellular matrix in the glomeruli and enhanced glycosylation of surface and matrix proteins. Reduction of nephrin, a structural protein of the slit diaphragm, can be observed in patients suffering from DN, compromising the filtration function. Elevated blood sugar inhibits thrombomodulin expression in glomeruli, which under normoglycemic conditions activates protein C, leading to reduced apoptosis of endothelial cells and podocytes. Finally, a number of growth factors and cytokines are dysregulated and lead to changes of the kidney milieu, activating inflammatory and wound healing

programs, with an enhanced recruitment of monocytes/macrophages into the various kidney compartments including the tubulointerstitial regions [18-20].

Clinically, DN is diagnosed by presence of albuminuria and can be stratified based on histological analysis of kidney biopsies [21]. The parameters analyzed are thickening of glomerular basement membranes and the mesangium, as well as the level of scarring (sclerosis) of kidney tissue and glomeruli with concurrent hyaline deposition [22]. Importantly, many patients with DN progress towards CKD even after glucose levels have been effectively reduced through medication [23]. The mechanisms driving progressive CKD are not well understood, but are believed to involve a complex chronic scarring process linked to enhanced leukocytic infiltrates. These infiltrates may act by modulating the status of homeostatic pathways within the target tissue either directly or indirectly, leading to morphological alterations as evidenced by increased ECM deposition by parenchymal fibroblasts and epithelial cells [24-27].

1.1.2 Alterations in signaling pathways during progressive DN

With the scope of morphological changes in DN, and the prevalence of infiltrating immune cells, dramatic changes in homeostatic signaling networks can be observed with disease progression [28-31]. To analyze and quantify these changes, a number of strategies have been employed ranging from various imaging techniques such as immunohistochemistry, to transcriptomic profiling techniques based on cDNA microarrays or next generation sequencing approaches, and finally by the application of proteomic analysis [32-35].

Using transcriptomic profiling, a strong association of the WNT signaling pathway with progressive DN has been previously described by our group [36, 37]. Similarly, the TGF β /SMAD (transforming growth factor beta / SMAD) pathway is strongly associated with disease progression [34]. As both of these pathways have been implicated in wound healing programs, as well as fibrotic processes, their activation seems to be largely context dependent. A potential explanation for this context dependency could be association with the Hedgehog pathway, which can exert control over WNT signaling during development [38], and has also been shown to activate fibroblasts during CKD, in part, through non-canonical mechanisms not currently understood [39, 40]. Since non-canonical activation of GLI1/GLI2 (the GLI name comes originally from

Glioblastoma), the central transcription factors of Hedgehog signaling pathway, has been shown to occur via kinase driven processes, JNK (Janus kinase) and other MAPK (mitogen-activated protein kinase) are interesting candidate pathways for non-canonical Hedgehog pathway activation [41]. JNK signaling is critical in mediating cytokine signals by recipient cells, and is overexpressed in progressively damaged DN kidneys, leading to a general association with the process of progressive fibrosis [42]. Finally, the more recently described Hippo signaling pathway, originally identified for its function to regulate organ size, has also been implicated in CKD [43]. Since it shares important pro-fibrotic target genes like connective tissue growth factor (CTGF) and cysteine-rich angiogenic inducer 61 (CYR61) with TGF β /SMAD signaling, the involvement of the Hippo signaling cascade is strongly suggested during fibrotic processes. Additionally, Hippo signaling has been shown to be highly receptive to mechanical cues that would arise during scarring and the resultant stiffening of tissue [43, 44].

1.1.3 Homeostatic signal transduction pathways

Regulatory protein networks help define homeostasis in cells and their ability to react to external stimuli. This makes the study of signaling protein interactions in cells a cornerstone of cell biology [45]. Signal transduction pathways usually originate at a receptor on the cell surface, which can bind either surface molecules of other cells, or factors present in the surrounding micromilieu of the cell [46]. In this way, cells can react to nutrients, stress inducing molecules (e.g. pathogen-associated molecular pattern, PAMPs or damage-associated molecular pattern, DAMPs) but also to secreted signaling molecules, such as cytokines or growth factors released from other cells or cell types [47-49]. Upon binding to the receptor, signals are transmitted via individual signaling molecules in a stepwise process. Generally, the signaling cascade ends with modulation of downstream target gene expression by either the activation or blockade of specific transcription factors associated with the pathway.

In this way, cells and tissues can react to a wide range of stimuli without the need for physical presence of each individual cell at the original stimulus. Most signal transduction pathways were originally identified via knock-out studies in embryogenesis, and usually disruption of these pathways led to extreme and often embryonic lethal phenotypes [50].

1.1.4 Hedgehog signaling

The Hedgehog signaling pathway was originally identified in *Drosophila melanogaster* via random mutagenesis studies during larval development [51]. Most of the pathway's signaling components are highly conserved in higher eukaryotes and remain incredibly important for embryogenesis [52]. The signaling cascade is also important for normal homeostasis, with disruptions having the potential to cause various cancer forms [53, 54]. In addition, the pathway has been shown to be very important in stem cells, where it can be induced to help control the replacement of cells in damaged tissues [55]. The two Hedgehog ligands Indian hedgehog (IHH) and Sonic hedgehog (SHH) are expressed in tubular epithelial cells, and Hedgehog signaling in the primary cilium is linked to widespread effects on renal homeostasis [56]. Defects in ciliary Hedgehog signaling are associated with polycystic kidney disease [57].

The human canonical Hedgehog cascade is triggered when one of the three Hedgehog ligands SHH, IHH or Desert Hedgehog (DHH) bind to Patched (PTCH) receptors. Canonical Hedgehog signaling can occur in an autocrine or paracrine manner. Binding of one of the three ligands to the PTCH1 receptor leads to blockage of Smoothed (SMO), an inhibitor of GLI1/2 activation. Release of this blockade in turn activates the GLI1/GLI2 transcription factors, leading to nuclear localization and transcription of target genes [52].

In addition to the canonical activation mode, there are non-canonical GLI1/2 activation modes originally identified in cancer studies [58, 59]. The TGF β /SMAD pathway can directly activate transcription of the GLI1 and GLI2 genes, and in turn, upregulate Hedgehog activity [60]. Also, activation of GLI1/2 by growth factors has been shown to occur via receptor tyrosine kinases (RTK), for example, the epidermal growth factor receptor (EGFR) and fibroblast growth factor receptor (FGFR), but also through heterotrimeric G-proteins [61, 62]. This mode of activation is mediated by phosphoinositide 3-kinase (PI3K) and/or MAPK/MEKs [63-65]. PI3K derived GLI1/2 activation is thought to occur via AKT serine/threonine kinase (AKT), while MAPK/MEK activation leads to ERK activation, and either direct activation of GLI1/2 via phosphorylation, or indirectly via Jun proto-oncogene (JUN) activation in the nucleus.

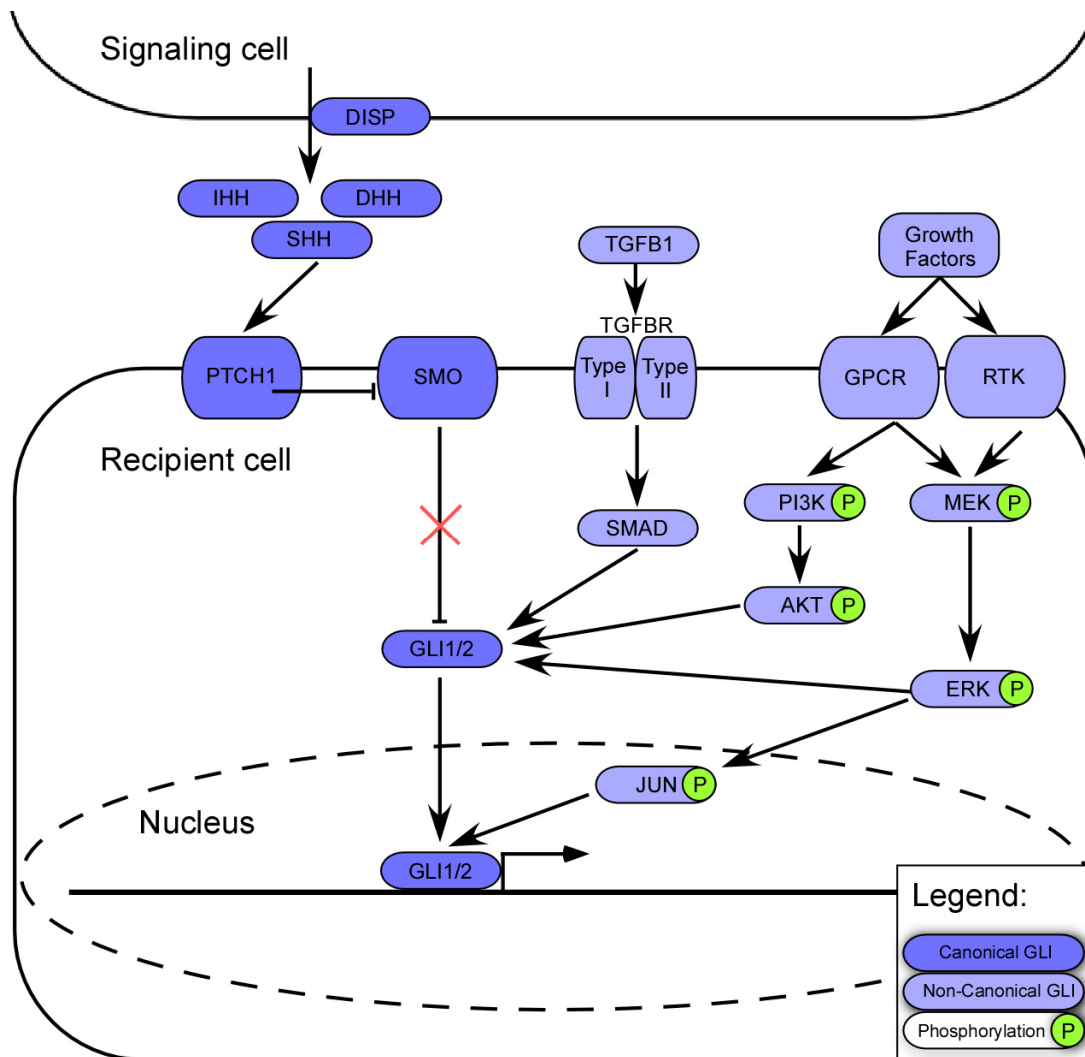


Figure 2. Canonical and non-canonical GLI activation in the Hedgehog signaling pathway. In the canonical Hedgehog signaling pathway, the binding of one of the three Hedgehog ligand molecules SHH, DHH or IHH to PTCH1 leads to inactivation of SMO, a potent inhibitor of GLI1/2 activation. This results in activation of GLI1/2 and translocation to the nucleus where transcriptional control of Hedgehog target genes occurs. Additionally, GLI1/2 can be activated via TGFβ/SMAD signaling and by growth factor associated receptors via kinase cascades as explained in chapter 1.1.4.

1.1.5 TGFβ/SMAD and BMP/SMAD signaling

The classical TGFβ signaling pathway, originally identified by the ability of TGFβ ligands to induce morphological changes in rat cell culture, has been shown to be centrally important in embryogenesis and in the maintenance of general tissue homeostasis, as well as in regulation of immune responses, wound healing and tissue fibrosis [66-68]. The TGFβ superfamily consists of a large number of related proteins, though the summary here will focus on the three classical TGFβ ligands, and the bone

morphogenetic proteins (BMPs). For all members of the TGF β family, a heterodimer of Type I and Type II TGF β receptors is required for signaling.

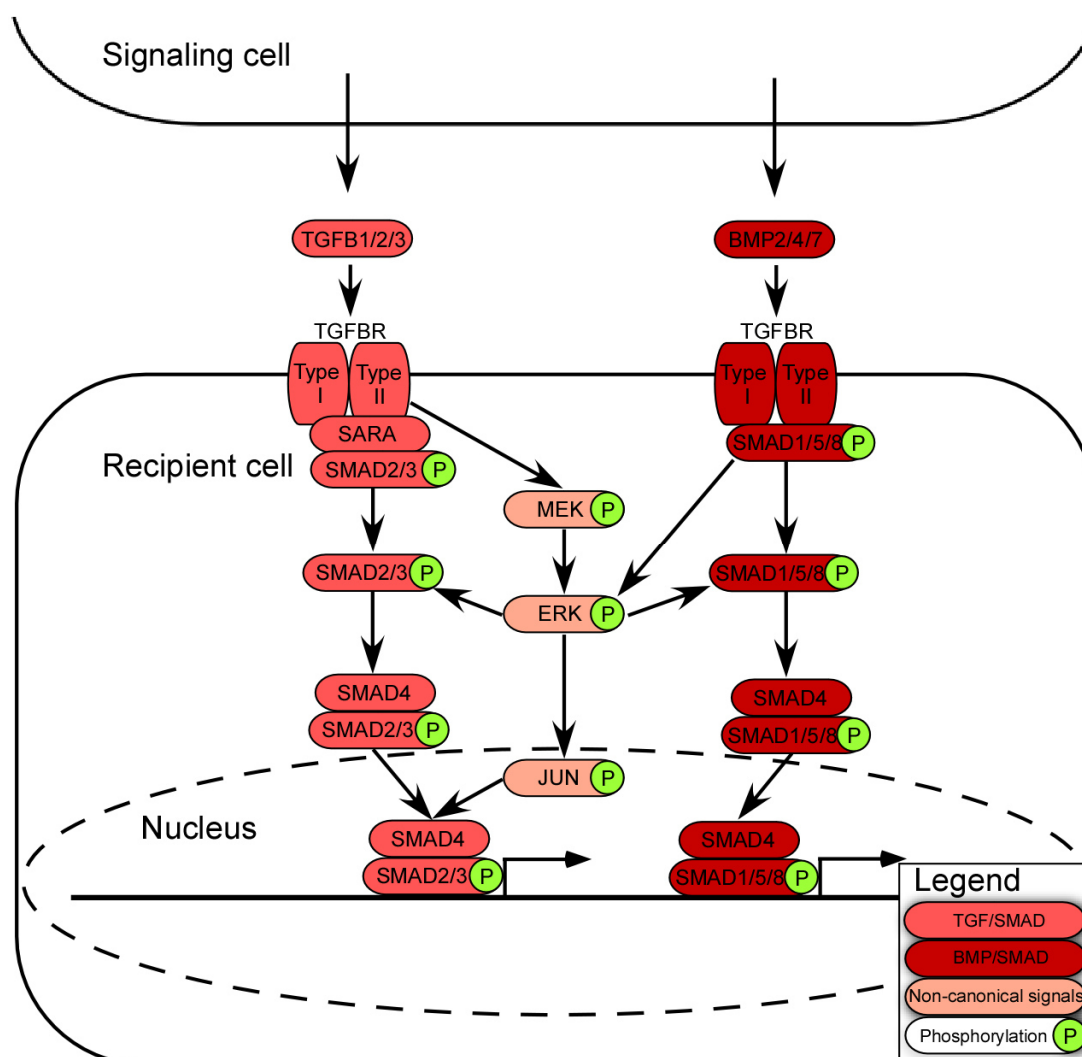


Figure 3. TGF β and BMP driven SMAD activation pathways. In the canonical TGF β signaling pathway, detection of one of the three ligand molecules (TGFB1-3) by a Type I/Type II receptor heterodimer leads to phosphorylation of R-SMADs. Phosphorylated R-SMADs bind to co-SMAD4 and are shuttled to the nucleus where they modulate transcription. BMP signaling occurs parallel with different SMADs. Additional signaling processes via other kinases are explained in chapter 1.1.5

Upon the binding of a TGF β ligand to a receptor dimer, the intracellular regulatory R-SMAD proteins become phosphorylated [69]. This occurs via the function of the SMAD anchor for receptor activation (SARA), acting as an adaptor protein. The unconventional nomenclature of SMAD proteins stems from the homology the mammalian proteins exhibit with both *Drosophila* “Mothers against decapentaplegic” (MAD) and *Caenorhabditis elegans* Sma [70]. Phosphorylated R-SMADs have a high affinity for recruitment of co-SMADs, SMAD proteins which are not phosphorylated,

but co-operate during signaling. In case of the canonical TGF β signaling cascade, SMAD2/3 act as R-SMADS with SMAD4 acting as a Co-SMAD. The resulting heterodimers are then shuttled into the nucleus and initiate transcription of target genes. In the highly similar BMP signaling cascade, BMP2/4/7 bind to the receptor dimer which leads to R-SMAD1/5/8 phosphorylation and binding to co-SMAD4 [70].

There are also non-canonical components of the signaling cascade [71-73]. MAP Kinases can also lead to R-SMAD phosphorylation, allowing downstream signaling of other pathways to regulate the activation of state of SMAD signaling. Interestingly, some components of TGF β /SMAD and BMP/SMAD signaling have been shown to feed back into MAPK/MEK and ERK pathways to modulate downstream JNK signaling [74].

1.1.6 WNT signaling

The WNT signaling network was originally identified in two independent studies, one using *Drosophila* mutagenesis as a developmental model, and one study on cancerogenesis [75-77]. Later it was found that the genes identified were actually functionally and structurally homologous to each other, and the gene family was dubbed WNT (a combination of “Wingless” from the *Drosophila* studies and “Integration”/INT from the cancer studies). These early findings highlighted the potential importance of WNT signaling in homeostasis and during development [78].

In the canonical WNT signaling pathway, one of the 19 human WNT ligands binds to a complex of a “Frizzled” receptor (FZD) and low-density lipoprotein receptor-related protein (LRP) [79]. This in turn leads to recruitment of the β -catenin destruction complex to LRP and deactivates it by dephosphorylation of Axin and Dishevelled (DSH). In this state, the normally unstable β -catenin accumulates in the cytoplasm, and is then shuttled to the nucleus where it enhances transcription via association with the T-cell factor/lymphoid enhancing factor (TCF/LEF) transcription factors. In addition to the canonical WNT signaling pathway, at least two other non-canonical signaling cascades have been identified, dubbed the WNT-Ca²⁺ pathway and the WNT-planar cell polarity (WNT-PCP) pathway. These pathways do not involve β -catenin [80].

In the WNT-Ca²⁺ pathway, named for its function in regulation of intracellular calcium levels, WNT ligands bind to Frizzled receptors, but in the context of heterotrimeric G-

proteins [81]. This leads to activation of specific domains of DSH, and via the G-protein interaction, activation of Phospholipase-C (PLC). PLC then cleaves phosphatidylinositol 4,5-bisphosphate (PIP₂) generating diacylglycerine (DAG) and inositol trisphosphate (IP₃). Detection of IP₃ by the endoplasmic reticulum (ER) triggers calcium release. Increased calcium then activates Ca²⁺/calmodulin-dependent protein kinase II (CaMKII) and Calcineurin. CaMKII in turn, activates the NFAT transcription factors [81, 82].

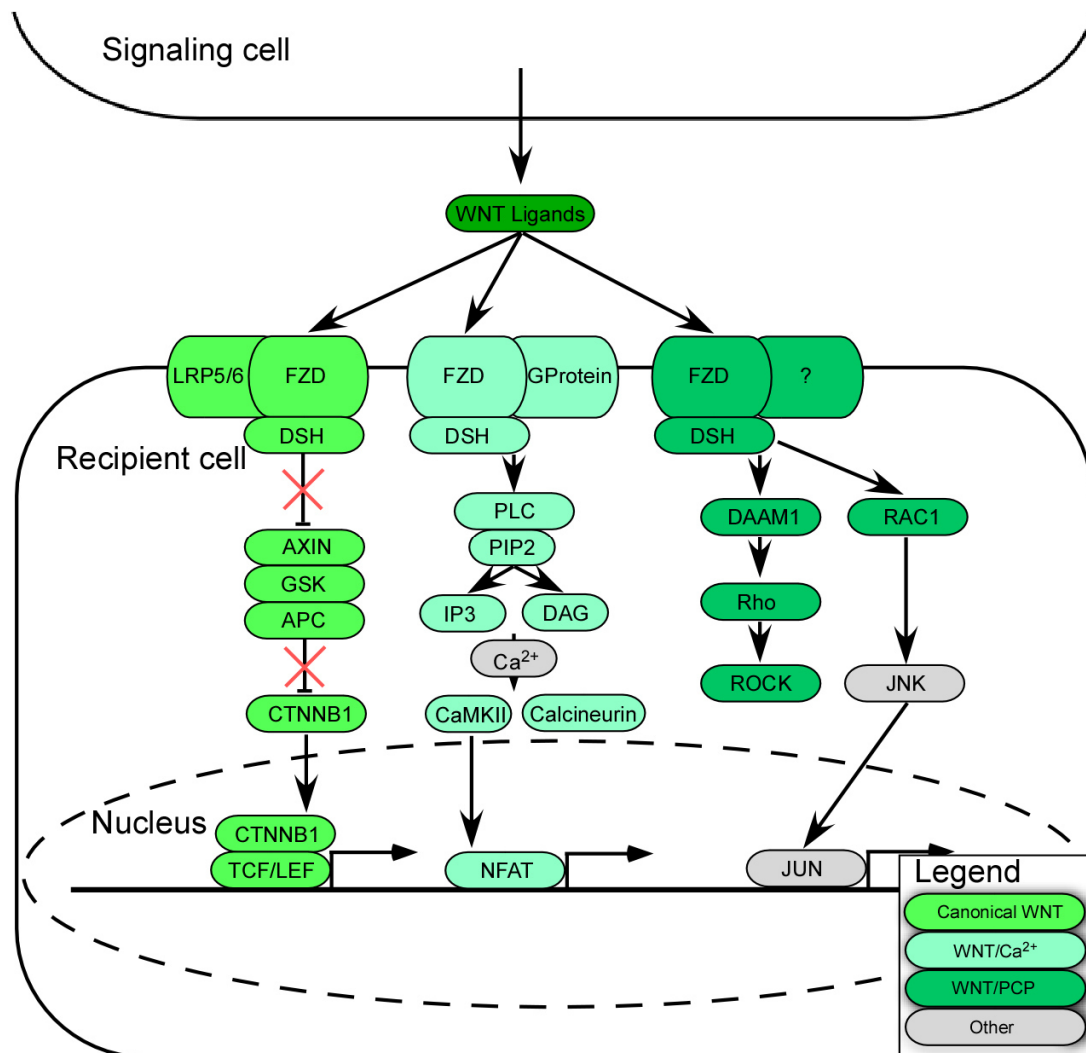


Figure 4. Canonical and non-canonical WNT signaling. The three known human WNT signaling pathways are comprised of canonical WNT/ β catenin, the WNT/Calcium pathway and the WNT planar cell polarity pathway. For a description of the three pathways refer to chapter 1.1.6

In the WNT/PCP pathway, WNT ligands bind to Frizzled receptors, and an as of yet unidentified co-receptor, to activate DSH, which then binds Dishevelled-associated activator of morphogenesis 1 (DAAM1) [83]. DAAM1 in turn activates the Rho

GTPase, and finally Rho-associated kinase (ROCK). The WNT/PCP pathway has been shown to regulate the cytoskeleton. Additionally, DSH can also activate JNK signaling via Ras-related C3 botulinum toxin substrate 1 (RAC1) [84].

1.1.7 Hippo signaling

The Hippo signaling pathway was originally identified in *Drosophila* developmental studies. Mutants in Hippo signaling exhibited overgrowths and other defects in organ size control [85]. More recently alterations of Hippo signaling genes have been described in various cancers highlighting the importance during normal tissue homeostasis [86, 87]. Follow-up studies have shown that Hippo signaling can be activated by loss of cell-cell contact and mechanical cues, as well as by some lipids and growth factors [88]. Hippo has been shown to be a major component in the regulation of renal interstitial fibrosis [43].

Under normal tissue conditions, Hippo signaling is deactivated, which manifests by phosphorylation of yes-associated protein 1 (YAP1) and WW domain-containing transcription regulator protein 1 TAZ(WWTR1), the transcriptional co-activators central to the pathway [89]. In the phosphorylated state, YAP1 and TAZ are retained in the cytoplasm, where they can modulate other pathways such as TGF β /SMAD and WNT, and also act on cell adhesion and polarization pathways together with the 14-3-3 proteins. The phosphorylation of YAP1 and TAZ is mediated by a kinase cascade comprising serine/threonine-protein kinase 4 (STK4, mostly referred to as MST1/2) and the downstream serine/threonine-protein kinase LATS (LATS1/2) kinases, together with the protein salvador homolog 1 (SAV1) and MOB kinase activator (MOB1A/B) scaffold proteins. How the initial activation of MST1/2 occurs in vertebrates is not entirely understood, but a few likely components have been identified or inferred from *Drosophila*: The atypical cadherins FAT1-4, the FERM domain-containing apical proteins FRMD6 and NF2 and the WW domain-containing apical proteins WWC1-3 [90-93]. If the activity of the signal transduction cascade is lost or inhibited, YAP1 and TAZ are no longer phosphorylated and are shuttled to the nucleus. There they cooperatively modulate transcription with specific families of transcription factors, most notably the Runt-related transcription factor (RUNX) and TEA domain family members (TEAD) [94].

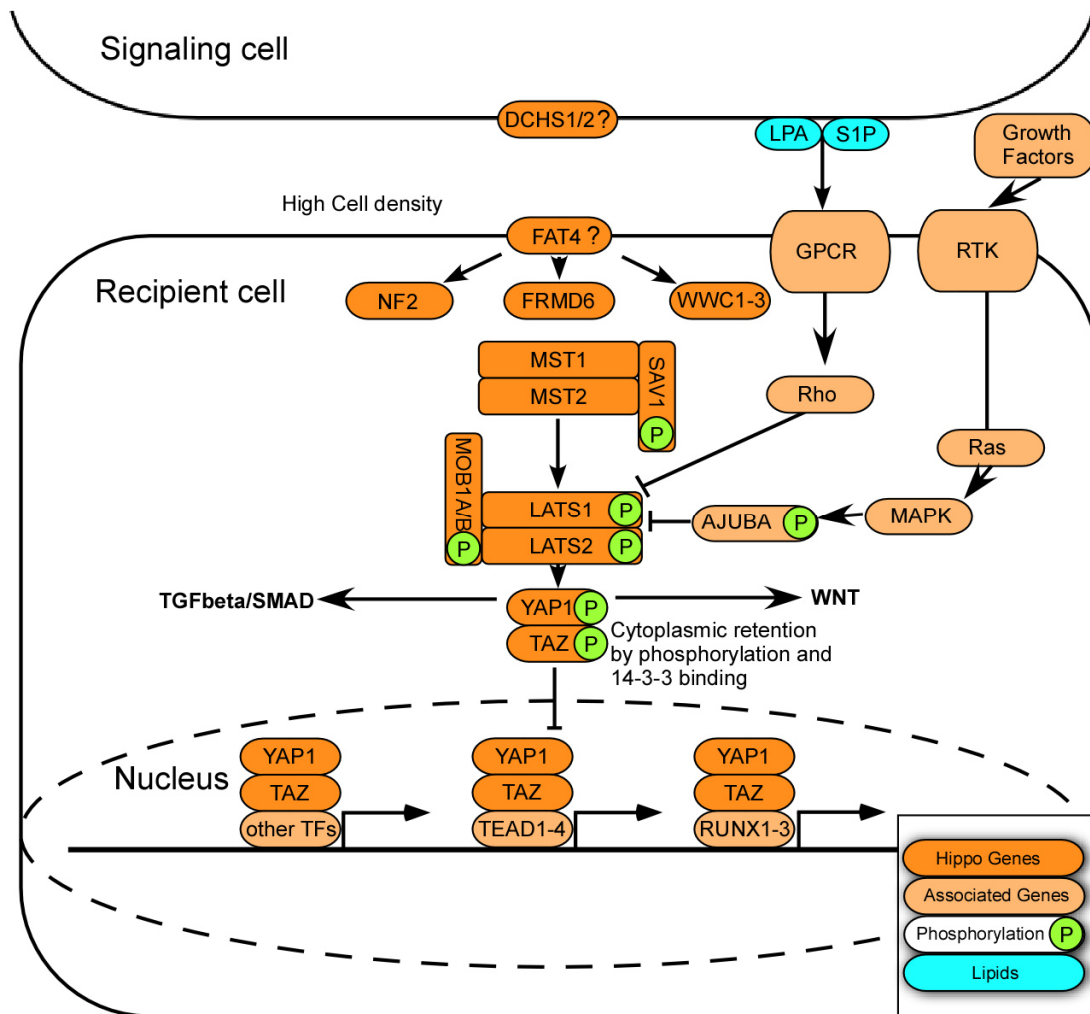


Figure 5. The Hippo signaling pathway. By an as of yet not fully understood mechanism, high cell densities lead to activation of the MST and subsequently phosphorylation of LATS kinases. LATS then phosphorylates YAP1 and TAZ, the transcriptional co-activators central to the Hippo signaling pathway. Phosphorylated YAP1 and TAZ are kept in the cytoplasm by phosphorylation and 14-3-3 protein binding. In low cell density situations, unphosphorylated YAP1 and TAZ are shuttled to the nucleus and modulate transcription. For a description of the three pathways refer to chapter 1.1.7

In addition to the core Hippo genes, there are additional modulations that occur through crosstalk with other pathways [95-97]. Some lipids such as lysophosphatidic acid and sphingosine-1-phosphate have been shown to block the Hippo phosphorylation cascade, leading to transcriptionally active YAP1 and TAZ [98]. This is thought to occur via the Rho GTPase. A similar blockage of phosphorylation has been shown for receptor tyrosine kinase (RTK) based on growth factor binding leading to activation of Ras, MAPK and phosphorylation of LIM Domain-Containing Protein Ajuba, which then blocks phosphorylation [99-101].

1.1.8 MAPK, JAK/STAT and JNK/SAPK pathways

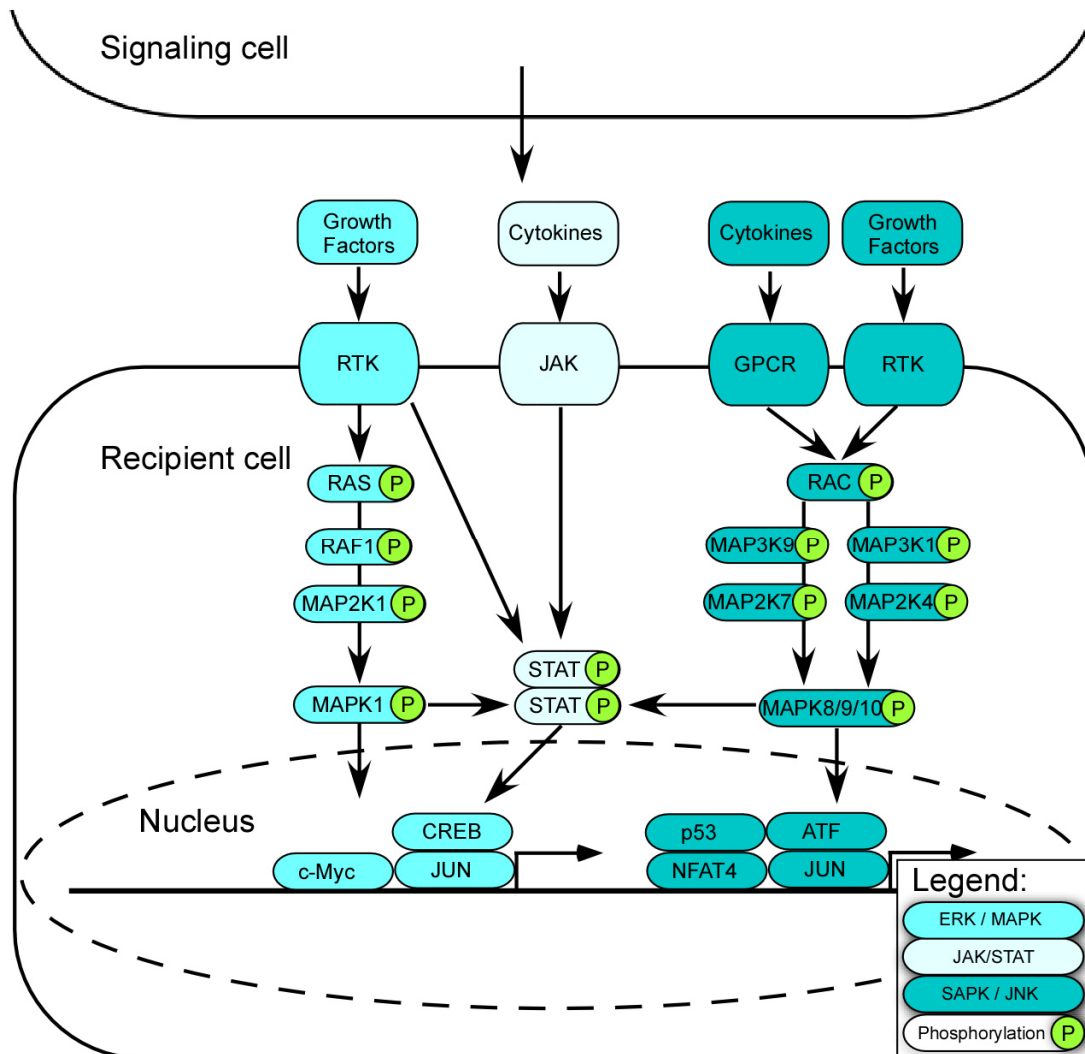


Figure 6. ERK/MAPK, JAK/STAT and SAPK/JNK pathways. Both the ERK/MAPK and SAPK/JNK pathways use tiered kinase cascades to transmit signals from cell surface receptors to transcription factors in to the nucleus. This complicated signaling mechanism allows for multiple levels of modulation and signal amplification inside the cell. JAK/STAT signaling shares many signaling components, but lacks the tiered mechanism. For specifics see chapter 1.1.8

The family of mitogen-activated protein kinases (MAPK) was originally identified in the context of growth factor signaling, but subsequently many more signaling processes involving MAPK were identified [102-104]. The general mechanism of MAPK is a tiered phosphorylation cascade usually starting with a MAPK kinase kinase (MAPKKK/MAP3K) which then phosphorylates, and activates a MAPK kinase (MAPKK/MAP2K) which in turn phosphorylates a final MAPK. This MAPK can then phosphorylate a wide range of proteins including transcription factors, or additional signaling molecules, to pass on a specific signal [105]. Signal specificity is usually

conferred by the associated receptors, but also by the binding affinity between the kinases, and in some cases, by the actions of specific scaffold proteins that tie signaling components to each other. While it may seem uneconomic for cells to have three steps of phosphorylation, this allows for multiple levels of regulation and signal amplification [106].

The extracellular signal–regulated kinases (ERK1/2, now also known only as MAPK) pathway was originally described as a morphogenic pathway that reacts to the presence of growth factors mediated through receptor tyrosine kinases (RTKs) such as epidermal growth factor receptor (EGFR) [107]. Upon binding a ligand, the receptor is autophosphorylated through a conformational change, which then allows the binding of docking molecules and guanine exchange factors, ultimately leading to the activation of RAS proteins (KRAS proto-oncogene, GTPase and HRAS proto-oncogene, GTPase). RAS can then go on to activate the RAF proto-oncogene serine/threonine-protein kinase, which phosphorylates the first MEK or MAPKK (MAP2K1/2). This leads to phosphorylation of ERK/MAPK, which can then regulate downstream transcription factors like Fos proto-oncogene, AP-1 transcription factor subunit (FOS), v-myc avian myelocytomatosis viral oncogene homolog (c-MYC or MYC), and cAMP responsive element binding protein (CREB) [103].

In contrast, the c-Jun N-terminal kinases (JNK/Janus kinases), also known as stress activated kinases (SAPK), are not only activated by growth factors, but also by a plethora of stress related signals [108]. Additionally, there is significant cross talk between the various regulatory cascades. JNK activation can start out with a G-protein coupled receptor (GPCR) or an RTK, both of which can trigger the activation of ras-related C3 botulinum toxin substrate 1 (RAC1), which can then in turn activate MAP3K9 or MAP3K1, and continue the signaling cascade through MAP2K7 or MAP2K4, and which ends with MAPK8/9/10 (also known as JNK1/2/3) [109]. These kinases then have the potential to activate a set of transcription factors such as the Jun proto-oncogene, AP-1 transcription factor subunit (c-Jun/JUN), activating transcription factor (ATF), tumor protein p53 (p53/TP53) and Nuclear factor of activated T-cells (NFAT4) [108].

Even though JAK/STAT signaling is not a true MAP kinase based process, it is very closely linked to MAPK/JNK. JAKs are bound to surface receptors and upon detection

of cytokines and growth factors their kinase activity is increased, and they recruit and phosphorylate STAT proteins [110, 111]. They then undergo dimerization and translocate to the nucleus where they can activate transcriptional targets. STATs however can also be phosphorylated by ERK and JNK, so JAK/STAT is not a truly separate pathway [112].

1.1.9 Interactions between signaling pathways

All of these homeostatic signaling pathways were originally defined in a very focused way. Generally, by the identification of interaction partners for previously identified pathway proteins, and thus, led to an expansion of the signaling cascades using phenotypic or transcriptional changes as read outs of their biologic importance [113]. However, while the pathway concept is a needed abstraction to grasp and study these mechanisms, experimental data suggest that, in reality, the individual pathways are much less clearly divided, and rather form larger networks by influencing each other (also referred to as pathway crosstalk) [114]. This can occur on various levels, with some being more obvious, such as the direct interaction of signaling proteins, some less so, like in the changes in the dynamics of transcription by competition or cooperative binding to DNA [115]. This also means that changes that, for example, occur from small genetic aberrations, can lead to defects in what at first look appear to be unrelated processes. Additionally, the interactions between pathways cause most signaling processes to occur in a context dependent manner, depending on either the type of recipient cell, or the type and status of the signaling cell [116-118]. This can be caused by different types of signaling molecules expressed, or by a lack of receptors for such a pathway, which together with the multitude of signals being exerted and received at a given time and in a specific micro milieu, can lead to unexpected activation patterns in the recipient cells.

Currently known signaling interactions of the homeostatic pathways detailed here are summarized in Figure 7. For most of these interactions there is no true 'upstream' or 'downstream' orientation, with the exception of the Hedgehog – WNT interaction, where WNT ligands are among the Hedgehog/GLI expressed target genes [38].

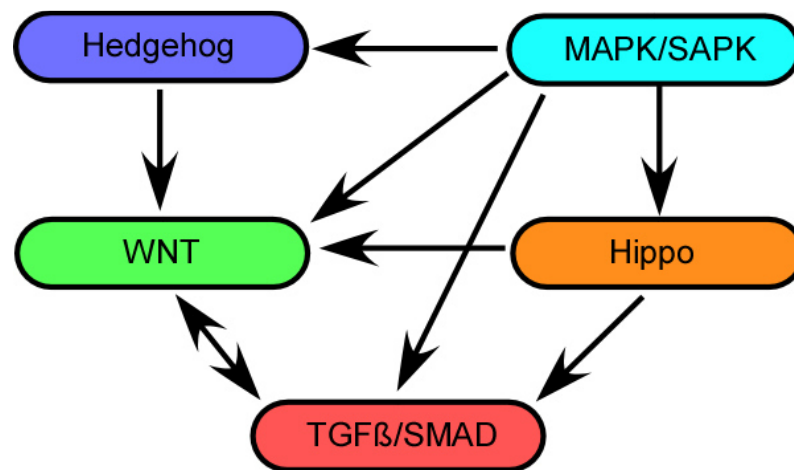


Figure 7. Interactions of signaling pathways. This scheme summarizes known interaction patterns between signaling pathways. For more information, see 1.1.9.

For the other pathways, the picture is less clear, as most interactions are cytoplasmatic and modulate, rather than cause, signaling events. This is especially true for the MAPK/SAPK networks which can have significant impact on the activation state of all of the other pathways [63, 119-123]. Hippo signaling has been also shown to modulate the activity of WNT and TGFβ/SMAD signaling, but mostly in the cytoplasmatic and thus phosphorylated and transcriptionally inert state of YAP1/TAZ [95, 97]. Additionally, some specific pro fibrotic target genes associated with the TGFβ/SMAD pathway are shared targets of Hippo signaling [87]. Finally, WNT – TGFβ/SMAD interactions have been studied in great detail because both of these pathways share important functions during wound healing and development, and both had been discovered relatively long ago [96, 124].

1.1.10 The human immune system

The immune system as a whole is a complex system comprised of organs, cell types and soluble factors, with the main function of defending the host organism from foreign pathogens. The most crucial aspect is thus the detection and elimination of foreign components, while tolerating the host. Upon detection of foreign, potentially harmful factors or antigens, an immune reaction is triggered [125, 126].

The human immune system is comprised of two major branches, the innate and the adaptive immune system. The innate immune system is much older evolutionarily, and allows the detection and direct action against pathogens by causing inflammatory reactions. It is comprised of dendritic cells, macrophages, granulocytes, mast cells,

natural killer (NK) cells and the complement system [127]. Upon detection of an antigen or danger signal (PAMP, pathogen associated molecular pattern) by pattern recognition receptors (PRR) the cells become activated, and start producing pro-inflammatory cytokines and chemokines to attract additional leucocytes to the source of the infection. NK cells kill infected and otherwise anomalous cells, such as cells with altered major histocompatibility complex (MHC) class I phenotypes. Phagocytes take up and kill pathogens. Lastly, the complement system, a series of secreted factors, generated in the liver bind to the surface of bacteria and other pathogens, and through a cascade of reactions, opsonize them to be targeted for destruction, while attracting more immune cells to the location [128].

After the original steps of host defense have begun, the adaptive immune system comes into play. The name adaptive stems from the capability to generate an antigen-specific response to pathogens, and then to memorize this response, to allow for faster host defense in the future [129]. The most important cells in the adaptive immune system are T- and B-cells. Both need to be activated by antigen contact to perform their functions. T-cells are subdivided into more subclasses, based on their expression of CD4 and CD8. Both types of T-cells express a specific receptor (T-cell receptor, TCR) and can only be activated by antigen presentation in context with a MHC molecule on an antigen-presenting cell (APC). Almost every cell can function as an APC, from “professional” immune cells like dendritic cells, macrophages and B-cells, to regular cells infected with pathogens. CD8 positive (+) cells use this co-receptor to detect antigens in context with MHC class I molecules on APCs and upon activation act as cytotoxic T-cells or killer T-cells, inducing apoptosis in the infected cell by release of cytotoxins [130-132].

CD4⁺ T-cells detect antigens presented by MHC class II molecules. MHC class II is expressed on antigen presenting cells like macrophages and dendritic cells, and CD4⁺ T-cells are not generally cytotoxic, earning them the name helper-T cells. Upon activation, they secrete cytokines, which activate CD8⁺ T-cells and macrophages and express the surface proteins required to activate B-cells. Not all CD4⁺ T-cells are pro-inflammatory though, as they can also mature to regulatory T-cells, which counteract inflammatory signals [133, 134].

Finally, B-cells can detect pathogens when they bind to antibodies on its surface. Upon binding, the complex of antibody and pathogen is taken up, cleaved proteolytically and presented on the cell surface in context with MHC class II molecules. Helper T-cells can then detect the antigen/MHC II complex and activate the B-cell. Upon activation, the B-cell begins to divide and differentiate into plasma cells, which then secrete large amounts of the detected antibody. This allows for a highly specific immune response and the specific targeting of pathogens by the immune system [135].

The adaptive immune system can form an immunological memory, which happens upon activation of T and B-cells, when some of their offspring form long-lived memory cells, which, upon reactivation allow for rapid and highly efficient immune responses to known pathogens [136].

1.1.11 Immune system in the kidney and the myeloid phenotype

ercDC/2⁺MoPh

The kidney resident immune cells are mostly comprised of dendritic cells and macrophages, which are largely restricted to the tubulointerstitial space [137-139]. Both of these cell types are categorized as “professional” phagocytes, meaning their main function is taking up pathogens, albeit in different functional contexts [140]. Macrophages, which contain many lysosomes, classically function to clear apoptotic cells, directly kill pathogens and to secrete pro inflammatory factors like interleukin-1 (IL1), interleukin-6 (IL6), and TNF-alpha (TNF α). However, more recently, additional functions have been identified, like the secretion of growth factors during healing processes and immune modulatory functions depending on their state of polarization [141-143]. In this regard, it is thought that the resident myeloid cells may also play key roles in the regulation of tissue homeostasis. Dendritic cells, classically defined by their role in antigen presentation to T and B-cells in the lymph nodes, can also influence immune regulation by modulating surrounding immune or parenchymal cells via the secretion of cytokines and chemokines [144-147]. The divide between different subpopulations of monocytic cells is now seen as a rather artificial separation, and a new concept of a myeloid phenotypic continuum has subsequently been proposed [148, 149]. This concept is supported by the identification of specific renal mononuclear phagocytes (rMoPh) in the kidney, myeloid derived cells that express both macrophage and DC markers, and thus do not easily fall into either category

[150]. One such phenotype of DC has recently been identified in human kidneys and originally described as “ercDC” for its tendency to be highly enriched in examples of renal cell carcinoma [151]. This myeloid subtype is characterized by expression of CD209/DC-SIGN and CD14, and for the purpose of this thesis, has been dubbed 2⁺MoPh (double positive, CD209⁺, CD14⁺ mononuclear phagocytes). Importantly, this cell type is also found in normal kidneys under homeostatic conditions. Reports have also suggested that 2⁺MoPh become enriched in CKD [139]. This phenotype is of special interest in progressive kidney disease. While it expresses T-cell activating markers, it is very inefficient at stimulating naïve T-cells and does not secrete IL-12 after CD40 ligand contact, while also expressing Fascin at lower levels than seen in IL-4/GM-CSF immature DCs (imDC). Both of these factors are required for the activation of T-cells, either by promoting the differentiation of T-cells or for the formation of the immunological synapse. *Ex-vivo* isolated 2⁺MoPh were recently used by our collaborator (Prof. Dr. Elfriede Nößner) for an in-depth transcriptomic and functional study of the cell type (Brech et al. submitted). Additionally, a 2⁺MoPh-like phenotype can be generated from peripheral blood monocytes *in-vitro* through co-culture with renal epithelial cell or renal cell carcinoma conditioned media allowing for more detailed characterization and experiments (Brech et al. submitted).

1.1.12 Renal damage, inflammation and fibrosis

The renal pathology caused by diabetes is considered a sterile inflammation, since there are usually no external pathogens involved [152]. It is thought to be caused by damage occurring to parenchymal cells and subsequent cell death and/or matrix remodeling with the release of damage-associated molecular patterns (DAMPs) which can be detected by DCs [137, 143-145, 147]. This damage promotes an influx of immune cells into the kidney, which then influence the surrounding parenchymal cells, a process that once a certain threshold is reached, can propagate itself. Coinciding with this increased infiltration of immune cells, fibrosis of the tubulointerstitium or glomerulosclerosis can be observed, a pathology in which aberrant deposition of extra cellular matrix (ECM) leads to destruction of the kidney fine structure and loss of function in the nephrons.

The mechanisms by which this deposition of ECM is induced are not fully understood, but the influx of immune cells may be a defining factor. Since not all kidneys undergo fibrotic processes, the composition of immune cells may be the deciding factor whether chronic damage or regeneration of damaged tissue occurs [153]. Similarly, while the changes occurring to signaling networks have been documented, separation of cause and effect has proven difficult, and it has not been shown whether alterations occur due to immune infiltrates or other sources secondary to the progressing disease process.

1.2 Rationale of this study

In broad terms, the aim of this study was to further our understanding of the alterations of signaling networks in the kidney in the context of progressing kidney damage and shifting composition of immune cell infiltrates. Specifically, to elucidate the potential effect of specific myeloid cell phenotypes on parenchymal cells. To this end, studies of signaling processes conferred by the 2⁺MoPh phenotype in comparison to classical imDC phenotype were conducted.

According to our hypothesis, the composition and level of myeloid infiltrates during DN, in comparison to healthy kidneys, may represent an important factor for the developing disease and during its advancement to ESRD. Specifically, myeloid infiltrates may directly alter the homeostatic status of key regulatory pathways in kidney parenchyma through a paracrine or juxtacrine manner. The presence of specific myeloid cells (2⁺MoPh) will have a measureable effect on the homeostatic pathways in model kidney parenchymal cells linked to tissue repair and fibrosis.

1.3 Specific Aims of this study

To better elucidate the pathophysiologic role of a defined myeloid cell population in DN, two strategies were employed: One based on transcriptomic analysis of diabetic nephropathy patient data, and one using a novel *in-vitro* system to study the direct effects on signaling exerted by the myeloid cells.

- In the first stage, diabetic nephropathy (DN) samples taken from human biopsies were analyzed transcriptomically via cDNA microarray technology to screen for alterations in known homeostatic pathways, as compared to biopsy samples taken from normal kidney transplants just prior to implantation. DN microarray samples were then screened using a bioinformatics tool for the presence of CD209/DC-SIGN⁺, CD14⁺ 2⁺MoPh to assess whether their presence was increased relative to healthy kidneys. To this end, a bioinformatic deconvolution method, which can distinguish between myeloid signatures, and effectively calculate the amount of these cells in complex transcriptomic data was applied.
- The second stage sought to validate the direct effects of 2⁺MoPh cells on the activation of relevant pathways in experimental parenchymal cells. To this end, a series of pathway specific reporter and expression vectors were designed and established for use as a platform for co-culture studies with immune cells. For this approach, HEK293 (renal) cells served as model parenchymal cells, and *in-vitro*-polarized immature DCs 'imDCs' and 2⁺MoPh were compared and contrasted for their ability to induce specific signaling pathways. The signaling pathways identified in the *in-vitro* screen were then analyzed in more detail in the transcriptomic DN database using diverse bioinformatics approaches.
- The ultimate goal was to identify core homeostatic pathways and associated genes that correlate with the presence of 2⁺MoPh during progressive DN as potential therapeutic targets.

2 Materials

2.1 Cell culture

2.1.1 Cells and cell lines

Cell line	Origin	Medium
Hek293, adherent human embryonic kidney cell line	ATCC CRL-1573, Manassas, Virginia (USA)	DMEM + 10 % FBS + 1% P/S
Mono-Mac-6, acute monocytic leukemia cell line	Leibnitz Institute DSMZ ACC124, Braunschweig, (Germany)	RPMI 1604 + 10% FBS + 1% NEAA + 1% Sodium pyruvate + 900µg/ml Insulin + 1mM Oxalacetic acid + 1 % P/S
THP-1, acute monocytic leukemia cell line	ATCC TIB-202, Manassas, Virginia (USA)	RPMI 1604 + 10% FBS + 1 % P/S
2 ⁺ MoPh, CD209 / DC-SIGN ⁺ , CD14 ⁺ monocytic phagocytes, generated from primary human peripheral blood mononuclear cells	Prof. Dr. Nößner, Core facility für Immunanalytik Helmholtz Zentrum Munich (Germany)	Assay medium: RPMI1640 + 10% FCS + 1% NEAA + 1% Sodium Pyruvate
imDC, IL-4/GM-CSF immature DCs, generated from primary human peripheral blood mononuclear cells	Prof. Dr. Nößner, Core facility für Immunanalytik Helmholtz Zentrum Munich (Germany)	Assay medium: RPMI1640 + 10% FCS + 1% NEAA + 1% Sodium Pyruvate

2.1.2 Culture media and additives

Name	Manufacturer
RPMI 1604 Medium +GlutaMAX	Gibco, Thermo Fisher Scientific, Waltham (USA)
Dulbeccos Modified Eagle Medium (DMEM) + GlutaMAX	Gibco, Thermo Fisher Scientific, Waltham (USA)
Fetal bovine serum (FBS)	Merck/Biochrom GmbH, Berlin (Germany)
Penicillin/Streptomycin (P/S)	Merck/Biochrom GmbH, Berlin (Germany)
Minimum Essential Medium Non Essential Amino Acids (NEAA)	Gibco, Thermo Fisher Scientific, Waltham (USA)
Sodium Pyruvate 100mM (100X)	Gibco, Thermo Fisher Scientific, Waltham (USA)
Human Insulin solution	Merck/Sigma-Aldrich GmbH, Munich (Germany)
Oxalacetic acid	Merck/Sigma-Aldrich GmbH, Munich (Germany)

Name	Manufacturer
Hygromycin B	Roche Diagnostics, Mannheim (Germany)
Puromycin	Invivogen, SanDiego (USA)
Zeocin	Invivogen, SanDiego (USA)
Blasticidin	Invivogen, SanDiego (USA)
Geneticin / G418	Merck/Sigma-Aldrich GmbH, Munich (Germany)
Doxycyclin Hyclate	Santa Cruz Biotechnology, Dallas (USA)

2.1.3 Cell culture chemicals

Name	Manufacturer
Dulbeccos Phosphate Buffered Saline (DPBS)	PAN-Biotech GmbH, Aidenbach (Germany)
Trypsin/EDTA Solution (T/E)	PAN-Biotech GmbH, Aidenbach (Germany)
Trypan Blue 0.4% Solution	Lonza AG, Basel (Switzerland)
Dimethyl sulfoxide (DMSO)	Merck, Darmstadt, (Germany)

2.2 Microbiology

2.2.1 Bacteria strains

Strain	Origin	Genotype
DH5 α	Addgene, Cambridge (USA)	F- endA1 glnV44 thi-1 recA1 relA1 gyrA96 deoR nupG Φ 80dlacZ Δ M15 Δ (lacZYA-argF)U169, hsdR17(rK- mK+), λ -
MACH-1 T1R	Invitrogen, Thermo Fisher Scientific, Waltham (USA)	F- Φ 80lacZ Δ M15 Δ lacX74 hsdR(rK-, mK+) Δ recA1398 endA1 tonA
DB3.1	Invitrogen, Thermo Fisher Scientific, Waltham (USA)	F- gyrA462 endA1 Δ (sr1-recA) mcrB mrr hsdS20(rB-, mB-) supE44 ara-14 galk2 lacY1 proA2 rpsL20(SmR) xyl-5 λ - leu mtl1

2.2.2 Bacterial media

LB Medium per liter		
10g	Bacto Tryptone	BD, Franklin Lakes (USA)
10g	NaCl	Roth, Karlsruhe (Germany)
5g	Yeast Extract	BD, Franklin Lakes (USA)

LB Agar Plates per liter		
10g	Bacto Tryptone	BD, Franklin Lakes (USA)
10g	NaCl	Roth, Karlsruhe (Germany)
5g	Bacto Yeast Extract	BD, Franklin Lakes (USA)
15g	Bacto Agar	BD, Franklin Lakes (USA)
SOC Medium		
5g	Yeast Extract	BD, Franklin Lakes (USA)
20g	Bacto Tryptone	BD, Franklin Lakes (USA)
10mM	NaCl	Roth, Karlsruhe (Germany)
2,5mM	KCl	Roth, Karlsruhe (Germany)
10mM	MgCl	Roth, Karlsruhe (Germany)
10mM	MgSO ₄	Roth, Karlsruhe (Germany)
20mM	Glucose	Roth, Karlsruhe (Germany)

2.2.3 Microbiology solutions

Ampicillin Stock solution		
50mg/ml	Ampicillin	Roth, Karlsruhe (Germany)
70%	Ethanol	Merck, Darmstadt, (Germany)
30%	H ₂ O	
Kanamycin Stock solution		
10mg/ml	Kanamycin	Roth, Karlsruhe (Germany)
100%	H ₂ O	
Chloramphenicol Stock solution		
34mg/ml	Chloramphenicol	Serva, Heidelberg (Germany)
100%	Ethanol	Merck, Darmstadt, (Germany)
Spectinomycin Stock solution		
100mg/ml	Spectinomycin	Merck/Sigma-Aldrich GmbH, Munich (Germany)
50%	DMSO	Merck/Sigma-Aldrich GmbH, Munich (Germany)
50%	H ₂ O	

Bacteria freezing medium, per liter		
132.3mM	KH ₂ PO ₄	Merck, Darmstadt, (Germany)
21mM	Sodium Citrate x 2H ₂ O	Merck/Sigma-Aldrich GmbH, Munich (Germany)
3.7mM	MgSO ₄ x 7H ₂ O	Roth, Karlsruhe (Germany)
68.1mM	(NH ₄) ₂ SO ₄	Roth, Karlsruhe (Germany)
459.3mM	K ₂ HPO ₄ x 3H ₂ O	Merck, Darmstadt, (Germany)
35.2% (w/v)	Glycerol	Roth, Karlsruhe (Germany)
	H ₂ O	
CaCl₂ Solution (for competent bacteria)		
60mM	CaCl ₂	Merck, Darmstadt, (Germany)
15% (w/v)	Glycerol	Roth, Karlsruhe (Germany)
10mM	PIPES, pH7	Merck, Darmstadt, (Germany)
	H ₂ O	

2.3 Buffers and solutions for molecular biology

Name	Manufacturer
Restriction enzyme buffers 1.1, 2.1, 3.1, Cutsmart	New England Biolabs, Ipswich (USA)
T4 DNA Ligase buffer	New England Biolabs, Ipswich (USA)
Antarctic Phosphatase buffer	New England Biolabs, Ipswich (USA)
Phusion HF buffer	New England Biolabs, Ipswich (USA)
Phusion GC buffer	New England Biolabs, Ipswich (USA)
Thermo Pol Buffer	New England Biolabs, Ipswich (USA)
dATP 100mM	Fermentas, Thermo Fisher Scientific, Waltham (USA)
dGTP 100mM	Fermentas, Thermo Fisher Scientific, Waltham (USA)
dTTP100mM	Fermentas, Thermo Fisher Scientific, Waltham (USA)
dCTP100mM	Fermentas, Thermo Fisher Scientific, Waltham (USA)

5X Tris Borate EDTA (TBE) Solution per litre		
54g	Tris	Roth, Karlsruhe (Germany)
27,5g	Borate	Merck, Darmstadt, (Germany)
20ml	0.5ml EDTA	Roth, Karlsruhe (Germany)
	H ₂ O	
6X Loading Buffer for Agarose Gels		
0.25% (w/v)	Bromphenol Blue	Roth, Karlsruhe (Germany)
0.25% (w/v)	Xylen-Cyanol FF	Merck, Darmstadt, (Germany)
30% (v/v)	Glycerol	Roth, Karlsruhe (Germany)
	H ₂ O	
Electroporation buffer 1M		
5mM	KCl	Merck, Darmstadt, (Germany)
15mM	MgCl	Roth, Karlsruhe (Germany)
120mM	Na ₂ HPO ₄ /NaH ₂ PO ₄ pH7.2	Merck, Darmstadt, (Germany)
50mM	Mannitol	Merck/Sigma-Aldrich GmbH, Munich (Germany)

2.4 Enzymes

Name	Manufacturer
DNase I	Qiagen, Hilden, (Germany)
RNase A	Roche, Basel (Switzerland)
T4 DNA Ligase	New England Biolabs, Ipswich (USA)
Taq DNA-Polymerase (5 U/μl)	New England Biolabs, Ipswich (USA)
Phusion DNA-Polymerase	New England Biolabs, Ipswich (USA)
Calf Intestinal Phosphatase	New England Biolabs, Ipswich (USA)
Antarctic Phosphatase	New England Biolabs, Ipswich (USA)
EcoRI	Roche Diagnostics, Mannheim (Germany)

Restriction Enzymes, New England Biolabs, Ipswich (USA)

AccI, AgeI-HF, AclI, ApaI, ApaLI, AvrII, BsrGI, BamHI, BglII, BstBI, ClaI, EcoRI, Eco53KI, EcoRV, FspI, KpnI-HF, MfeI, HindIII-HF, MluI, NcoI, NdeI, NheI, NotI-HF, PaeI, PciI, PmlI, PvuI, SacII, Sall, SapI, Scal-HF, SfiI, XbaI, XhoI,

2.5 Size Standards for electrophoresis

Name	Manufacturer
1 kb ladder	Thermo Fisher Scientific, Waltham (USA)
2 log ladder	New England Biolabs, Ipswich (USA)

2.6 Recombinant proteins and peptides

Name	Manufacturer
rhWNT3A	R&D/bio-technie, Minneapolis (USA)
rhTGFB1	Acris/Origene, Herford (Germany)
rhSHH	Bio-Techne GmbH, Wiesbaden (Germany)
rhEGF	Bio-Techne GmbH, Wiesbaden (Germany)

2.7 Small molecule agonists and antagonists

Name	Manufacturer/Source
Rapamycin	LC Laboratories, Woburn (USA)
PD98059	Merck/Sigma-Aldrich GmbH, Munich (Germany)
Wortmannin	Merck KGaA, Darmstadt (Germany)
GW3965	Gift from Prof. Gröne, Heidelberg (Germany)
GANT61	Merck/Sigma-Aldrich GmbH, Munich (Germany)
Lysophosphatidic Acid	Enzo, Farmingdale (USA)

2.4 Primers

Primer name	Sequence
TCF7_FW_P5P2	GGGGACAAC TTTGTATACAAAAGTTGTAAGCTCGGATCCA CTAGTAAC
TCF7_RV_P5P2	GGGGACCACTTTGTACAAGAAAGCTGGGTTGCCTCAGAA GCCATAGAG
Gli1_FW_P5P2	GGGGACAAC TTTGTATACAAAAGTTGTACCTCTGAGACGC CATGTTC
Gli1_RV_P5P2	GGGGACCACTTTGTACAAGAAAGCTGGGTTCCCTTAGGAA ATGCGATCTG
SMAD4_FW_P5 P2	GGGGACAAC TTTGTATACAAAAGTTGTATTAGTGAACCGT CAGATCTC
SMAD4_RV_P5 P2	GGGGACCACTTTGTACAAGAAAGCTGGGTTGTGGTTTGTGTC CAAAC TCATC
SMAD3_FW_P5 P2	GGGGACAAC TTTGTATACAAAAGTTGTACAGAGCTCGTTT AGTGAACC
SMAD3_RV_P5 P2	GGGGACCACTTTGTACAAGAAAGCTGGGTTCACTGGAGT GGCAACTTC
Yap1S127A_FW P5P2	GGGGACAAC TTTGTATACAAAAGTTGTACAGTCGACACCA TGGACTAC
Yap1S127A_RV_ P5P2	GGGGACCACTTTGTACAAGAAAGCTGGGTTCTGCCTGAG GGCTCTATAAC
CMV_Pro_FW	GGGGACAAG TTTGTACAAAAAAGCAGGCTTACGATGTACG GGCCAGATA
CMV_Pro_RV	GGGGACAAC TTTTGTATACAAAGTTGTAGCAGTGGGTTCT CTAGTTAGC
Yap1WT_FW_P 5P2	GGGGACAAC TTTGTATACAAAAGTTGTAAGCTCGGATCCA CTAGTAAC
Yap1WT_RV_P5 P2	GGGGACCACTTTGTACAAGAAAGCTGGGTTAGCGAGCTCT AGCATTTAGG
CMVTO-fw	GGGGACAAG TTTGTACAAAAAAGCAGGCTTAAGGCCCTTT CACTCATTAG
CMVTO-rv	GGGGACAAC TTTTGTATACAAAGTTGTCCGGTGTCTTCTAT GGAG
TAZ_FW_P5P2	GGGGACAAC TTTGTATACAAAAGTTGTAGTGAACCGTCAG AATTGATC
TAZ_RV_P5P2	GGGGACCACTTTGTACAAGAAAGCTGGGTTCACTGGAGT GGCAACTTC
NR1H2_fw_GW	GGGGACAAC TTTGTATACAAAAGTTGTAATGTCCTCTCCTA CCACGAGTTC
NR1H2_rv_Stop GW	GGGGACCACTTTGTACAAGAAAGCTGGGTTTCACTCGTGG ACGTCCCAGAT
NR1H3_fw_GW	GGGGACAAC TTTGTATACAAAAGTTGTAATGCCCACTCT GCTGGG
NR1H3_rv_STO P GW	GGGGACCACTTTGTACAAGAAAGCTGGGTTTCATTTCGTGC ACATCCCAGATCTC
Gaussia_P5P2_ FW	GGGGACAAC TTTGTATACAAAAGTTGTAATCCAGCCACCA TGGGAGTC
Gaussia_P5P2_ r v	GGGGACCACTTTGTACAAGAAAGCTGGGTTGGCCGCTTA GTCACCACC

2.5 Plasmids and vectors

Name	Manufacturer
pcDNA6.2/V5-PL-DEST	Thermo Fisher Scientific, Waltham (USA)
pcDNA6/TR	Thermo Fisher Scientific, Waltham (USA)
pT-Rex-DEST30	Thermo Fisher Scientific, Waltham (USA)
pHOOK2	Thermo Fisher Scientific, Waltham (USA)
pGL3-Promoter	Promega, Fitchburg (USA)
pN3 Bar-Gluc	Gift from Peter Neth, LMU Munich
pBlue-loxP-PGK-gb2-hyg-loxP	BCCM/LMBP #6665, Zwijnaarde (Belgium)
NR1H2 cDNA clone	HsCD00438678, DNASU, Tempe (USA)
NR1H2 cDNA clone	HsCD00004021, DNASU, Tempe (USA)
NR1H3 cDNA clone	HsCD00442548, DNASU, Tempe (USA)
GLI K12	#16419, Addgene, Cambridge (USA)
WWP-Luc	#16451, Addgene, Cambridge (USA)
pCEP4 Smad4	#16483, Addgene, Cambridge (USA)
SBE4-Luc	#16495, Addgene, Cambridge (USA)
pHR TCF4	#16514, Addgene, Cambridge (USA)
pcDNA Flag Yap1	#18881, Addgene, Cambridge (USA)
Luciferase-pcDNA3	#18964, Addgene, Cambridge (USA)
3XFlag pCMV5-TOPO TAZ WT	#24809, Addgene, Cambridge (USA)
3XFlag pCMV5-TOPO TAZ (S89A)	#24815, Addgene, Cambridge (USA)
8xGTIIC-luciferase	#34615, Addgene, Cambridge (USA)
pcDNA3-HA-TCF1	#40620, Addgene, Cambridge (USA)
pENTR-3xFLAG-YAP1-S127A	#42239, Addgene, Cambridge (USA)
SMAD3 WT expression vector	Gift from Prof. Groene, DKFZ, Heidelberg (Germany)
SMAD3 constitutively active mutant expression vector	Gift from Prof. Groene, DKFZ, Heidelberg (Germany)

2.6 Kits

Kit	Manufacturer
InnuPREP Plasmid Mini Prep	Analytik Jena AG, Jena (Germany)
InnuPREP Plasmid Midi Prep	Analytik Jena AG, Jena (Germany)
ZymoPURE Plasmid Maxiprep Kit	Zymo Research Corp, Irvine (USA)
Exo-Spin Exosome Purification Kit	Cell Guidance Systems Ltd, Cambridge (UK)
MultiSite Gateway Pro Plus	Thermo Fisher Scientific, Waltham (USA)
Gateway LR Clonase II Plus	Thermo Fisher Scientific, Waltham (USA)
Gateway BP Clonase II	Thermo Fisher Scientific, Waltham (USA)
Purelink RNA Mini Kit	Thermo Fisher Scientific, Waltham (USA)
BioLux <i>Gaussia</i> Luciferase Assay Kit	New England Biolabs, Ipswich (USA)
Pierce BCA Protein Assay Kit	Thermo Fisher Scientific, Waltham (USA)

2.7 Other laboratory equipment

Device	Manufacturer
vapo.protect thermocycler	Eppendorf, Hamburg (Germany)
Thermomixer comfort	Eppendorf, Hamburg (Germany)
Megafuge 1.0R	Thermo Fisher Scientific, Waltham (USA)
Biofuge pico	Thermo Fisher Scientific, Waltham (USA)
Rotanta 460R	Hettich, Tuttlingen (Germany)
L70 Ultracentrifuge	Beckman, Brea (USA)
Lumat LB 9507	Berthold, Bad Wildbad (Germany)
GENios plate reader	Tecan, Männedorf (Switzerland)

2.8 Chemicals

Name	Manufacturer
Agarose ultrapure	Thermo Fisher Scientific, Waltham (USA)
Aqua ad injectabilia	Braun, Melsungen (Germany)
β -Mercaptoethanol	Roth, Karlsruhe (Germany)
Bromphenolblue	Sigma Aldrich, Taufkirchen (Germany)
Calciumchloride (CaCl ₂)	Merck, Darmstadt (Germany)
Ethylenediaminetetraacetic acid (EDTA)	Merck, Darmstadt (Germany)
Acetic acid	Merck, Darmstadt (Germany)
Ethanol, absolute	Merck, Darmstadt (Germany)
Ethidiumbromid 1%	Merck, Darmstadt (Germany)
Isopropanol	Merck, Darmstadt (Germany)
Methanol, absolute	Merck, Darmstadt (Germany)
Magnesiumchloride	Merck, Darmstadt (Germany)
MOPS (3-(N-morpholino)propanesulfonic acid)	Roth, Karlsruhe (Germany)
MTT 3-(4,5-dimethylthiazol-2-yl)-2,5-diphenyltetrazolium bromide	Sigma Aldrich, Taufkirchen (Germany)
Sodium Acetate	Merck, Darmstadt (Germany)
Sodium chloride	Sigma Aldrich, Taufkirchen (Germany)
tris(hydroxymethyl)aminomethane (Tris)	Merck, Darmstadt (Germany)
Hydrochloric acid	Roth, Karlsruhe (Germany)

2.8 Disposables and other materials

Name	Manufacturer
Cell culture plates	TPP, Trasadingen (Switzerland)
Cell culture flasks	TPP, Trasadingen (Switzerland)
Cell scrapers	TPP, Trasadingen (Switzerland)
Conical centrifuge tubes 15ml/50ml	BD Biosciences, Franklin Lakes, USA

2.9 Antibodies for flow cytometry

Specificity	Label	Species /	Clone	Manufacturer	Dilution	Staining
CD14	PB	Mouse IgG2a, κ	M5E2	BD	1:25	Surface
CD14	PerCP-Cy5.5	Mouse IgG1, κ	61D3	eBioscience	1:10/1:5+	Surface
CD163	PerCP Cy5.5	Mouse IgG1, κ	GHI/61	Biologend	1:10	Surface
CD209	APC	Mouse IgG2a, κ	DCN46	BD	1:10	Surface
CD209	PE	Mouse IgG2b, κ	DCN46	BD	1:10/1:4+	Surface
CD40	FITC	Mouse IgG1, κ	5C3	BD	1:10	Surface
CD64	FITC	Mouse IgG1, κ	22	Beckman Coulter	1:10	Surface
CD80	PE	Mouse IgG1, κ	L307.4	BD	1:16.6	Surface
HLA-DR/ MHC-II	FITC	Mouse IgG2a, κ	L243	BD	1:25	Surface
Isotype	-	Mouse IgG1, κ	MOPC21	BD	1:500	intracellular
Isotype	A700	Mouse IgG1, κ	MOPC21	BD	*	Surface
Isotype	APC	Mouse IgG1, κ	11711	R&D Systems	*	Surface
Isotype	APC	Mouse IgG2a, κ	HOPC 1F/12	Jackson	*	Surface
Isotype	FITC	Mouse IgG1, κ	MOPC21	BD	*	Surface
Isotype	FITC	Mouse IgG2a, κ	G155-178	BD	*	Surface
Isotype	FITC	Mouse IgM	IS5-20C4	Miltenyi Biotec	*	Surface
Isotype	PE	Mouse IgG1	MOPC21	BD	*	Surface
Isotype	PE	Mouse IgG2b, κ	MPC-11	Biologend	*	Surface
Isotype	PE	Ratte IgG2a, κ	R35-95	BD	*	Surface
Isotype	PE-Cy7	Mouse IgG1, κ	MOPC21	BD	*	Surface
MerTK	APC	Mouse IgG1, κ	125518	R&D Systems	1:5	Surface
MSR1	APC	Mouse IgG2B	351615	R&D Systems	1:5	Surface
VSIG4	-	Rabbit	Polyclonal	abcam	1:50	Surface

* adjusted to antibody used

2.10 Software

Software	Manufacturer	Usage
Prism	Graphpad Software, La Jolla (USA)	Statistical tests and Graphing
Canvas 12	ACD Software, Victoria (Canada)	Diagrams and Illustrations
R including the bioconductor package	Open source projects, found at their respective websites https://www.bioconductor.org/ and https://www.r-project.org/	Microarray analyses including deconvolution analyses
Genomatix Software suite	Genomatix GmbH, Munich, (Germany)	Pathway mapping
Progenesis QI software for proteomics 2.0	Nonlinear Dynamics, Newcastle upon Tyne (UK)	Proteomics

3 Methods

3.1 Microarray analysis

3.1.1 Samples

A total of 17 DN samples (calculated eGFR MDRD mean of 44, median of 46 and standard deviation of 25) and 30 living donor (LD) controls were obtained from the European Renal cDNA Bank (ERCB) and microdissected for microarray analysis [154]. To this end, total RNA from the tubulointerstitial compartments was isolated, reverse transcribed, linearly amplified, and hybridized on Affymetrix microarrays in collaboration with Prof. M. Kretzler, University of Michigan, Ann Arbor [35, 36, 155, 156].

3.1.2 Robust multichip average (RMA) analysis, batch correction and filtering

In initial analyses of microarray samples, all data was normalized using the RMA Algorithm [157] and annotated at EntrezGene level using current Custom CDF Files from Brainarray (<http://brainarray.mbni.med.umich.edu/Brainarray/>) [158]. All data was batch corrected [159] and log transformed using the GenePattern pipeline [160]. Filtering for expressed genes was done by applying a cutoff of the median of the non-human Affymetrix control probe sets plus two times their SD.

3.1.3 GeneRanker analysis

Processed gene lists were assigned to biologic processes using the GeneRanker software, which is part of the Genomatix software suite (Munich, Germany). Analysis was carried out using default parameters and using the literature mining based pathway database [161].

3.1.3 Deconvolution analysis to selectively identify 2⁺MoPh cells in complex data

To estimate the proportion of 2⁺MoPh cells in mixed samples (i.e. the 2⁺MoPh score), the procedure suggested by Abbas [162] was followed. First, 61 2⁺MoPh marker genes were identified using pamr (nearest shrunken centroid method) on a training set comprising 6 and 182 samples taken from 2⁺MoPh cells, and various control cell types, respectively. Then the mean expression values for each marker gene in all 2⁺MoPh samples were calculated. The coefficient of a linear model of marker gene expression

value in each mixed sample based on the corresponding means was obtained from the ercDC pool, that then served as an estimate of the fraction of 2^* MoPh, the deconvolution score of the mixed sample. This was done in collaboration with Prof. Dr. E. Nößner and Dr. D. Brech, Helmholtz Zentrum München and Dr. Tobias Straub, LMU Core Facility, Bioinformatics Biomedizinisches Centrum.

3.1.4 Weighted Gene Correlation Network Analysis (WGCNA)

A signed coexpression network was generated using the Weighted Gene Correlation Network Analysis (WGCNA) package as implemented in the R statistical software with the default parameters and a minimum module size set to 30 [163].

3.2 Cell culture

3.2.1 General cell culture

The culture of human cells and cell lines was performed in a laminar flow hood to prevent contamination. All reagents were pre-warmed to 37°C in a water bath prior to use. All cells were incubated at 37°C and 5% CO₂.

For subculturing, adherent cells were washed with PBS and subsequently detached using Trypsin-EDTA solution at room temperature. The reaction was stopped by adding double the volume of medium containing 10% FCS (or more if the medium contained less FCS) and the cells were pelleted by centrifugation for 3 min at 220 x g (rt). Subsequently, the cell pellet was resuspended in fresh medium and a fraction was seeded into the respective cell culture vessel.

Suspension cells were resuspended prior to subculturing and subsequently a fraction of the culture medium according to the desired split factor was transferred into a new cell culture flask, which was then filled up with fresh medium to the desired end volume.

3.2.2 Freezing and thawing of cells

All cells were frozen in 20% of their respective culture medium + 60% FCS + 10% DMSO in sealable cryotubes. The tubes were cooled to -80°C over a 24 h period in an isopropanol container prior to transferring them into a liquid nitrogen container. For thawing, the frozen cell suspensions were rapidly thawed in a 37°C water bath and immediately transferred into a cell culture vessel filled with prewarmed medium. The medium was replaced after 18 h to remove DMSO.

3.2.3 Counting cells

Cell counts were determined using a Neubauer chamber. The cover slip was attached to the chamber so that “Newton’s rings” were visible. This is used as a means of determining optimal distance between counting chamber and cover slip, and is important as the chamber is calibrated to the resulting volume. One part of the cell suspension was mixed with Trypan Blue solution in a 1:3-1:5 ratio, depending on cell line and density, staining dead cells blue. 10 µl of this mixture were immediately pipetted into the chamber. Only living cells were counted in all the quadrants of the chamber. The number of cells per ml suspension could then be calculated. The count (x) multiplied by the dilution and divided by the quadrants counted gave a number of $x \cdot 10^4$ cells/ml cell suspension.

3.3 Molecular biology

3.3.1 Freezing and thawing of bacteria

For long-term storage of *E. coli* strains, 900 µl of an overnight culture was mixed with 100 µl freezing solution for bacteria (10x) and frozen at -80°C. To establish cultures from frozen cells, a small amount of frozen bacteria was streaked onto an appropriate agar plate and incubated at 37°C overnight. Subsequently, a liquid culture in LB Medium was established from a single colony on that plate.

3.3.2 Preparation of agar plates

For the preparation of microbiological agar plates, 1X LB medium was prepared with an added 1.5% of Agar and autoclaved. Upon reaching a temperature of 60°C, when required, appropriate antibiotics were added (Ampicillin: 100 µg/ml final concentration; Kanamycin: 50 µg/ml final concentration; Chloramphenicol: 25µg/ml final concentration) and the solution was cast in Standard 10cm Petri dishes. Plates were stored in plastic bags at 4°C.

3.3.3 Restriction digestion of DNA

DNA was cut using restriction enzymes. To cut 1 µg DNA, 1 unit of restriction enzyme was used per hour. In cases when large amounts of DNA had to be cut, the amount of enzyme and/or the incubation time was increased accordingly. To minimize unspecific cutting due to high Glycerol content, no more than 10% of Enzyme final volume was used. All digestions were performed in a buffer suitable for the respective

enzyme(s) (diluted to 1x) at the temperature suggested by the manufacturer (37-65°C).

3.3.4 Separation of DNA fragments by electrophoresis

To separate DNA fragments for analytical or preparative purposes, agarose gel electrophoresis was used. The concentration of agarose was chosen according to the expected fragment sizes and varied between 0.6% and 3% agarose. Gel solutions were prepared in 0.5x TBE buffer with added ethidium bromide and heated in a microwave oven to dissolve the agarose and cast in horizontal gel chambers.

For the electrophoresis, all samples and a size standard [2 log ladder, New England Biolabs, Ipswich (USA)] were mixed with loading buffer for agarose gels (6x) to yield a 1x final concentration of loading buffer and loaded into the wells. Using 0.5x TBE buffer at 170 V, electrophoresis was performed and the gels were subsequently photographed under UV light for documentation. In the case of preparative gels, the respective bands were cut out of the gel under UV light and DNA was extracted from the gel fragments using a commercial kit (Qiagen Gel Extraction Kit) according to the manufacturer's instructions.

3.3.5 Determination of DNA and RNA concentrations

The concentrations of DNA and RNA in solutions were determined using a Nanodrop ND-1000 spectrophotometer [Thermo Fisher, Waltham (USA)]. All determinations were performed according to the manufacturer's instructions using the appropriate buffer as control (Water, TE, Elution Buffer).

3.3.6 Dephosphorylation of DNA ends

In case cleavage and separation of plasmids led to compatible overhangs, to prevent re-ligation of linearized vectors, their 5' DNA ends were dephosphorylated. To this end, 5 units of Antarctic phosphatase per pmol 5' ends was added to the sample and the mixture was incubated at 37°C for 1 h. The reaction was stopped by heat inactivation at 65°C for 15 min. Prior to the next cloning step, the dephosphorylated DNA was purified using a commercially available kit (Qiagen PCR Cleanup Kit) according to the manufacturer's instructions.

3.3.7 Assembly of short synthetic DNA elements for reporter constructs

To synthetically generate short (up to 200 base pairs) inserts for reporter vectors, single stranded Oligos were ordered [Thermo Fisher, Waltham (USA) or Biomers, Ulm (Germany)]. These oligos were designed such that the two strands would be compatible for annealing by designing them as reverse complements of each other. In addition, the oligos were designed with overhangs compatible to the ones created by restriction enzymes, allowing for direct ligation into cleaved vector backbones.

3.3.8 Ligation of DNA fragments

For ligation of vector backbone and insert DNA, separate reactions were prepared using an insert:vector molar ratio of 3:1 and 10:1, respectively. A third reaction containing only vector DNA served as negative control. All reactions were performed in a total volume of 20 μ l containing 400 U (1 μ l) T4 DNA ligase and 2 μ l 10x T4 DNA ligase buffer overnight at room temperature.

3.3.9 Preparation and transformation of competent *E. coli* MACH-1

Chemically competent *E. coli* were prepared in-house as a vessel for propagation and selection of cloned plasmids. To this end, 4 ml of an overnight liquid culture of *E. coli* MACH-1 in LB medium was diluted 1:100 into fresh LB medium and incubated at 37°C and 250 rpm and left to grow till reaching an OD_{600nm} of 0.375. Subsequently, the suspended bacteria were aliquoted into 50 ml aliquots, incubated on ice for 5 min and afterwards centrifuged for 10 min at 1600 x g (4°C). After discarding the supernatant, each aliquot of bacteria was resuspended in 10 ml ice-cold CaCl₂ solution and the centrifugation step repeated. After that, the supernatant was discarded again, each aliquot of bacteria was resuspended in 10 ml fresh ice cold CaCl₂ solution and stored on ice for 30 min. Following another centrifugation as detailed above, the pelleted bacteria were resuspended in 2 ml CaCl₂ solution and frozen at -80°C in 50 μ l Aliquots. For transformation of competent *E. coli* MACH-1 bacteria using ligation reactions, varying amounts of DNA were used, depending on the cloning method, but corresponding to 10-100 ng DNA. The frozen bacteria were rapidly thawed and 50 μ l of suspension were added to the DNA. Following an initial incubation on ice for 10 min, the mixture was heated to 42°C for 45 sec and immediately cooled on ice again. The transformed bacteria were suspended in 250 μ l SOC medium and incubated for 60 min at 37°C and 400 rpm. Subsequently, the suspension was plated onto agar plates containing the appropriate antibiotic for selection of successfully transformed colonies

and incubated over night at 37°C. The next day, single colonies were picked and transferred into liquid cultures in order to prepare plasmid DNA.

3.3.10 Isolation and analysis of plasmid DNA from transformed bacteria

Plasmid DNA was isolated from transformed bacteria using commercially available kits (Innuprep Plasmid Mini kit for liquid cultures up to 1.5 ml; ZymoPURE Plasmid Maxi kit for liquid cultures up to 150 ml) according to the manufacturers' instructions. Following plasmid DNA isolation, analytical restriction digestions were performed using appropriate restriction enzymes (see 3.3.3) and the resulting fragments were analyzed by gel electrophoresis (see 3.3.4).

3.3.11 Polymerase chain reaction (PCR)

For the cloning steps presented here, a large number of Polymerase chain reactions, some with large products, were carried out using a Polymerase with a 3'->5' exonuclease function [Phusion High-Fidelity DNA Polymerase, New England Biolabs, Ipswich (USA)] to ensure a very low level of mismatches. All PCR products were evaluated and purified by agarose gel electrophoresis to remove primers and potential falsely primed products.

The general PCR protocol used was:

Step	Temperature	Time	Number of cycles
Initial denaturation	98°C	5 min	1
Denaturation	98°C	30s	
Annealing	Depends on Primers	30s	30
Extension	72°C	30s / kbase	
Final extension	72°C	10 min	1

3.3.12 Sequencing of DNA

DNA sequencing, using the Sanger method of chain-terminating dideoxynucleotides, was performed by GATC Biotech, Konstanz. Since a large number of constructs were sequenced, there is a large number of individual primers that were used for the sequencing of PCR templates. The most commonly used however were:

Vector	Primer Name	Sequence
pSBTET.Reporter Variants	Enhancer_FW	CATGTCTGGTCTCGAATCCATC
pSBTET.Reporter Variants	Enhancer_RV	CGATGCAGATCAGGGCAAAC
pENTR221 Variants	M13 FW	TGTAACACGACGGCCAGT
pENTR221 Variants	M13 RV	CAGGAAACAGCTATGACC
pSBDEST Variants	T7	TAATACGACTCACTATAGGG
pSBDEST Variants	pSBDEST_RV	GGTTCCTTCCGGTATTGTC
pSBDEST Variants	V5_RV	ACCGAGGAGAGGGTTAGGGAT

3.4 Cloning Strategies

3.4.1 Adaptation of the pGL3-Promoter vector for *Gaussia* Luciferase

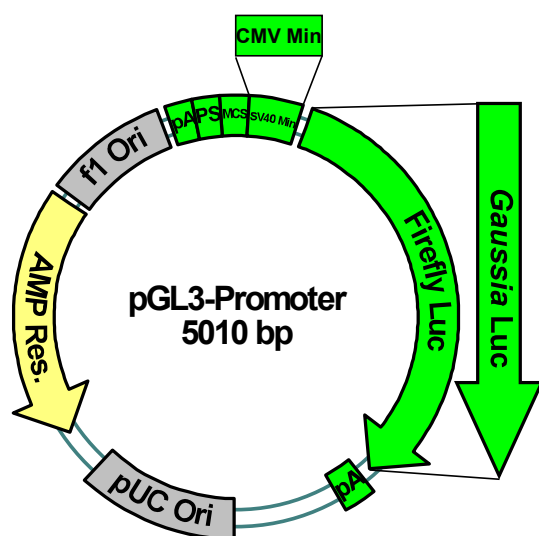


Figure 8. Cloning scheme for the generation of the reporter vectors, Step 1. In the first cloning step, the minimal promoter element and the luciferase were to be replaced in the commercially available pGL3-Promoter vector. For details refer to 3.4.1

The first step in the generation of the reporter vectors (see 3.4.2) was modification of the commercially available pGL3-Promoter Vector [Promega, Fitchburg (USA)]. The original pGL3-Control Promoter reporter vector used Firefly Luciferase optimized for low background activity, and a minimal Promoter based on the Simian virus 40 (SV40). To reduce background activity, this minimal promoter had already been reduced to the core 197 bp.

In a first cloning step, the intracellular Firefly luciferase was replaced with the codon optimized version of the secreted luciferase taken from *Gaussia princeps*, obtained

via PCR from the WNT specific reporter vector pN3-BAR-Gluc. After a few preliminary experiments, the background activity level with this SV40 minimal promoter was deemed too high, and the SV40 minimal promoter was replaced by a 35 bp long stretch of the cytomegalovirus promoter (CMV Min) which significantly reduced background activity. The resulting vector was named pGL3-CMVMin-GLuc.

3.4.2 Modifications of pCDNA6/TR for Sleeping Beauty compatibility

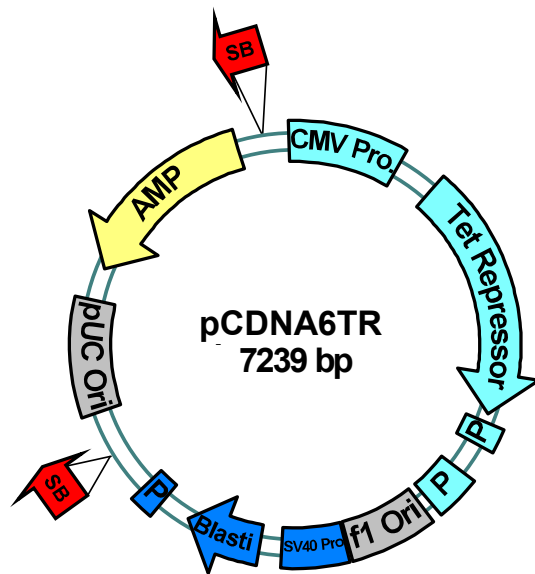


Figure 9. Cloning scheme for the generation of the reporter vectors, Step 2. In the second cloning step, Sleeping Beauty transposase inverted terminal repeats were integrated into the pCDNA6/TR vector. For details refer to 3.4.2

As a basis for the generation of the complex pSBTET.Reporter vectors, the commercially available pcDNA6/TR [Thermo Fisher, Waltham (USA)] vector was chosen. This vector was deemed suitable as it already contained an optimized and humanized expression cassette for the TET-Repressor protein from the Tn10 transposon in enteric bacteria [164]. In these bacteria, the TET-repressor protein serves to tightly regulate expression of the resistance gene for tetracycline. This regulatory capacity has been adapted for use in inducible eukaryotic systems to allow for rapid and highly sensitive de-repression of Tet-Operator controlled promoters. To further optimize the potential for the generation of stable transfectants, the principle expression cassettes for both the eukaryotic selective marker Blasticidin and the expression cassette for the TET-Repressor protein were flanked with recognition sites (inverted and direct repeats) for the Sleeping Beauty (SB) transposase [165-167]. This allowed efficient introduction of transfected genetic cargo into the host cell genome when co-transfected with an expression vector for the SB transposase, thus generating stable transfectants. The resulting vector was named pCDNA6TR/ITR.

3.4.3 Generation of pSBTET.Reporter by fusion of the modified pGL3 Promoter and pCDNA6/TR-ITR

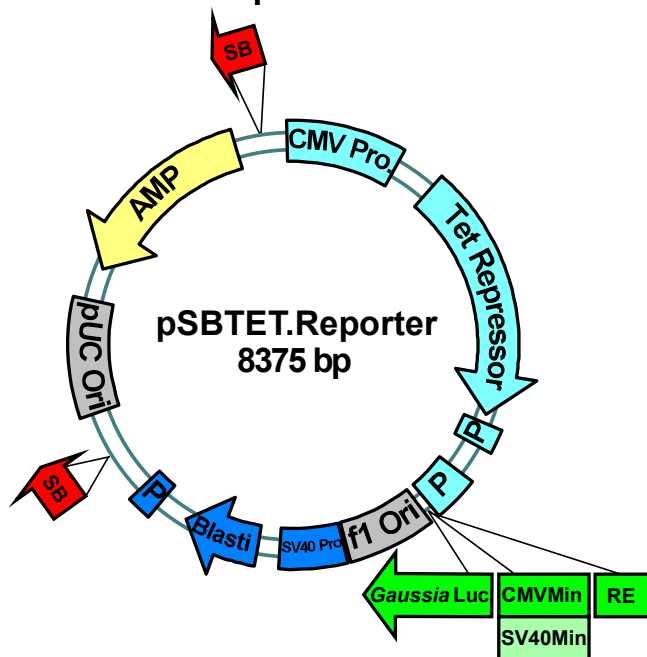


Figure 10. Cloning scheme for the generation of the reporter vectors, Step 3. In the final cloning step, a fusion of the generated pGL3-Promoter based reporter element and the Sleeping Beauty-adapted backbone was generated. For details refer to 3.4.3

The final step for the generation of the pSBTET.Reporter plasmids was fusion of the aforementioned (3.4.1 and 3.4.2) pGL3-CMVMin-GLuc and pCDNA6TR/ITR vectors resulting in a vector that was Sleeping Beauty transposable, expressing the TET-Repressor and carrying a *Gaussia* luciferase based reporter cassette, with expression of the Blasticidin selection marker to screen for stable transfectants. The plasmids were cut and ligated together resulting in the pSBTET.reporter. [168]

3.4.4 Generation and insertion of transcription factor specific reporter elements

To generate transcription factor specific reporter elements to act as pathway reporters, single stranded oligomers were assembled as in 3.3.7 with compatible XhoI, PstI overhangs and ligated into the cleaved pSBTET.reporter vector backbone as detailed in 3.3.8.

Sequences of reporter elements:

AP-1 Binding element (6x multimer): TGA⁺CTCA, Linker Sequence: TCAAGCA
(<https://www.addgene.org/40342/> [169])

GLI binding element (8x multimer): GACCACCCAC
(http://www.sabiosciences.com/reporter_assay_product/HTML/CCS-6030L.html)

TEAD binding element (8x multimer): ACATTCC, varying linker sequences
(<https://www.addgene.org/34615/>, [170])

LXR binding element (3x multimer): TGACCAGCAGTAACC
(http://www.sabiosciences.com/reporter_assay_product/HTML/CCS-0041L.html)

TCF/LEF binding element (12x multimer): ATCAAAG,
[171]

SMAD binding element (5x multimer): AGCCAGACAGT
(http://www.sabiosciences.com/reporter_assay_product/HTML/CCS-017L.html)

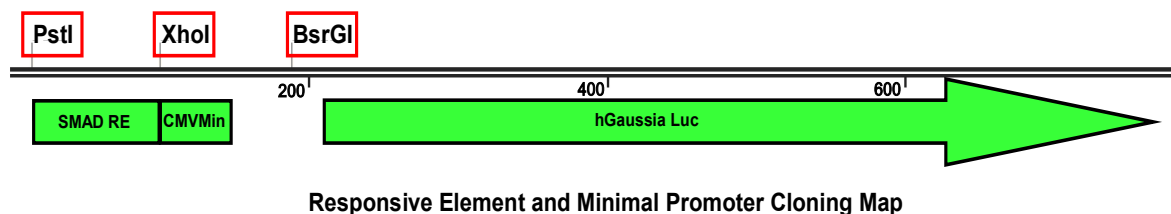


Figure 11. Accessible Cloning Sites in pSBTET.Reporter vectors.

Magnified region of pSBTET.SMAD serves as illustration of restriction sites available to modify these vectors. The minimal promoter is replaced by digests with XhoI and BsrGI, while the transcription factor responsive elements are replaced by PstI and XhoI digests. This allows for easy adaptation of the reporter vectors to other pathways, or even replacement of both RE and Minimal Promoter with a full human promoter by digest with PstI and BsrGI.

3.4.5 Generation of pSBDEST by Fusion of pCDNA6/TR-ITR and pcDNA6.2 V5 PL-DEST

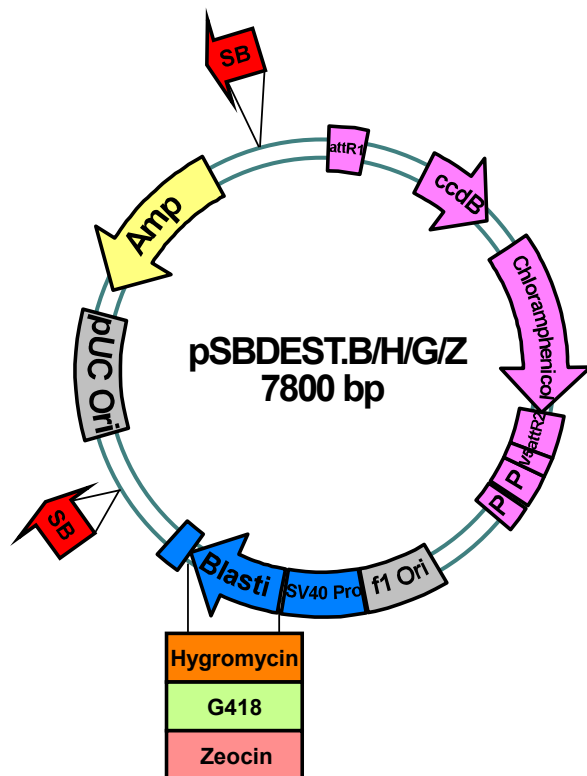


Figure 12. Cloning scheme for the generation of the Destination vectors. Similar to the reporter vectors, MultiSite Gateway compatible destination vectors were adapted to Sleeping Beauty transposase-ready vector by the addition of ITRs, in addition, variants with other selective markers were generated to allow for co-transfection with the Blastidicin selection carrying reporter vectors, or multiple destination vectors. For details see 3.4.5

To generate a highly flexible cloning system, also compatible with the Sleeping Beauty transposon strategy, a promoterless commercial multi-site Gateway cloning vector was modified. Multi-Site Gateway cloning allows the rapid generation of complex transgenes via the recombination of up to four fragments into a single Destination vector in a defined orientation and order. Since the backbone region of pCDNA6TR/ITR had high sequence identity to pCDNA6.2/V5-PL-DEST, this vector was selected and used as donor for the Gateway cassette. Both pCDNA6TR/ITR and pCDNA6.2/V5-PL-DEST were cut using BgIII. This digest cleaved out the TET-Repressor expression cassette from pCDNA6TR/ITR, but retained the backbone, including the Sleeping Beauty compatible ITRs/DRs. The same enzymatic digest of pCDNA6.2/V5-PL-DEST released the Gateway cloning acceptor cassette. After agarose gel purification, the resultant fragments were ligated, resulting in pSBDEST.B. Additionally, the system was made more flexible by replacing the Blastidicin selection marker with a selection of either Hygromycin, G418/Geneticin or Zeocin, resulting in pSBDEST.H, pSBDEST.G and PSBDEST.Z [168]. This allows the parallel selection of multiple plasmids in the same cell.

3.4.6 Generation of Entry Clones

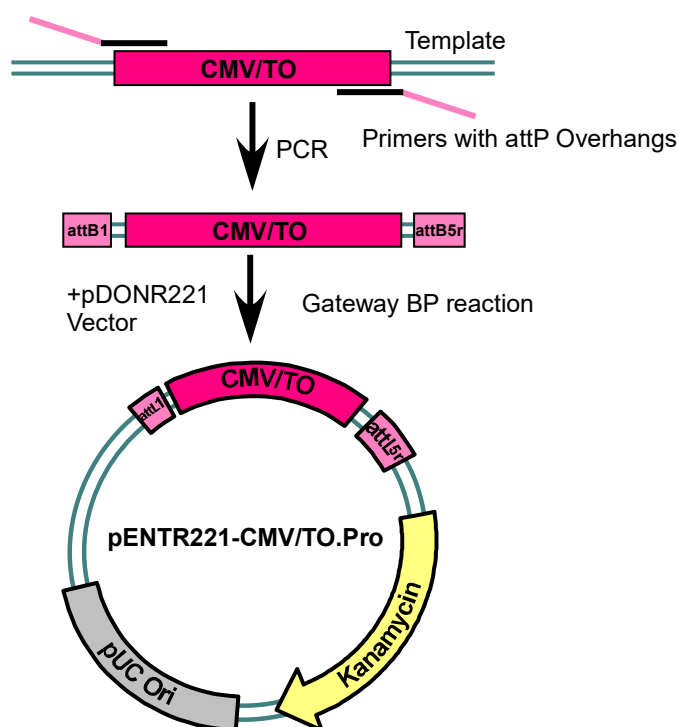


Figure 13. Cloning of compatible Entry Clones. For the generation of compatible Multi-Site Gateway Entry clones, PCR products with attP overhangs were generated for sequences of interest. This was accomplished by using primers consisting of a homologous region and Gateway-cloning compatible attP overhangs. In a so-called “BP-reaction” the overhangs are recombined into a donor vector. For details see 3.4.6

Entry clones serve as building blocks for MultiSite Gateway reactions. To generate an entry clone, a template was PCR amplified using specific primers carrying long, vector and reaction specific overhangs which allowed for recombination reactions. All PCR reactions were carried out as specified in 3.3.11.

Entry clones for various promoters and coding DNA sequences (CDS) were generated in BP reactions according to the Multi-Site Gateway Manual, using the donor vectors supplied in the MultiSite Gateway Pro Plus Kit [Thermo Fisher, Waltham (USA)]. PCR Templates for these constructs were purchased from either Addgene (Cambridge, USA) or DNASU (Tempe, USA), for a list see Section 2.5.

To verify the all Entry clones, each individual clone was screened through restriction digests and gel electrophoresis; positive clones were then verified by partial sequencing.

3.4.7 Generation of Expression vectors

To generate expression constructs, two-fragment Multi-Site Gateway reactions were carried out using an Entry clone for a desired promoter fragment, and a second Entry clone carrying the CDS for the gene of interest (see Figures 14 and 15). The only Gateway-Destination vectors used were pSBDEST variants. All MultiSite Gateway LR reactions were carried out according to the Multi-Site Gateway Manual and using Gateway LR Clonase II Plus [Thermo Fisher Scientific, Waltham (USA)]. To verify all Expression clones, each one was screened by restriction digests and gel electrophoresis and positive clones then verified by sequencing.

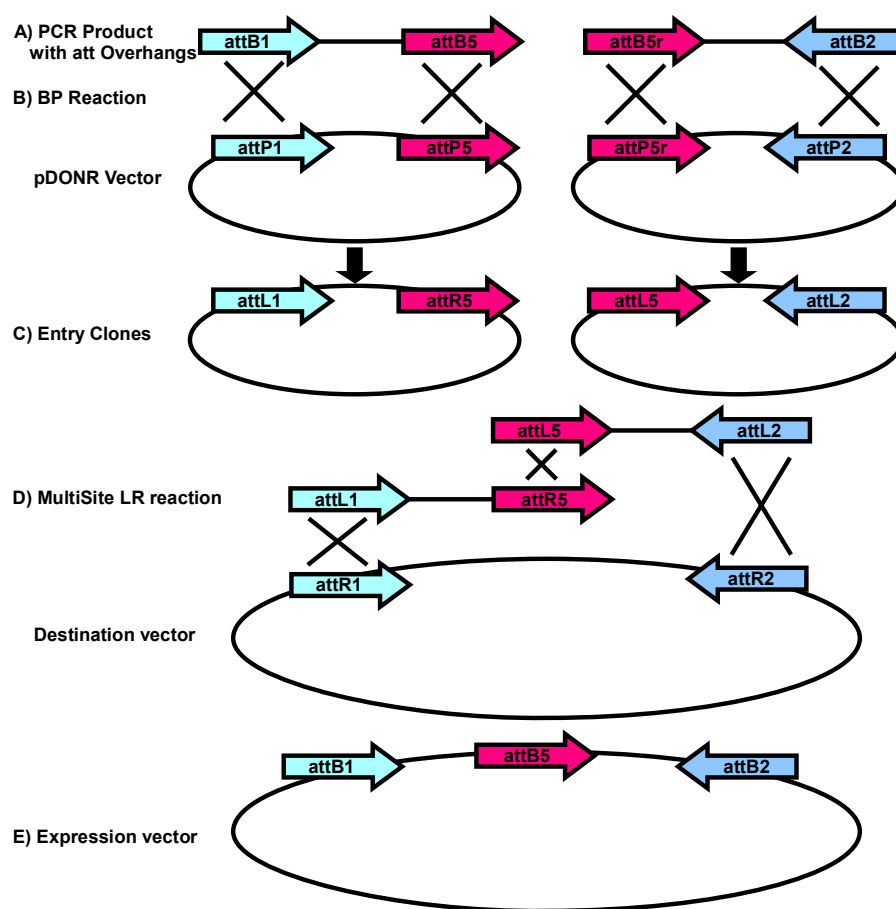


Figure 14
Overview of multi-site Gateway cloning.

Gateway cloning is a cloning strategy based on Integrase (Int) from Phage λ and Integration host factors (IHF a and IHF b) from *E. coli* in tandem with specific overhangs required for recombination. **A** Using specific primer overhangs, PCR products are generated with flanking Gateway cloning compatible recombination sequences (*attB* sites). **B-C** via *in-vitro* BP reactions with compatible donor vectors, Entry clones are generated, with resulting *attL* recombination sites. **D** In an LR reaction (another *in-vitro* reaction), recombination between fitting LR overhangs leads to directed and ordered insertion of multiple entry clones into a destination vector. **E** The resulting expression vector carries the inserts in sequence. By recombination *attB* sites have been generated. Both BP and LR reactions are strictly selected by 2 mechanisms: Positive selection via Kanamycin/Ampicillin selection in the donor/entry vector backbone and negative selection by *ccdB*. *ccdB* is a suicide gene in *E. coli* and every donor or destination vector carries it. If it isn't replaced by recombination, transfected *E. coli* die. So only *E. coli* which are Kanamycin/Ampicillin resistant from recombined vectors survive.

clones are generated, with resulting *attL* recombination sites. **D** In an LR reaction (another *in-vitro* reaction), recombination between fitting LR overhangs leads to directed and ordered insertion of multiple entry clones into a destination vector. **E** The resulting expression vector carries the inserts in sequence. By recombination *attB* sites have been generated. Both BP and LR reactions are strictly selected by 2 mechanisms: Positive selection via Kanamycin/Ampicillin selection in the donor/entry vector backbone and negative selection by *ccdB*. *ccdB* is a suicide gene in *E. coli* and every donor or destination vector carries it. If it isn't replaced by recombination, transfected *E. coli* die. So only *E. coli* which are Kanamycin/Ampicillin resistant from recombined vectors survive.

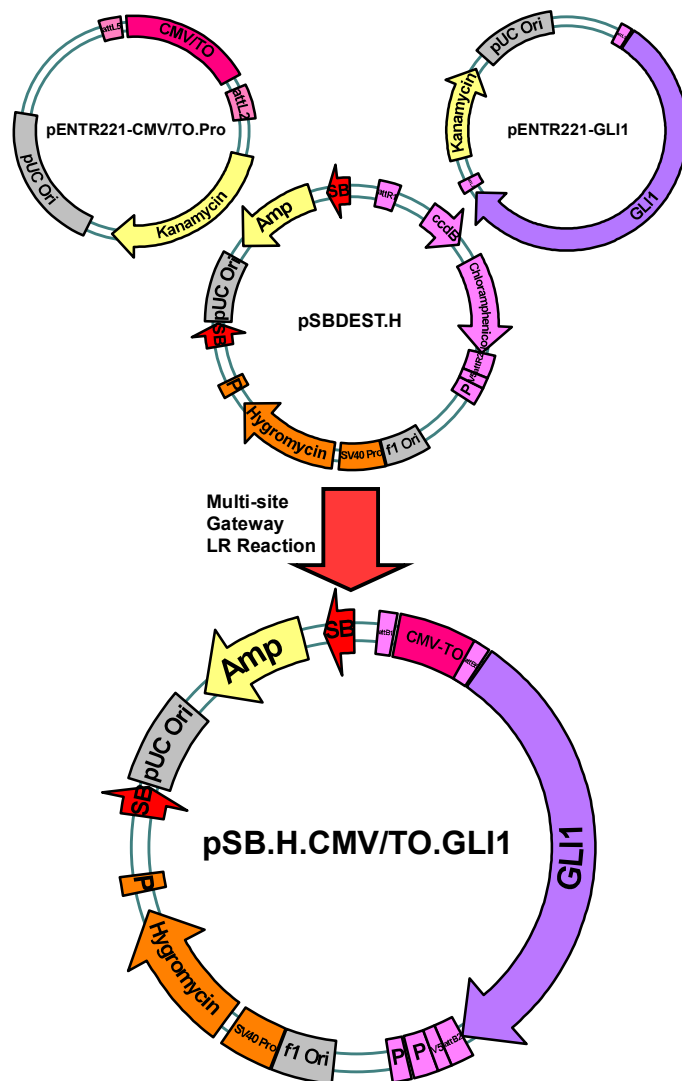


Figure 15 Example of the multi-site Gateway reactions performed in this study. Multi-site gateway cloning was used to generate an inducible GLI1 overexpression vector under the control of the CMV/TO promoter. The principle of the technique is explained in figure 15.

3.5 *In vitro* experiments

3.5.1 Stable transfection of cells by electroporation

To generate stable transfectants in cell lines, host cells were co-transfected with a Sleeping Beauty transposase compatible reporter, and/or expression vector, and an additional expression plasmid carrying the transposase enzyme gene in 2:1 ratio.

Electroporation was used as the main strategy to transfect cells. In practice, electroporation reactions were carried out using either an Amaxa Nucleofector IIB [Lonza, Basel (Switzerland)] or the NEON transfection system [Thermo Fisher, Waltham (USA)]. Both systems are highly optimized for small volumes and specific

cell lines. For both systems cells were grown to roughly 80% confluency, detached and counted and finally electroporated according to the table below.

Cell line	AMAXA Protocol	NEON protocol 10µl	NEON protocol 100µl
HEK293	Q-030	1x10 ⁶ , 950V, 30ms	1x10 ⁶ , 1050V, 30ms

After electroporation, the cells were seeded into fresh cell culture flasks and after 24 hours medium was replaced and selection was started.

3.5.2 Antibiotic selection for transformants

To select for transformants, electroporated cells were subjected to antibiotics for 7 to 10 days, according to manufacturer's instructions. To determine the lethal dosage of each antibiotic per cell line, an individual experiment using a dilution row was carried out in advance of the generation of stable transfectants. In these experiments, cells were subjected to increasing amounts of antibiotics, which were replenished every 2-3 days, while monitoring cell health and proliferation microscopically. To prevent experimental artifacts later on, concentrations were biased to the higher concentration in cases of doubt. The final concentrations per antibiotic used can be found in the table below.

Cell Line	Blasticidin concentration	Hygromycin concentration	Zeocin concentration	G418 concentration
Hek293	8 µg/ml	150 µg/ml	150 µg/ml	600 µ/ml

3.5.3 Stimulation and validation of reporter cell lines

To assess the effects of specific treatments on stable reporter cell lines, cells were detached, counted and seeded out in 96-well format (10,000 - 20,000 cells / well). Depending on the stimulation needed, this was performed in in 50µl or 100µl medium, so that either a highly concentrated stimulation could be added in a 1µl scale or up to 50µl of a less concentrated compound could be added. Two hours after seeding out the cells to the 96-wells, stimulations were added. After 24, 48 or 72 hours (depending on the experiment) the effects on the cell line were assayed.

3.5.4 Overexpression methods

Overexpression studies were carried out similar to other stimulation experiments. Here however, the cells were stably transfected with the Tet-Repressor carrying reporter vectors and an inducible expression vector utilizing the CMV/TO promoter. When the Tet-Repressor protein is present in the cells, it forms dimers that block transcriptional activity of the CMV promoter. Upon tetracycline or doxycycline stimulation, these dimers are disrupted by a conformational change and the Tet-Repressor monomers no longer block the CMV promoter.

Since Doxycycline has 48 hours of cell culture half-life, compared to the 24 hours of Tetracycline, all experiments presented here used doxycycline-based activation. Two hours after seeding the inducible cell line into 96-wells, at least three replicates were activated with 1µg/ml Doxycycline, with the controls being left untreated.

3.5.5 Co-culture assays

Co-culture assays were carried out similar to stimulation experiments. 10,000 – 20,000 reporter cells were seeded out in 50µl per 96-well plate well in the same medium as the co-cultivated cells. After 2 hours for the reporter cells to attach to the wells, varying amounts of cells were added to the wells in 50µl volume. 48 hours later reporter activity was assayed.

3.5.6 Luciferase Assays

Since all reporter constructs described here use *Gaussia* luciferase as a reporter protein, its presence was assayed by addition of its substrate, coelenterazine, and subsequent measurement of the amount of light generated in the reaction to coelenteramide. coelenterazine and the appropriate reaction buffer was purchased in form of the BioLux *Gaussia* Luciferase Assay Kit [New England Biolabs, Ipswich (USA)] and measurements were done using 20µl of cell culture supernatant with 50µl of the prepared substrate / buffer solution after 45 seconds incubation using a Berthold Lumat LB 9507 Luminometer with 10s measurements.

3.5.7 Harvesting and concentration of serum-free supernatants

To assess whether soluble components of culture supernatants were capable of driving specific pathway activation, serum-free supernatants were generated and concentrated. To harvest serum-free supernatants, cells were seeded out in high densities in 24 well plates in medium containing no antibiotics or serum. 72 hours later

supernatants were harvested and centrifuged at 200 x g for 10 minutes to pellet remaining cells, the supernatants were then taken off again and the centrifugation step repeated, again taking the supernatant off. The cell-free and serum-free supernatant was then concentrated using an Amicon Ultra-15 10kDa Spinfilter [Merck, Darmstadt (Germany)] at 2000 x g. Supernatants were concentrated up to 10 fold and used in reporter assays as described above. All centrifugations were carried out in a Rotanta 460R centrifuge [Hettich, Kirchleugern (Germany)]. In cases where supernatants were to be freed from non-soluble components, they were centrifuged at 100,000 RCF in a L70 Ultracentrifuge [Beckman, Brea (USA)].

3.5.8 Exosome Preparation

Exosomes were prepared from harvested serum-free supernatants after 72 hours for conditioning either using an in-house ultracentrifugation method or using the commercially available Exo-Spin Purification Kit [Cell Guidance Systems, St Louis (USA)] as per manufacturer's instructions. For the ultracentrifugation method, the following centrifugation profile was used: 10 minutes 300 RCF, 20 minutes 2000 RCF [both Rotanta 460R, Hettich, Kirchleugern (Germany)], 30 minutes 10,000 RCF, 70 minutes 100,000 RCF [both L70 Ultracentrifuge, Beckman, Brea, (USA)] and then resuspended in sterile PBS.

3.5.9 Determination of protein content

Protein content for exosome preparations was determined colorimetrically using the Pierce BCA Protein Assay Kit [Thermo Fisher, Waltham (USA)], a two-component assay reagent set to measure total protein concentration compared to a protein standard. Measurements were done using a Genios Plus plate reader [Tecan, Männedorf, (Switzerland)].

3.6 Quantitative real-time PCR

3.6.1 RNA Purification

RNA was isolated from various cell lines using the PureLink RNA Mini Kit [Thermo Fisher, Waltham (USA)] according to manufacturer's instructions. The optional DNase I [Qiagen, Hilden (Germany)] digestion step was included to remove residual genomic DNA from the samples. RNA was eluted in 30 µl using RNase free water.

3.6.3 Quantification of RNA

Purified RNA was quantified using the Quant-IT RNA assay for the Qubit Fluorometer [Thermo Fisher, Waltham (USA)]. Measurements are based on and made specific for RNA by the chemistry of the Quant-it dyes that upon binding RNA increase their fluorescence several hundred-fold. All measurements were carried out based on the manufacturer's instructions.

3.6.4 Reverse Transcription

Due to the fragile nature of RNA, all samples were transcribed into cDNA through reverse transcription. The resulting cDNA was quantified in a following qPCR reaction step. As primers designed for qPCR are usually cDNA specific, they will only amplify cDNA and not genomic DNA. In cases where of genes with only one exon or the 18S-rRNA, it is impossible to design cDNA specific primers. To control for these problems, and to exclude a PCR signal from genomic DNA contamination in the sample, the so-called RT- sample was added to the reverse transcription step. Here, 0.2 µg of total RNA, possibly containing genomic DNA contamination, was added to a set of reactions. These reactions equaled the RT+ batch with the exception of the reverse transcriptase enzyme. Since no reverse transcription could take place in these samples and RNA cannot be measured in qPCR, each signal that was produced by the RT had to originate from the combination of a cDNA unspecific primer and genomic DNA contamination. For the reverse transcription, 2 µg of total RNA, as measured in 3.6.3, was added to the RT+ reaction mix and in a final volume of 40µl.

Reagent	RT+	RT-
First-strand buffer (5x)	1x	1x
dNTP	1.5 mM	1.5 mM
DTT	13.4 mM	13.4 mM
Rnasin	2.5 U/µl	2.5 U/µl
Acrylamid, linear	0.7 µM	0.7 µM
Hexanucleotides (10x)	0.2x	0.2x
Superscript II	4.4 U/µl	-

Both reaction batches were incubated at 42°C, slowly shaken in a thermo block for 1.5 hours. For subsequent qPCR reactions, the RT+ samples were to be diluted 1:10, whereas the RT- batch remained undiluted, leading to equal amounts of RNA in the RT+ and RT- reactions. All samples were stored at -20°C, until further use.

3.6.5 Quantitative PCR (qPCR)

qPCR is a method used to determine the relative amount of mRNA for a specific gene at a certain time point. The method is generally used while comparing different tissues, during drug treatments and to verify the presence of transgenes in engineered cell types. The method uses cycles of PCR amplification of specific products while detecting fluorescent signals. While there are multiple variants of qPCR, here only the SYBR green method was used. In this method a DNA intercalating dye, which is only detectable in its DNA bound state, serves as the readout which is measured in real time by the qPCR cycler device. Earlier detection of the signal means more relative abundance of the original mRNA in comparison to other samples. To control that the signal does not originate from unspecific products or DNA contamination, an additional step has to be included. After the amplification cycles, a melting curve of the products is generated which uses the loss of fluorescent signal as a readout. This way, the loss of signal from small DNA molecules can be separated from the loss of signal of bigger molecules allowing to assess specificity (single peak).

Reagent	Amount
SYBRGreen mastermix (10x)	1X
SYBRGreen Primer FW	10pM
SYBRGreen Primer RV	10pM
Taq polymerase	0.03U/ μ l

H₂O was added to the mastermix to reach a final volume of 18 μ l. For qPCR 2 μ l of the RT+ (1:10) dilution or 2 μ l of the RT- samples were added to the master mix, to reach a final volume of 20 μ l per well. Experiments were set up in duplicates. qPCR was performed on an ABIPrism7000 Sequence Detection system [Thermo Fisher, Waltham (USA)]. After an initial hold of 2 minutes at 50°C and 10 minutes at 95°C, the samples were cycled 40 times at 95°C for 15 seconds, and 60°C for 60 seconds. All primers are summarized in the supplementary table 1. The expression of candidate genes was normalized to the reference gene 18S rRNA [172].

3.6.6 Calculation of regulation

The presence of a fluorescent signal in a qPCR reaction is determined with a threshold, dubbed Cycle Threshold (CT). This threshold is reached at a certain cycle in the qPCR reaction. If a sample has a low CT value it has come up in an early PCR cycle indicating relatively high abundance of the template, whereas if it is detected late (in a higher cycle number) and has a high CT value the template was less abundant. Since the method yields relative values instead of absolutes, it is dependent on the use of reference genes (also called house-keepers). These reference genes allow for comparisons across different samples. To optimize the CT value, the baselines for each individual gene were adjusted based on the fluorescence curves, positioning them in the linear portion of the curve. The so calculated CT values were then used to calculate fold changes using the Pfaffl method [173].

3.7 Microscopy of Kidney sections

3.7.1 Sample preparation

Kidney samples were dehydrated with 70% ethanol for 5 hours, then 96% ethanol for 2 hours, 100% ethanol for 3.5 hours, xylene for 2.5 hours and paraffin for 4 hours. Paraffination was done using liquid paraffin. To mount the samples on glass slides, 2 μ m sections were cut using a microtome. Deparaffination was done 3 times in Xylene for 5 minutes. For rehydration, samples were incubated 3 times in 100% Ethanol for 3 minutes, then 2 times in 95% ethanol for 3 minutes and finally for 3 minutes in 70% ethanol. Then samples were washed twice for 5 minutes in PBS.

3.7.2 Immunohistochemistry

To prepare samples for immunohistochemistry, samples were first cleared from internal peroxidase, to do so, the samples were incubated in 3% H₂O₂ in Methanol for 20 min in the dark, then washed twice in PBS for 5 minutes. For both YAP1 and TAZ(WWTR1) antibodies antigen retrieval was done using an autoclave for 20 minutes in pH6 citric acid buffer. Blockage of endogenous biotin was done using a commercially Avidin/Biotin blocking kit. YAP1 antibody was diluted 1:100 in 10% skimmed milk powder in PBS. TAZ(WWTR1) antibody was diluted 1:50 in PBS. Detection was done for 1 hour at room temperature. To detect the primary antibodies, biotinylated secondary antibodies (5 μ g/ml in PBS) were used for 30 minutes. After incubation a commercially available kit (Vectastain) was used to detect bound

antibodies according to manufacturer's instructions. For counter-staining methyl green was used and again quickly washed with 96% ethanol, then 100% ethanol and followed by xylol. To mount the slides, Vectamount [Vectorlabs, Burlingame (USA)] mounting medium was used.

3.8 Generation of 2⁺MoPh and imDC cells

3.8.1 Isolation of mononuclear cells from peripheral blood

Mononuclear cells were isolated from venous blood from healthy donors (peripheral blood mononuclear cells, PBMCs). To prevent coagulation of blood, 50ml Syringes with added 1000 U Heparin were used. Blood samples were then mixed with the same volume of RPMI medium and layered on top of 15ml Ficoll in a 50 ml tube. Density gradient centrifugation (2000 rcf, 20 minutes, no brakes) served to separate the blood components. Erythrocytes and granulocytes sink into the Ficoll layer while thrombocytes float to the top. The middle phase contains the PBMCs, which was carefully taken off and put into a fresh 50ml tube, 1:1 mixed with RPMI medium and centrifuged for 12 minutes to remove remaining Ficoll. Supernatant was discarded and the cell pellet filtered through a cell sieve and counted.

3.8.2 Positive isolation of monocytes from PBMC

Isolation of monocytes from PBMC was done using the MACS technology (magnetic cell sorting) at 4°C. Monocytes were selected with CD14 microbeads according to manufacturer's protocol with the cell pellet being resuspended in 10µl volume per 10⁷ cells. CD14 positive monocytes were then differentiated to either imDC or 2⁺MoPh subtypes.

3.8.3 *In-vitro*-differentiation of myeloid cell types from monocytes

All myeloid cells were cultivated in 6 well plates. To generate 2⁺MoPh from monocytes, 7 x 10⁶ cells were transferred to 3ml AIM-V-Medium (3% human serum) or 1ml of RCC26 conditioned supernatant in 3ml VLE-medium (6% human serum). For the generation of imDC cells, monocytes were cultivated in 4ml AIM-V-medium (1% human serum) supplemented with 80 ng/ml GM-CSF and 80 ng/ml recombinant human IL-4 protein. These media were replaced after two days and cells harvested on day 7.

3.9 Fluorescence activated cell scanning (FACS) Analysis

Fluorescence activated cell scanning (FACS) analysis was used to detect surface or cytoplasmic factors via antibodies coupled to a fluorochrome. It was used to characterize the *in-vitro* generated 2⁺MoPh and imDCs, and the myeloid cell lines Mono-Mac-6 and THP1 (see addendum). For surface staining, 5×10^4 to 2×10^5 cells were suspended and washed with 500 μ l ice cold FACS buffer in a 1.5 ml FACS tube. After centrifugation, the supernatant was discarded except for 50 μ l, and the concentrated cells were stained with antibodies. Samples were mixed by vortexing and incubated for 25 min at 4°C in the dark. Then the samples were washed with 500 μ l FACS buffer and after centrifugation the supernatant discarded so that 100 μ l were left. To control for dead cells, 10 μ g/ml propidium iodide was added shortly before data acquisition. To be able to correct for unspecific events and define thresholds, a compensation matrix was generated by including single stained compensation beads. 70 μ l FACS buffer were added to 15 μ l positive or negative control beads [Miltenyi Biotec, Bergisch-Gladbach (Germany)] and stained with 1 μ l of each antibody, then incubated for 25 min at 4°C in the dark. Similar to the cell samples, the compensation beads were washed in 500 μ l FACS buffer and after centrifugation, the supernatant discarded with 100 μ l being left in the tube. Using these compensation beads, the software can determine the thresholds for both positive and negative signals, which is important when fluorochromes have overlapping spectra. All measurements were done using a LSR II-Flow cytometer and analyzed with the FlowJo Software suite. Antibodies are listed in table 2.9.

3.10 Mass spectrometry

3.10.1 Sample preparation for mass spectrometry

Supernatants were proteolysed with trypsin [Promega, Mannheim (Germany)] using a modified filter aided sample preparation protocol [174].

3.10.2 LC-MS/MS analysis

Mass spectrometry (MS) data were acquired using a data-dependent top-10 method on a Q Exactive (QE) high field (HF) mass spectrometer [Thermo Fisher, Waltham (USA)] in cooperation with Dr. C. von Törne, Proteomics Core Facility, Helmholtz Zentrum München. Samples were automatically loaded to the online coupled RSLC [Ultimate 3000, Thermo Fisher, Waltham (USA)] HPLC system. A nano trap column

was used [LC Packings, Sunnyvale, CA (USA)] before separation by reversed phase chromatography [PepMap, 50 cm, 75 μm ID, 2 μm /100 \AA pore size; LC Packings, Sunnyvale, (USA)] at 50°C. Peptides were eluted from column at 300 nl/min using increasing acetonitrile (ACN) concentration (in 0.1% formic acid) from 3% to 40 % over a 90 minute gradient. MS spectra were recorded within a mass range from 300 to 1500 Da at a resolution of 60,000. Fragmentation was performed via higher energy collisional dissociation (HCD) with a target value of 3e6 ions determined with predictive automatic gain control (AGC). Precursor peptides were isolated with a 1.6 m/z window. Resolution for HCD spectra was set to 15,000 at m/z 200 with an AGC target of 1e5 and maximum ion injection time of 100 ms. The normalized collision energy was 28. The underfill ratio was defined as 1%. Dynamic exclusion was set to 30 seconds.

3.10.3 Protein identification and label-free quantification

The acquired spectra of the different samples were loaded and analyzed using Progenesis Q1 software for proteomics [Version 2.0, Nonlinear Dynamics, Waters, Newcastle upon Tyne (UK)] for precursor-based label-free quantification as previously described [175]. The proteome of native adult Muller glial cells from murine retina. Mol Cell Proteomics) with the following adjustments: Samples were allocated to their respective experimental groups imDC 46hours and 2*MoPh 46 hours. Peptide identification with Mascot (MatrixScience, London (UK) version 2.5.1) using the Ensembl Human protein database (release 80, containing 100208 sequences). Search parameters used were 10 ppm peptide mass tolerance, 20 mmu fragment mass tolerance.

4 Results

4.1 Bioinformatic characterization of DN samples and calculation of 2⁺MoPh presence

It is now well established that regulatory pathways, strongly associated with renal development, can often become reactivated as a response to tissue damage. This reactivation is thought to underlie aspects of wound repair [176, 177]. The dysregulation, or over-activation of these pathways, has been linked to biologic processes underlying the pathophysiology of chronic renal disease [36, 37, 39, 40]. Myeloid cells have been implicated as key effector leukocytes in the repair of damaged tissue, and in many instances, are thought to help drive chronic fibrosing tissue damage [137, 138, 143-147, 150]. The goal of this thesis was to determine if a myeloid subtype previously identified in normal renal tissue, and found to be increased in many examples of renal disease, could potentially contribute to the damage seen in progressive diabetic nephropathy [139, 151]. To this end, we sought to determine if the presence of these myeloid cells could be directly linked to the activation of regulatory pathways associated with the progression of tissue damage seen in diabetic nephropathy.

4.1.1 Dysregulation of developmental/regulatory pathways in the context of diabetic nephropathy

As a first step, transcriptomic data from a cohort of patient human renal tissue was analyzed for the activation of pathways commonly associated with development and repair. Microdissected kidney samples representing the tubulointerstitial compartments of patients diagnosed with diabetic nephropathy, and taken during routine biopsies, were made available through the European Renal cDNA Bank (ERCB) [154]. The transcriptomic data was subsequently analyzed for the presence of dysregulated homeostatic pathways.

The transcriptomic profiles of all samples had been previously measured using Affymetrix microarray technology. To identify and verify general alterations of homeostatic pathways, the kidney samples from progressed diabetic nephropathy (DN) patients were compared to samples taken from living donor (LD) transplant kidneys prior to implantation, the cleanest dataset available as an approximation of “normal” human control kidneys. Analysis of this transcriptomic dataset was done in

collaboration with Prof. Dr. M. Kretzler and V. Nair [University of Michigan, Ann Arbor (USA)] using procedures described in the methods section (3.1). For all bioinformatic analyses, 17 DN samples were used in total with a calculated eGFR MDRD [178] mean of 44, median of 46 and standard deviation of 25, and compared to a set of 30 LD controls. Transcriptomic profiles were generated from microdissected tubulointerstitial regions of the renal biopsy samples, using Affymetrix cDNA microarrays. Briefly, after quality control of the samples, normalization and batch correction procedures were carried out. Upon comparison of the DN samples to the LD controls, 2739 genes were found to be significantly altered. Within this set of genes, many exhibited comparably small differences. To address this, a second filtering step using a fold change of at least a 1.3 fold threshold was applied. The results showed a set of 874 regulated genes that were then analyzed for alterations of homeostatic pathways. To allow for an unbiased approach, the Genomatix software suite, which contains a number of bioinformatics tools was used to analyze expression data. The GeneRanker program, which determines association of an input gene list with either pathway (canonical or based on literature mining), Gene Ontology (GO) terms or additional gene-sets based on diseases, transcription factors (TFs) or tissue profiles was applied. For this analysis, the pathway based literature mining approach was used, as this approach retains canonical/core pathway genes, but also extends the list based on published literature.

Pathway	Genomatix Pathway id	<i>p</i> -value	Obs.	Exp.
TGFβ/SMAD Signaling	PW_SMAD_HOMO_SAPIENS	1,87E-04	49	28,95
MAPK (JAK) Signaling	PW_JAK_HOMO_SAPIENS	1,99E-04	30	14,96
MAPK (STAT) Signaling	PW_STAT_HOMO_SAPIENS	1,66E-03	41	25,48
Canonical WNT Signaling	PW_βCATENIN_HOMO_SAPIENS	5,75E-03	56	39,86
Integrin Signaling	PW_INTEGRIN_HOMO_SAPIENS	4,11E-10	46	16,99
Myeloid Differentiation	PW_MYD88_HOMO_SAPIENS	6,46E-05	24	10,13

Table 1. Dysregulated homeostatic pathways in DN. Abbreviated list of gene sets identified as overrepresented by GeneRanker. In addition to the pathways listed here, a large set of inflammatory gene sets was identified, for full list see addendum 6.1.1. Obs. = number of observed genes, Exp. = number of expected genes.

This was an important step as it would potentially allow for the identification of non-canonical signaling processes, which were suspected to play a role in DN. GeneRanker determines significance by calculating an expected amount of genes from the size of the input gene list and the number of genes in a given pathway while considering the number of genes in the genome as frame of reference. If a pathway is overrepresented, a p -value can be calculated to judge reliability.

The GeneRanker analysis showed significant dysregulation of at least four major homeostatic signaling pathways: TGF β /SMAD signaling, MAPK signaling, canonical WNT signaling and Integrin signaling (see table 1). Similar findings had previously been published for other datasets generated from microdissected kidney tissue [35, 36, 156]. Integrins are a diverse group of transmembrane receptors which modulate cell-cell adhesion [179]. This signaling is strongly associated with the homeostatic status of cells, as well as the signaling seen during contact. A large number of immune-associated gene sets were also found to be significantly altered (see addendum 6.1). Interestingly, myeloid differentiation was identified as being one of the altered gene sets.

4.1.2 Detection of 2⁺MoPh in complex tissues by deconvolution analysis

Our previous studies [139, 143, 146, 147, 150, 151], as well as the transcriptomic changes in myeloid differentiation seen during the progression of DN, prompted further study of the kidney resident myeloid cell composition. The recently identified 2⁺MoPh myeloid cell type, characterized by the expression of the surface markers CD209/DC-SIGN and CD14, exhibits expression of classical DC, and in parallel, macrophage-associated genes [151]. Originally, this phenotype was identified as being enriched in clear cell renal cell carcinoma (and was thus called 'ercDC', enriched in renal cell carcinoma DC). The cell type is also found in the interstitium of healthy kidneys and becomes increased in number in many progressive kidney pathologies [139, 151]. To analyze whether 2⁺MoPh could be detected in DN, transcriptomic profiles of *in-vitro* generated 2⁺MoPhs, as well as a series of other myeloid subtypes were obtained through our collaborators Prof. Dr. Elfriede Nößner and Dr. D. Brech [Helmholtz Zentrum, München (Germany)].

This data was then used by collaborators in the BMC, Core Facility Bioinformatics [Dr. Tobias Straub, Munich, (Germany)] as the input data for the generation of a

bioinformatics-driven deconvolution strategy to predict the presence of 2⁺MoPh cells with a high degree of accuracy within the transcriptomic data derived from complex tissues (Brech et al. submitted). Deconvolution strategies employ sets of marker genes and their dynamics to calculate proportions of cell types in complex tissues [162]. The deconvolution strategy developed for 2⁺MoPh was able to specifically segregate these cells from other myeloid cell subtypes (blood isolated CD1c⁺DC, CD141⁺DC, slanDC, monocytes; as well as *in-vitro* generated M1 macrophages, M2 macrophages and imDC) in a series of proof of principle studies and was thus judged to be specific for the 2⁺MoPh phenotype (Brech et al. submitted).

Analysis of DN transcriptomic data using the deconvolution method identified an enhanced presence of 2⁺MoPh signatures in the tubular interstitium of DN patients in comparison to healthy living donor control kidneys.

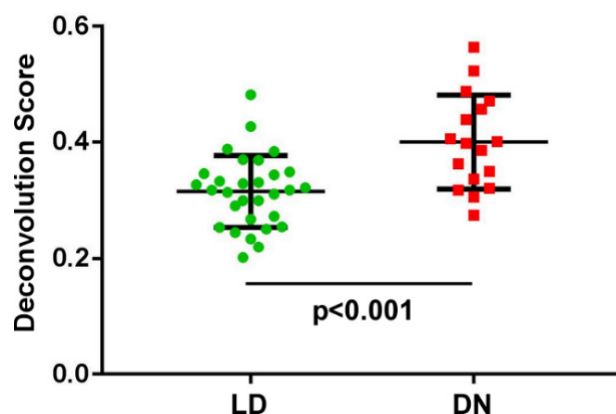


Figure 16. Deconvolution scores for 2⁺MoPh in microdissected tubular tissue. From ERCB living donor (LD) and diabetic nephropathy (DN) cDNA microarrays, a deconvolution score was calculated as an estimation of 2⁺MoPh presence. DN samples show a significant increase in score.

Additionally, the deconvolution signature was found to significantly correlate with a decrease in glomerular filtration rate in the diseased kidneys as determined by eGFR MDRD (estimated glomerular filtration rate, modification of diet in renal disease) – a measurement of renal function.

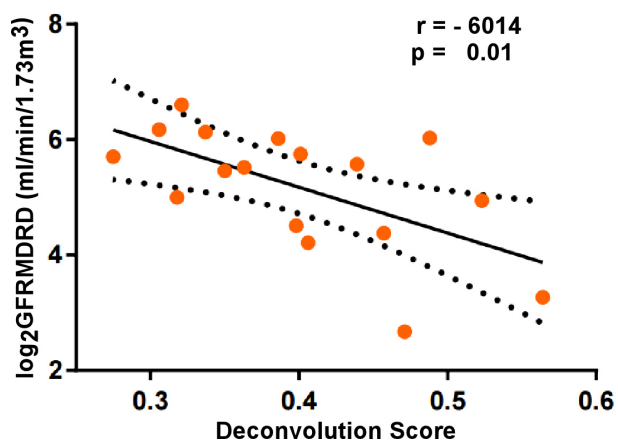


Figure 17. Association of glomerular filtration rate with 2⁺MoPh presence in DN. Yellow dots indicate deconvolution scores as a measurement of 2⁺MoPh presence in individual patient samples. There is a significant negative correlation with glomerular filtration rate. ($r =$ correlation coefficient)

Together, these findings supported our hypothesis that enhanced levels of 2⁺MoPh are a factor in the development or progression of CKD caused by diabetes. To test this hypothesis in more detail, we then sought to determine if 2⁺MoPh cells could directly influence changes in the homeostatic status of parenchyma, as evidenced by the transcriptomic profiling in 4.1.1

4.2 Cloning and Establishment of the Vector Platform

To study the potential effect of 2⁺MoPh on resident kidney cells, an *in-vitro* cell co-culture system was developed, which also required the design of a novel reporter and expression vector system [168]. An important feature of the vectors designed, was the ability to monitor the activation status of specific regulatory pathways. This was achieved by generating a series of reporter cassettes for transcription factors associated with the activation of select pathways. Additionally, the intricacies and interactions of the modulated pathways could be studied through the overexpression of key pathway genes. To this end, a mechanism for inducible expression was employed. To work efficiently with stably transfected reporter cell lines, both a mechanism to efficiently generate genomic insertions, and a set of different selective markers were also needed. The use of stable vector integration with selection, and pathway reporters with controlled transgene expression allowed the direct comparison of activation states between stimulated and unstimulated, but genetically identical, cells, thus greatly reducing potential variation between experiments and samples as commonly seen in transient assays.

An additional component of this vector platform was the capacity for high throughput cloning to rapidly generate the complex transgenes required in the expression vectors. To do so, Gateway cloning, a highly efficient and well established recombination-based cloning strategy was chosen [180]. The Multi Site Gateway technology was adopted for use in the vector platform. This tool allows cloning of up to four inserts into an acceptor vector dubbed the “destination vector” in an orientation specific manner.

Potential additional issues addressed included potential promoter competition due to multiple inserted copies, general issues of transfection efficacy, and it was also unclear whether all the complex transgenes involved in the vector platform would function together as intended when inserted into host cell lines.

4.2.1 Cloning of pathway reporter vectors

The reporter vector pSBTET-Reporter [168] was based on the pGL3-Promoter, pN3-Bar-Gluc and pcDNA6.2/V5-PL-DEST vectors and was generated in a multistep cloning procedure as detailed in the methods section. In each cloning step, verification was carried out using sequencing, functional assays (luciferase activity), or both. The resultant pSBTET-Reporter represents a next generation reporter vector with a number of advantages over classical Firefly luciferase reporter vectors:

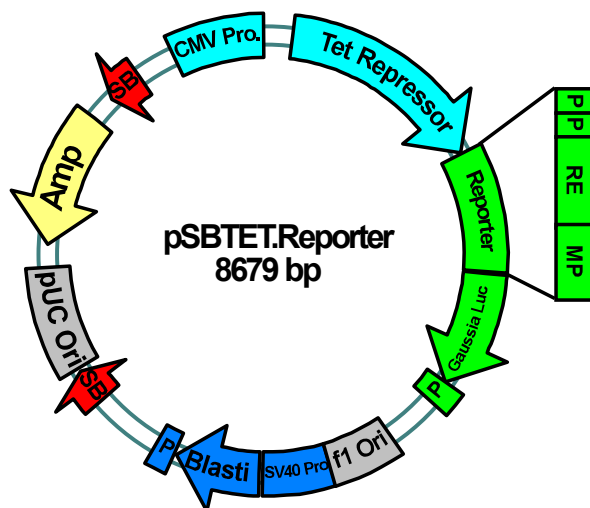


Figure 18. Final version of pSBTET-Reporter vector.

This resulting vector allows for active, stable integration into host cells via Sleeping Beauty transposition, dramatically raising insertion frequency. Additionally, it carries constitutive expression of the TET-repressor gene, which is needed for Doxycycline based de-repression systems. Finally, the Reporter cassette driving humanized *Gaussia* luciferase allows for monitoring the activity of transcription factors. Since *Gaussia* luciferase is secreted into the supernatant, resulting reporter cells can

be monitored in time courses without cell lysis. (also see 3.4)

- It included the TET-Repressor [164] protein which allows for repression and de-repression of compatible promoters, and thus a basis for inducible expression or knockdown systems where required.
- The vectors use secreted *Gaussia* luciferase [181] as reporter protein, allowing measurements of luciferase activity without cell lysis. A property that makes the vectors useful for time courses and rapid screening approaches.
- The inclusion of Sleeping Beauty transposase [165-167] compatible inverted terminal repeats/direct repeats allows efficient stable integration of transgenes into host cell genomes by an active mechanism, largely without size restrictions and the need for viral systems and S2 biosafety levels.

The basic pSBTET-Reporter was then used as a basis to generate pathway specific reporter vectors by introducing binding sites for pathway-associated transcription factors. As described in 3.4.4, reporter vectors for TGF β /SMAD signaling, canonical

WNT signaling, Hippo signaling, Hedgehog signaling and AP-1/MAPK signaling were generated. These pathways were chosen in part based on the initial pathway screen of the DN samples and also because of their known interactions and crosstalk, which was deemed of central importance to draw a more complete picture of whether alterations of one pathway co-occurred with alterations of other pathways. This approach also expands the bioinformatic screening possibilities, as the pathway mapping software currently used is dependent on previously archived classical pathway data. We sought to also include the potential of non-canonical modes of pathway activation, for example, those less well defined processes induced through growth factors and cytokines, that may be responsible for some of the modulation of the homeostatic milieu seen during progressive DN.

The Hedgehog signaling pathway, originally identified during embryonal patterning, has been shown to also play a role in tissue regeneration, tissue homeostasis, wound healing, and has been implicated in moderating aspects of progressive renal damage [31, 40, 52, 56]. TGF β /SMAD signaling is involved in tissue homeostasis, wound healing, fibrosis and immune responses [16, 67, 68, 96, 182]. The canonical β -catenin centric WNT pathway is a complicated regulatory network. It has been implicated in cancer, tissue homeostasis, wound healing, cell migration and in control over proliferation and differentiation. This pathway is also strongly associated with progressive renal fibrosis, including the damage seen during DN [28, 31, 36, 37, 96]. Finally, the HIPPO pathway and its central transcriptional co-activators YAP1 and TAZ are new subjects of interest. The described functions of this pathway range from regulation of organ size, to responses to external stimuli such as mechanical stress, wound healing and a major role in fibrotic renal diseases [43, 44, 96, 124]. As there is no single transcription factor targeted by the HIPPO pathway, the associated TEAD transcription factors were used as the basis for the reporter vector [99]. LXRs were also studied as a candidate pathway, since these nuclear receptors are intricately tied to the regulation of innate immune responses exemplified by their role in myeloid cell polarization [183, 184], and chronic renal disease [185, 186].

4.2.2 Cloning of Gateway Destination vectors

A similar approach as detailed in 3.4.4 was used to generate a set of highly flexible Gateway cloning [180] destination vectors [168]. The Multi-Site Gateway cloning platform (summarized in figures 14 and 15) allows the integration of up to four fragments in a direction and orientation specific manner, while also providing strong bacterial selection mechanisms to simplify the search for correct clones [187]. Multi-Site Gateway cloning allows the rapid design and generation of protein expression vectors by recombination of a promoter with a coding sequence for a gene of interest.

Again, Sleeping Beauty transposase compatible inverted terminal repeats/direct repeats were included to facilitate the integration of resultant vectors into host cell genomes. The resulting Multi-Site Gateway destination vectors were further adapted by generating a set of four vector variants with different eukaryotic selection markers.

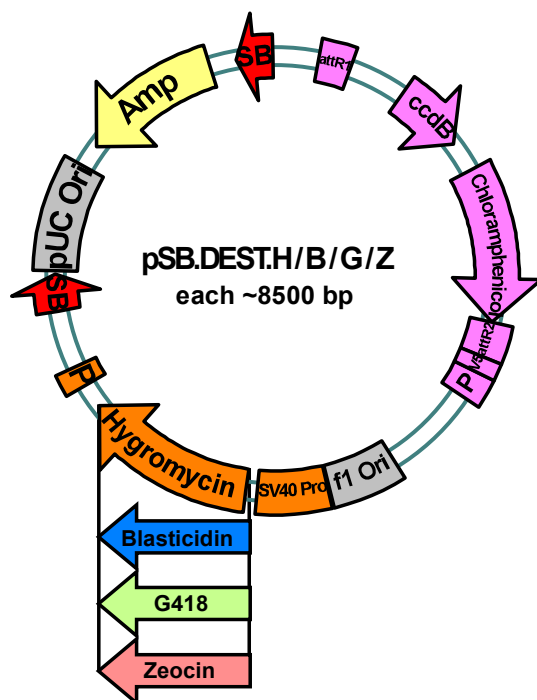


Figure 19. Final version of pSB.DEST vectors. The finalized plasmid serves as a multi-site Gateway cloning destination vector while still allowing for highly efficient integration into host cells via Sleeping Beauty transposition. The choice of selective markers allows for combinations of multiple stably inserted plasmids. Multi-site Gateway cloning allows for the integration of up to four entry clones between attR recombination sites.

The resulting vectors were verified by sequencing, and used in Multi-Site Gateway LR reactions, leading to the generation of all expression vectors used in this study. In cases where inducible expression vectors were necessary, the TET-Repressor blockable CMV/TO promoter was used as an entry clone, leading to the generation of Doxycycline inducible expression vectors.

4.2.3 Cloning of Entry Clones

Two types of Multi-Site Gateway Entry Clones were generated. attL1/attL5r Entry clones were used for promoter fragments while attL5/attL2r were used for coding DNA sequences of genes of interest. This allowed for the combination of any promoter entry clone with any CDS entry clone to generate expression vectors. Cloning for each entry clone was done via PCR and BP reactions with compatible pDONR221 vectors.

Type	Insert	Resulting vector
attL1/attL5r	CMV/TO Promoter	pENTR221-CMV/TO Pro
attL1/attL5r	CMV Promoter	pENTR221-CMV Pro
attL5/attL2r	Human YAP1 CDS, wildtype	pENTR221-YAP1 WT
attL5/attL2r	Human YAP1 CDS, S127A mutant	pENTR221-YAP1 CA
attL5/attL2r	Human WWTR1(TAZ) CDS, wildtype	pENTR221-TAZ WT
attL5/attL2r	Human WWTR1(TAZ) CDS, S89A mutant	pENTR221-TAZ CA
attL5/attL2r	Human GLI1 CDS	pENTR221-GLI1
attL5/attL2r	Human NR1H2 CDS	pENTR221-NR1H2
attL5/attL2r	Human NR1H3 CDS	pENTR221-NR1H3
attL5/attL2r	Human TCF7 CDS	pENTR221-TCF7
attL5/attL2r	Human MYDGF CDS	pENTR221-MYDGF
attL5/attL2r	Human WNT1 CDS	pENTR221-WNT1
attL5/attL2r	Human WNT3 CDS	pENTR221-WNT3
attL5/attL2r	Human WNT3A CDS	pENTR221-WNT3A
attL5/attL2r	Human SMAD3 CDS, wildtype	pENTR221-SMAD3
attL5/attL2r	Human SMAD3 CDS, active mutant	pENTR221-SMAD3 CA

Table 2. Entry clones generated for this study. Using PCR overhangs and pDONR221 vectors from the MultiSite Gateway cloning kit, a series of Entry clones was generated by PCR and BP reactions.

4.2.4 Cloning of Expression Vectors

Using the cloned Multi-Site Gateway entry clones and destination vectors, Expression vectors were generated via Multi-Site Gateway LR Reactions. The resultant vectors were verified by sequencing.

First Entry Clone	Second Entry clone	Resulting vector
pENTR221-CMV/TO Pro	pENTR221-YAP1 WT	pSB.H.CMV/TO.YAP1 WT
pENTR221-CMV/TO Pro	pENTR221-YAP1 CA	pSB.H.CMV/TO.YAP1 CA
pENTR221-CMV/TO Pro	pENTR221-TAZ WT	pSB.H.CMV/TO.TAZ WT
pENTR221-CMV/TO Pro	pENTR221-TAZ CA	pSB.H.CMV/TO.TAZ CA
pENTR221-CMV/TO Pro	pENTR221-GLI1	pSB.H.CMV/TO.GLI1
pENTR221-CMV/TO Pro	pENTR221-NR1H2	pSB.H.CMV/TO.NR1H2
pENTR221-CMV/TO Pro	pENTR221-NR1H3	pSB.H.CMV/TO.NR1H3
pENTR221-CMV/TO Pro	pENTR221-TCF7	pSB.H.CMV/TO.TCF7
pENTR221-CMV/TO Pro	pENTR221-MYDGF	pSB.H.CMV/TO.MYDGF
pENTR221-CMV Pro	pENTR221-WNT1	pSB.H.CMV.WNT1
pENTR221-CMV Pro	pENTR221-WNT3	pSB.H.CMV.WNT3
pENTR221-CMV Pro	pENTR221-WNT3A	pSB.H.CMV.WNT3A
pENTR221-CMV/TO Pro	pENTR221-SMAD3 WT	pSB.H.CMV/TO.SMAD3 WT
pENTR221-CMV/TO Pro	pENTR221-SMAD3 CA	pSB.H.CMV/TO.SMAD3 CA

Table 3. Expression vectors clones generated for this study. Expression vectors for genes of interest were generated by MultiSite Gateway LR reaction, using the pSB.Dest.H vector as a basis.

4.2.5 Transfection of cell lines using Nucleofection techniques and the SB100 Transposase

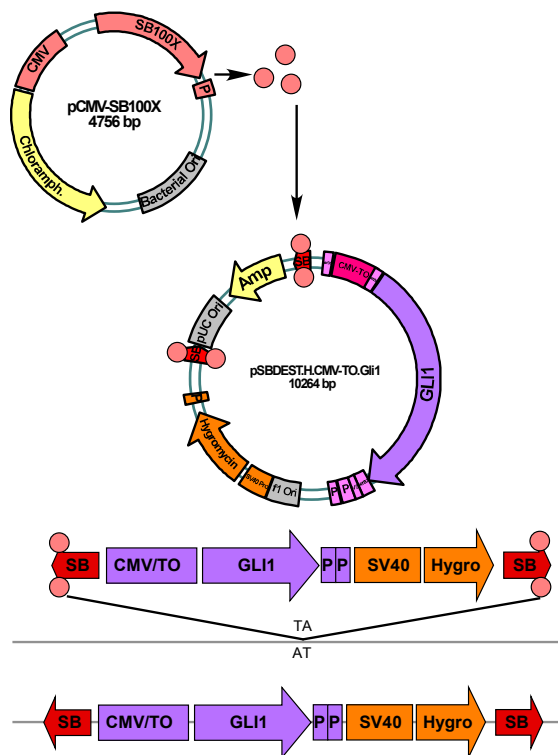


Figure 20. Sleeping beauty transposition mediated stable integration of transgenes into host cells.

The vector carrying the genetic cargo (here exemplified by the aforementioned CMV/TO GLI1 expression vector) is co-transfected with pCMV-SB100X. This leads to the production of SB100 transposase protein inside the host cell. SB100 transposase then binds to Sleeping Beauty inverted terminal and direct repeats (SB) and, by transposition, stable integration of the genetic cargo semi randomly into the host cell genome.

As HEK293 cells were originally isolated from embryonal kidneys, they were chosen as the experimental “parenchymal” cell line for these studies. Additionally, due to their fast growth and high transfectability, HEK293 cells are well established expression cells for the production of recombinant proteins.

To achieve high levels of transfection, next generation electroporation methods were employed. AMAXA [Lonza, Basel (Switzerland)] uses electroporation cuvettes. One downside of this system is that work with small volumes is difficult due to the cuvette shape. In addition, it is impossible to fine tune parameters and settings for delivery of the pulse. By contrast, the NEON [Thermo Fisher, Waltham (USA)] transfection system uses specific pipette tips, which double as electroporation chamber and can thus also work with volumes as low as 10µl, allowing for high cell numbers in low volumes and in parallel high plasmid concentrations. In addition, one has more flexibility in optimizing transfection parameters. The superiority of the NEON system was demonstrated in a panel of three cell lines. In each case the NEON electroporator showed brighter GFP reporter signals, with comparable cell death (data not shown).

Using NEON and SB technology, reporter and expression plasmids, and co-transfection with the pCMV(CAT)T7-SB100X transposase expression plasmid [166] allowed efficient transposase-mediated co-insertion of the TET-Repressor cassette, and the reporter cassette, (with different selective markers) into the host cell genome.

4.2.6 Proof of principle stimulation experiments for validation of the vector platform

To test the validity of the reporter genes within the vector platform, HEK293 cells were transfected with individual reporter constructs for a series of homeostatic pathways. For each pathway, a previously described control activator for the pathway reporter was used to validate the system. In each experiment, stably transfected cells were plated in a 96-well format and stimulated as described.

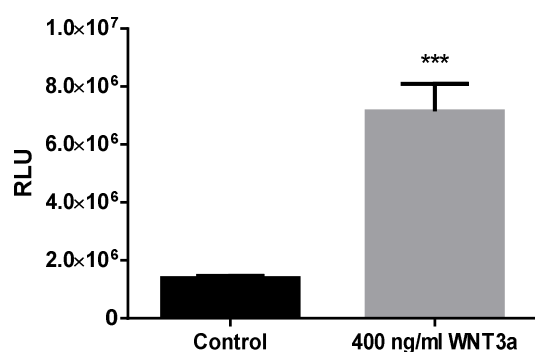


Figure 21. Stimulation of canonical WNT reporter HEK293 cells with recombinant human WNT3A protein.

To assess activity of the TCF/LEF reporter cassette, stable transfected HEK293 cells were treated with 400ng/ml WNT3A for 48 hours after which *Gaussia* luciferase reporter activity was assessed in the culture supernatant. Treatment with WNT3A strongly activates the TCF/LEF transcription factors and thus

the reporter element, leading to increased luciferase expression. (three wells per group, experiment representative of three individual experiments, *** = $p < 0.0005$)

For the Hedgehog pathway, recombinant human epithelial growth factor (EGF) protein, which activates the associated GLI1 transcription factor was used [188]. The commercially available and in house over-expressed versions of the canonical Hedgehog ligands are generally found to be very inefficient for activation of these and other reporter constructs at physiological concentrations (data not shown). This is thought to be due to incomplete posttranslational modification of the ligands and is consistent with data for commercially available vectors employing similar reporter elements (http://www.sabiosciences.com/reporter_assay_product/HTML/CCS-6030L.html). For the TGF β /SMAD reporter, recombinant human TGFB1 protein was used to activate the reporter construct [189]. To assess viability of the canonical WNT reporter construct, reporter cells were treated with the canonical WNT ligand WNT3A [190]. Examples for each of these experiments can be found in the supplemental data.

4.2.7 Proof of principle: induced overexpression of genes within the vector platform

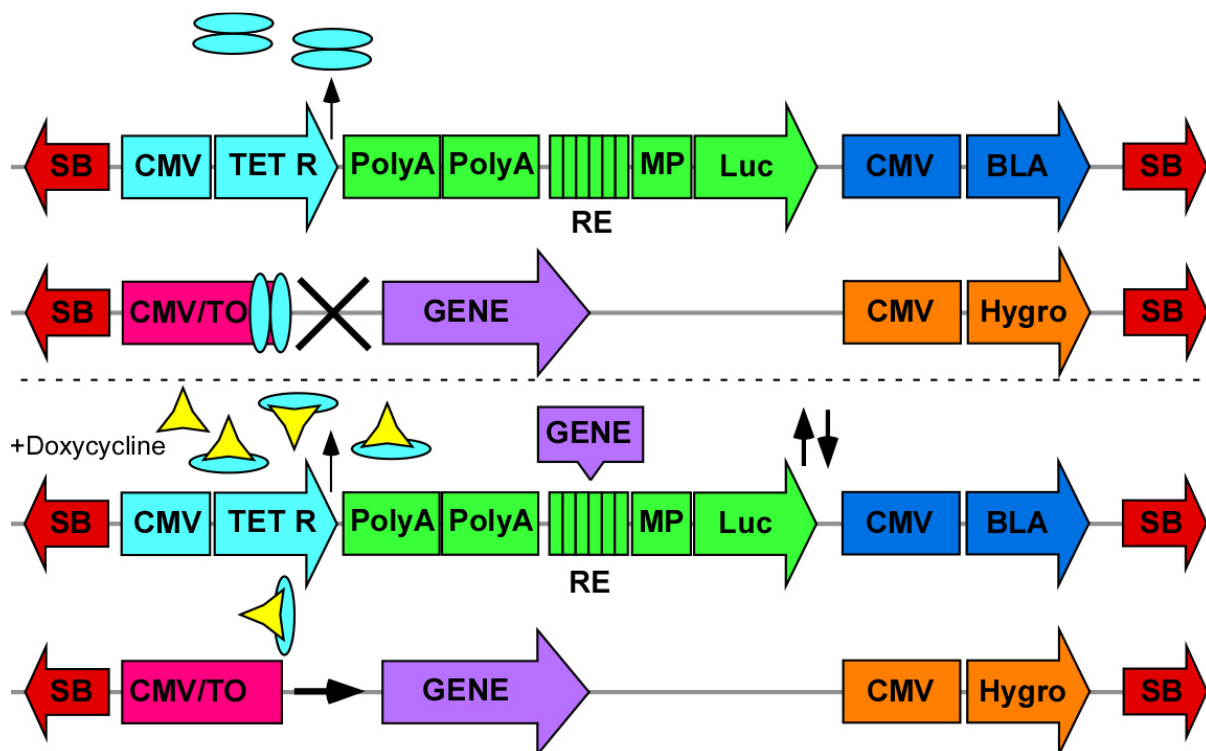


Figure 22. Explanation of inducible-expression and reporter vector system. The vector system generated here allows inducible overexpression/knockdown of genes with only 2 stably integrated vectors. One vector carries constitutive expression of the Tet-Repressor gene, a luciferase reporter cassette and Blasticidin selection. The other vector allows for Gateway engineered and Doxycycline inducible overexpression, with a number of selective markers exemplified by Hygromycin here. Both vectors can be stably integrated into cells with the SB100 transposase. In unstimulated cells, the Tet-Repressor molecules form dimers and bind to binding sites introduced into the CMV Promoter, blocking transcription. Upon Doxycycline stimulation, the Tet-Repressor molecules bind Doxycycline, which leads to a conformational change, monomerization and loss of DNA binding capacity. This then activates the transgene in the second plasmid (purple). The transgene will then have effects on the host cell, potentially modulating activation of the reporter cassette (green) of the first plasmid.

After validating the pathway-specific reporter constructs, as a next step the de-repression/gene activation system was verified *in-vitro*. HEK293 cells were transfected either in sequence (first the reporter then an overexpression construct) or together. As an example of this principle, inducible expression vectors for pathway associated transcription factors based on the de-repressible CMV/TO promoter [191] were generated. These constructs were blocked by TET-Repressor protein dimers expressed by the reporter vector. Upon stimulation with Doxycycline, a conformational change in the TET-Repressor protein was induced causing it to monomerize and

detach from DNA, allowing transcription from the now open CMV promoter. This approach could be used, for example, for the induced overexpression of a gene linked to the biology of the specific pathway reporter vector (see figure 22). This approach is exemplified here with transcription factors directly driving reporter activity.

As a proof of concept, an inducible GLI1 expression cassette was introduced in Hek293 cells engineered to monitor the activity of the Hedgehog pathway. GLI1 is a well-studied transcription factor associated with Hedgehog signaling [192]. For canonical WNT, TCF7 was used. TCF7 is a high mobility group (HMG) box transcription factor activated by β -catenin stabilization, a hallmark of the pathway [193]. For TGF β /SMAD signaling, SMAD3 was overexpressed [194]. Example experiments for each of these signaling platforms can be found in the addendum (see 6.2). These results showed that the two vectors stably introduced into the reporter cells could efficiently interact to provide the required signals.

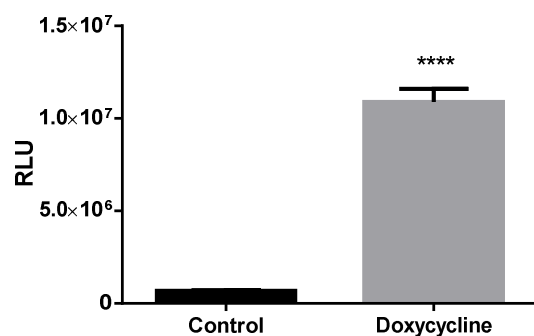


Figure 23. Hek293 Hedgehog reporter stimulation by overexpression, proof of principle.

Hek293 Hedgehog Reporter cells were transfected with a Doxycycline-inducible GLI1 overexpression construct. After 48 hours of Doxycycline treatment, luciferase expression and activity was strongly increased. (three wells per group, experiment representative of three individual experiments, **** = $p < 0.0001$)

As a further step for validation of *in-vitro* activity of the inducible overexpression vectors, a qPCR assay using GLI1 and GLI2 as readouts was employed. Hek293 cells carrying both the Hedgehog reporter with the included TET-Repressor expression cassette, as well as the inducible GLI1 expression construct were stimulated with either recombinant human EGF protein or Doxycycline to induce the expression of GLI1. qPCR for GLI1 was used as an additional readout of Hedgehog/GLI1 activation since activation of Hedgehog signaling will increase mRNA levels for GLI1 [195]. Treatment with EGF showed increased GLI activity for both GLI1 and GLI2, while Doxycycline induced overexpression of GLI1 led to highly increased levels of GLI1 but not GLI2.

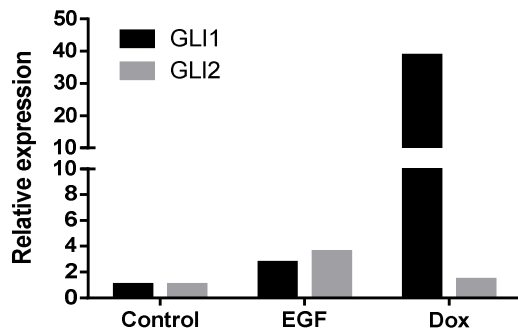


Figure 24. qPCR for GLI1 and GLI2 in an inducible GLI1 overexpression background. Hek293 Hedgehog Reporter cells were transfected with a Doxycycline-inducible GLI1 overexpression construct and relative mRNA levels for GLI1 and GLI2 assessed by quantitative real time PCR. Treatment with recombinant human EGF protein for 48 hours induced expression of both GLI1 and GLI2, while Doxycycline

based induction of GLI1 overexpression only increased levels of GLI1. (Data representative of two 48 wells per group.)

4.3 *In-vitro* model for myeloid infiltrate driven signaling alterations in the kidney

Using the tools described in 4.2, a series of experiments were designed to mimic and characterize potential alterations of homeostatic signaling pathways in kidney parenchymal cells conferred by contact with 2⁺MoPh and related imDC cells using reporter engineered HEK293 cells as model parenchymal cells.

4.3.1 Flow cytometric characterization of myeloid cells

To verify whether the lab cultivation and polarization to classical imDCs (IL-4/GM-CSF immature DCs) and the 2⁺MoPh phenotype was successful, the surface markers of the resulting cell populations were analyzed by flow cytometry (see figure 25). The markers included CD209/DC-SIGN, CD163, CD14, the defining markers for the 2⁺MoPh cell type [151] and markers to define to define DC or macrophage polarisation: CD40, HLA-DR and CD80 mainly expressed by DCs, CD64 expressed by M1 macrophages, MerTK expressed by M2 macrophages [196, 197]. The *in-vitro* derived 2⁺MoPh were positive for these markers. imDC were positive for CD209, but negative for CD163 and CD14. They expressed HLA-DR, the costimulatory molecules CD40, CD80 at about the same intensity as 2⁺MoPh. The M1 polarization marker CD64 was only marginally expressed while MER-TK was highly expressed.

All data involving myeloid differentiation or characterization was generated in collaboration with Prof. Dr. E. Nößner and Dr. D. Brech (Immunoanalytics- Core Facility & Research Group Tissue Control of Immunocytes, Helmholtz Zentrum München)

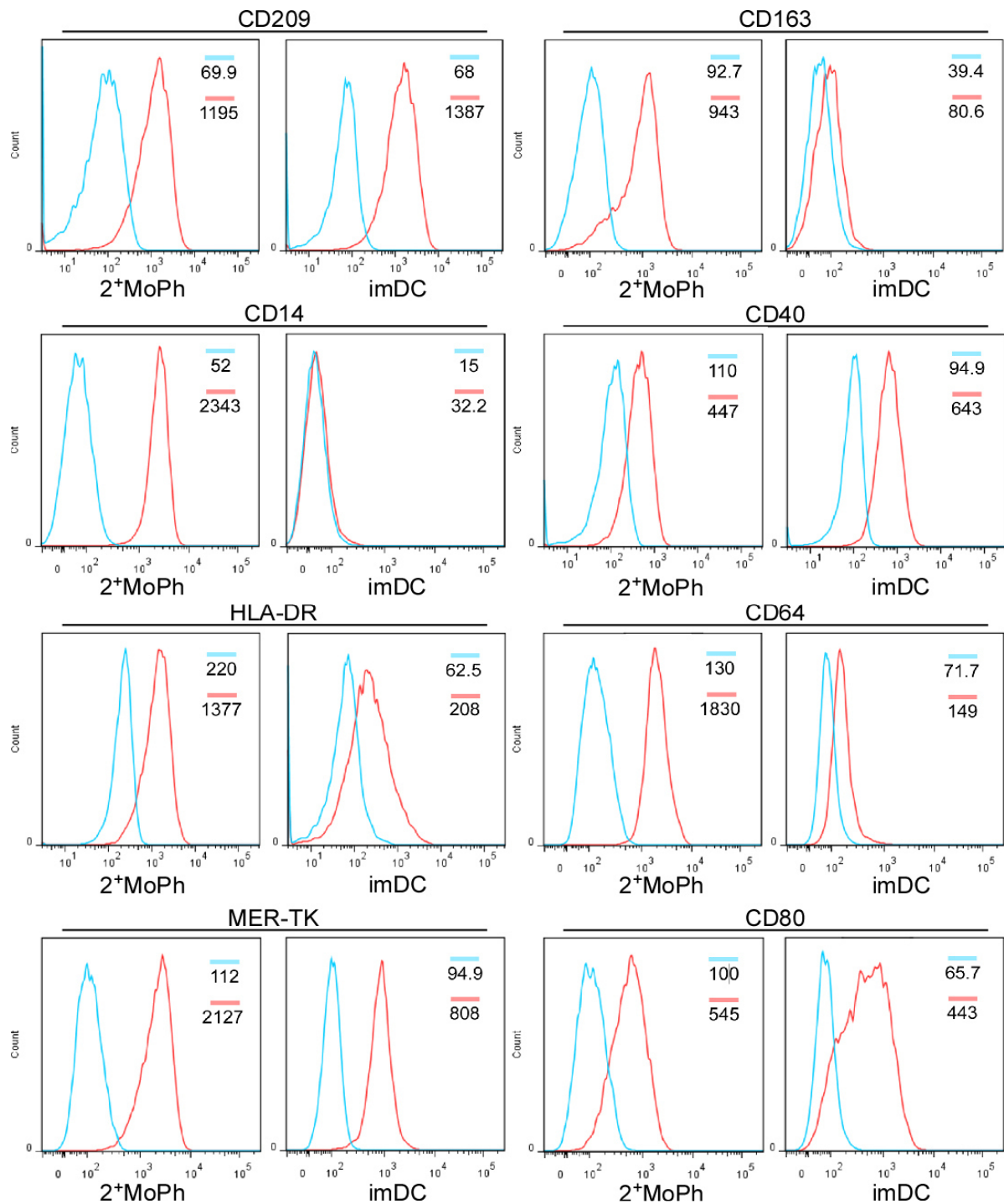


Figure 25. Flow cytometric characterization of 2⁺MoPh and imDC. *In-vitro* polarized 2⁺MoPh cells were characterized by flow cytometry. Red curves indicate the corresponding marker specific antibody, blue curves indicate the corresponding isotype controls. Cells were stained according to the protocol in 3.9. Numbers are median intensity of fluorescence.

4.3.2 2⁺MoPh and related myeloid cells can activate homeostatic pathways by co-incubation with reporter cells

To better understand the potential effect of different myeloid cells on the homeostatic milieu of experimental renal parenchymal cells, 2⁺MoPh and imDC cells were co-cultured with HEK293 cells engineered to express a series of reporters linked to homeostatic pathways associated with progressive renal damage, and additional candidate signaling networks.

In a pilot experiment to determine if the myeloid cells were toxic for the reporter cells, 2⁺MoPh and imDCs were co-cultured with HEK293 cells. To mimic varying degrees of immune-infiltration, the ratio between the model interstitial cells and the infiltrate was adjusted by adding different amounts of 2⁺MoPh/imDCs and no cytotoxic or growth impeding effects could be detected microscopically.

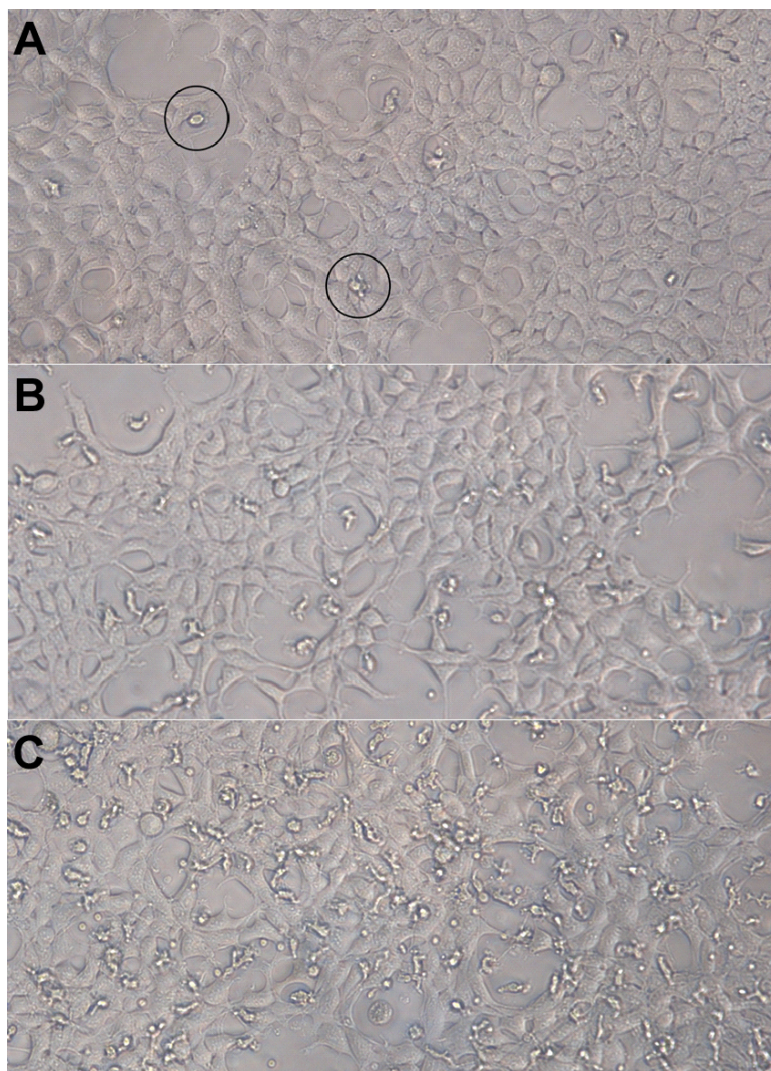


Figure 26. Varying amounts of myeloid cells co-cultured with 20,000 HEK293 reporter cells
20,000 HEK293 reporter cells were seeded in 96-well format and either
A) 100 myeloid cells
B) 10,000 myeloid cells
C) 40,000 myeloid cells added in co-culture for 48 hours. No cell death or growth impediment of HEK293 cells was observed.

Using a panel of reporters (see 4.2.1.), co-incubation experiments were performed using 20,000 HEK293 reporter cells plated into 96-wells, and after 48 hours 40,000 imDC or 2⁺MoPh were added to the wells. 48 hours later conditioned supernatant was sampled and reporter activity measured.

The results showed robust activation of the Hedgehog, MAPK and TGF β pathways, with less activation of WNT and LXR by 2⁺MoPh. imDCs had only minor effects on the various reporters. The HIPPO/TEAD pathway was slightly induced by 2⁺MoPh, but not by imDCs.

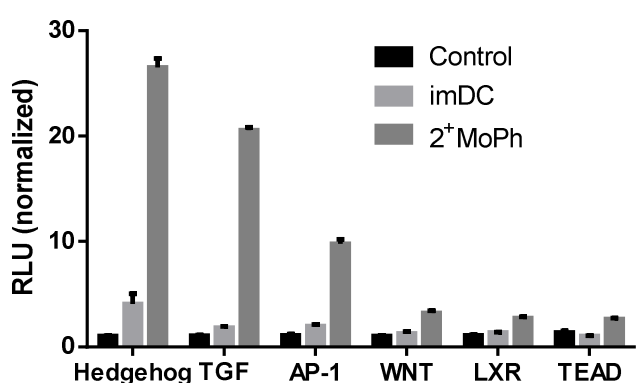


Figure 27. Hek Reporter cells co-cultured with primary, polarized myeloid cells. 20,000 Hek293 reporter cells were co-cultured for 48 hours with 40,000 imDC or 2⁺MoPh cells. Supernatants were sampled for luciferase activity. Co-culture with 2⁺MoPh lead to robust activation of the Hedgehog, TGF β and AP-1 reporters, less effect was observed on WNT and LXR, while HIPPO/TEAD signaling was largely

unaffected. Co-culture with imDCs yielded less signal than co-culture with 2⁺MoPh. (three wells per group, experiment representative of three individual experiments, changes are all highly significant between imDC and 2⁺MoPh treatment, all $p < 0.005$).

These results suggest that the 2⁺MoPh cells may have direct effects on the homeostatic pathways of parenchymal cells. As a next experiment, the dose dependent nature of the response was assessed using Hedgehog reporter cells and titrating the amount of 2⁺MoPh cells applied to the 96-wells.

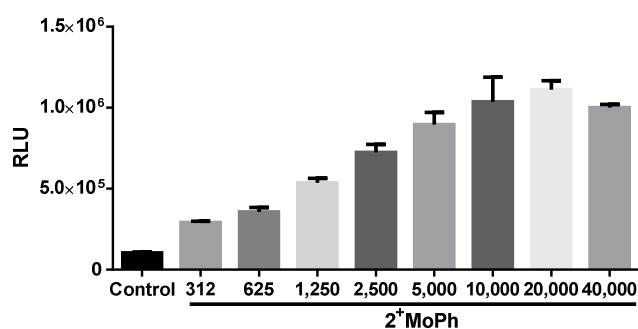


Figure 28. Hedgehog Reporter titration with 2⁺MoPh cells. 20,000 HEK293 Hedgehog reporter cells were co-cultured with serial dilutions of 2⁺MoPh cells. (three wells per group, experiment representative of two individual experiments).

A robust dose-dependent response was found. The experiment was then expanded to the other homeostatic pathways. A dose dependency could be shown for each reporter. Here, HIPPO/TEAD was not included due to its dependency on contact inhibition (also see addendum 6.5). Each pathway showed a dose dependency similar to that seen for the Hedgehog pathway.

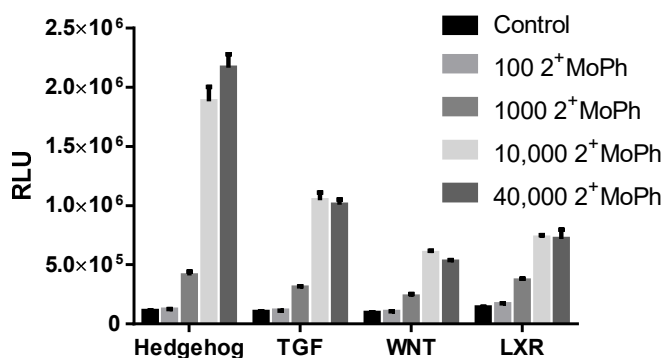


Figure 29. Reporter titration with 2⁺MoPh cells. 20,000 HEK293 reporter cells for Hedgehog, TGF β , WNT or LXR signaling were co-cultured with dilutions of 2⁺MoPh cells. (three wells per group, experiment representative of three individual experiments).

4.3.3 The factor(s) responsible for the activation of these pathways are secreted by 2⁺MoPh cells

To define whether the signals produced by myeloid cells were transduced through cell-cell contact, by soluble factors in the media, or by exosomes, various treatments of serum free supernatants were tested. To help facilitate these, and related experiments, experimental myeloid cell lines were tested for potential ability to activate the same pathways identified in the 2⁺MoPh experiments. The identification of a myeloid cell line would be helpful as the primary myeloid cells were difficult to generate, and generally showed poor viability under the serum starvation conditions needed to perform many of the following experiments.

To this end, THP1 and Mono-Mac-6 cell lines which were originally derived from patients with acute monocytic leukemia, and show suitable growth characteristics, were tested [198, 199]. Surface marker characterization of the Mono-Mac-6 and THP-1 cell lines are found in the addendum (6.3).

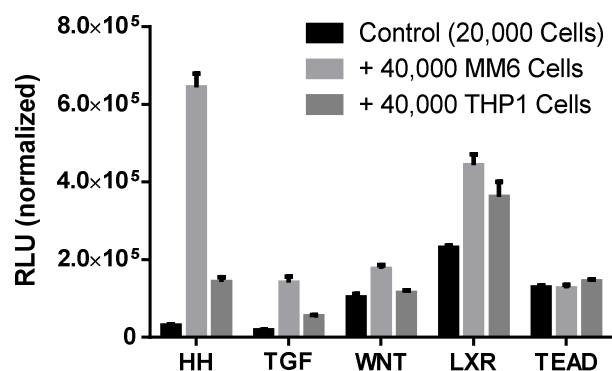


Figure 30. Hek293 Reporter cells co-cultured with myeloid cell lines.

To test whether model parenchymal cell reporter lines could be activated by co-incubation with myeloid cell lines, a panel of HEK293 reporter lines were co-incubated with the myeloid leukemia lines Mono-Mac-6 (MM6) and THP1. Reporter cells for Hedgehog, TGF β , and, to a lesser degree, LXR and WNT

signaling pathways showed induction following co-incubation, while TEAD was unchanged. 20,000 Hek293 reporter cells were co-incubated with 40,000 myeloid cells for 48 hours in 96-well plates, 100 μ l volume per well. Secreted *Gaussia* luciferase reporter activity was measured from the growth media. Data represent relative light units (RLU) normalized to assay medium or myeloid conditioned assay media. Experiment representative of three individual experiments, three wells per treatment group. Changes are highly significant ($p < 0.0005$) for HH, TGF, WNT and LXR reporters when co-incubated with Mono-Mac-6 cells.

The cell lines were then tested in co-culture with a panel of reporter cells. The Mono-Mac-6 cell line strongly activated the Hedgehog reporter as well as the TGF β , WNT and LXR reporters. TEAD was not activated. Due to technical problems, AP-1 activation experiments using Mono-Mac-6 cells were done individually, but also showed strong activation for Mono-Mac-6 cells (see supplement 6.3.1). THP-1 cells showed the same general activation profile, but the level of stimulation was far weaker than that seen with the Mono-Mac-6 cells. The Mono-Mac-6 results showed a good correlation with the data generated from the 2⁺MoPh cells, and were used in a series of experiments to help characterize the nature of the signal driving activation seen. The overall level of activation seen were generally weaker with Mono-Mac-6 than with 2⁺MoPh cells.

A series of Mono-Mac-6 cells dilutions was used in co-culture experiments using the Hedgehog and TGF β reporter HEK293 cell lines. A strong dosage dependency was observed.

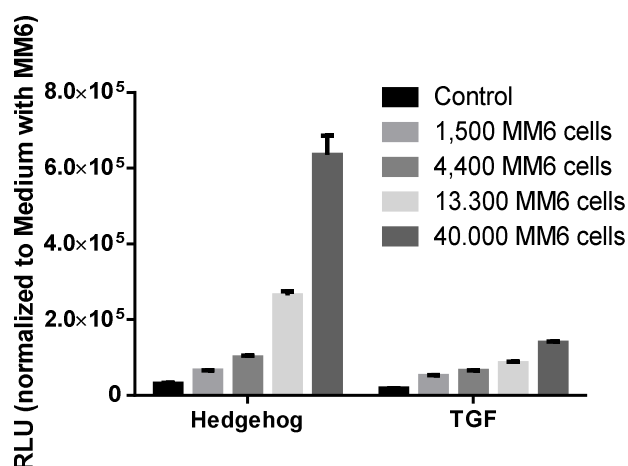


Figure 31. Mono-Mac-6 titration with Hek293-reporter lines. To assess whether the effects shown in figure 30 are dose-dependent, a serial dilution of Mono-Mac-6 (MM6) cells was added to 20,000 Hek293 cells reporter cells in 96-well format for 48 hours. TGFβ and Hedgehog reporter lines showed a dose dependent increase in signal, with the Hedgehog signal being stronger. Three 96-wells per group, experiment representative of three individual experiments.

To assess whether the signal(s) delivered by myeloid cell lines could also be conferred by conditioned medium from Mono-Mac-6 cells, Hedgehog and TGFβ reporter HEK293 cells were tested in parallel in a stimulation experiment.

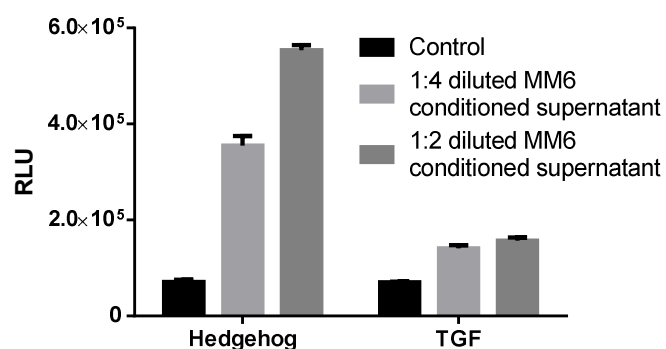


Figure 32. Mono-Mac-6 conditioned media stimulation of Hek293 reporter cell lines.

As Mono-Mac-6 (MM6) co-incubation had strong effects the next question was whether the effect depended on cell-cell contact or was also conferred by conditioned Mono-Mac-6 medium. Since there was a strong dosage-dependency observed in the co-

culture experiments, 20,000 Hek293 Hedgehog and TGFβ reporter cells were seeded in 96-well plates and stimulated for 48 hours with dilutions of Mono-Mac-6 conditioned (72h) medium. Similar to the findings in direct co-culture, activation of the Hedgehog signaling pathway was stronger than for TGFβ/SMAD signaling. Three 96-wells per group, experiment representative of three individual experiments.

While this experiment showed that conditioned supernatants could activate the reporter cells in a dose dependent manner, it also became clear that the activation potential of these supernatants was much reduced in comparison to co-culture. To increase the efficacy of the Mono-Mac-6 supernatants, the harvested, serum-free supernatants were then concentrated to increase their stimulation potential. This was done using concentration spin columns with a 10kDa cut-off as described in the methods section.

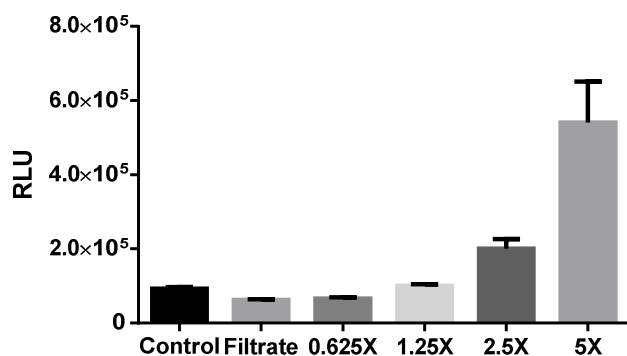


Figure 33. Concentrated Mono-Mac-6 conditioned media stimulated Hek293 Hedgehog reporter cells.

To amplify effects seen with conditioned medium, the serum-free Mono-Mac-6 conditioned medium was concentrated to 10X using spin filters with 10kDa exclusion. This led to a maximum final concentration of 5X in the assay by dilution with FCS

containing assay medium. Results show a dramatic increase in signal with increased concentration. Three 96-wells per group, experiment representative of three individual experiments

The concentrated supernatants showed an enhanced potential to activate the reporter cell lines, while diluting the concentrated supernatant reduced efficacy, again indicating a dose dependency. Having determined that the signal did not require direct cell-cell contact, the nature of signal(s) within the conditioned media were further shown to be sensitive to heat denaturation and protease treatment. The results strongly suggest secreted protein(s)/peptide(s) as the activating factor(s).

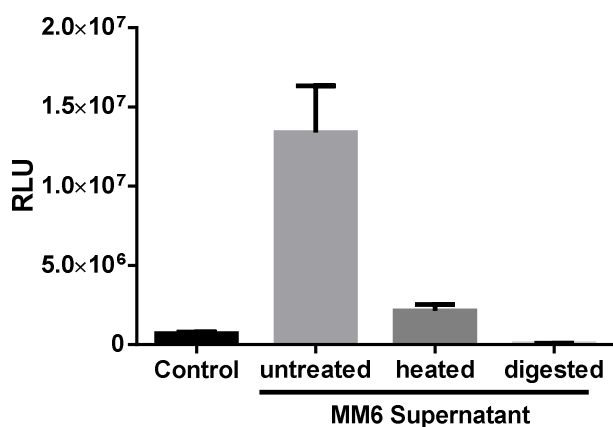


Figure 34. Destruction of signal conferring components in Mono-Mac-6 supernatants.

Mono-Mac-6 (MM6) supernatant was either heated at 98°C for 30 minutes or digested with Proteinase K in a 1:50 w/w dilution (enzyme / protein content) for 60 minutes and then heat inactivated for 10 minutes at 98°C. The resulting inactivated supernatants were used to stimulate 20,000 Hedgehog reporter carrying HEK293 cells for

48 hours. Heat inactivation dramatically reduced activation of reporter cells, Proteinase K digest removed the signal. Single experiment with five individual 96-wells per treatment group.

Exosomes are secreted by many cell types, including myeloid cells. They are small lipid encapsulated microbodies between 30 and 100nm in diameter that can activate target cells either through molecules on their surface, or other factors delivered to the target cell upon exosome fusion or uptake [200]. To determine if exosomes present in the supernatants could influence luciferase production by the reporter cells, exosomes

were purified either using a previously described ultracentrifugation method, or using a commercially available exosome preparation kit.

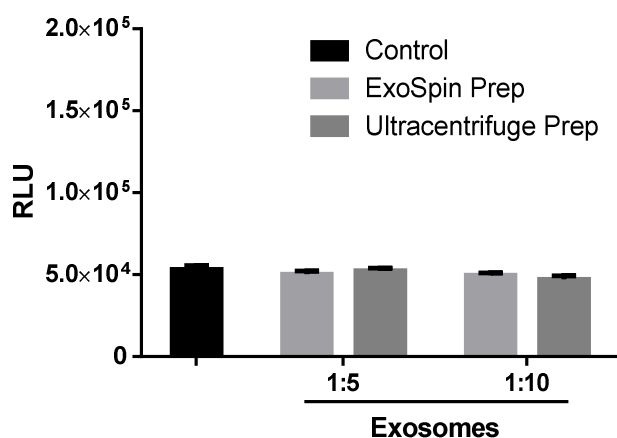


Figure 35. Exosome treatment of Hek293 Hedgehog reporter cells.

Exosomes were prepared from 48h conditioned, serum-free Mono-Mac-6 medium using two different techniques, and used to stimulate HEK293 Hedgehog reporter cells for 48 hours. Exosomes were prepared from 52ml of conditioned medium for each preparation with a final $\sim 100\mu\text{l}$ resultant concentrated exosome volume (Undiluted concentrations: ExoSpin Prep: 0.35mg/ml, Ultracentrifuge Prep:

0.27mg/ml). Addition of concentrated exosomes had no effect on Hek293 Hedgehog reporter cells. Controls are untreated Hek293 reporter cells. Two experiments with three 96-wells per group.

Neither preparation technique showed any activation of the Hedgehog reporter cell line, even though this reporter showed the strongest activation with the full supernatants and in co-culture experiments. Since this result suggested that the signal was transduced by a soluble factor, depletion of exosomes from the supernatants should not diminish the activation seen with complete supernatant. To verify this, complete supernatant was cleared of non-soluble components, such as exosomes, by ultracentrifugation.

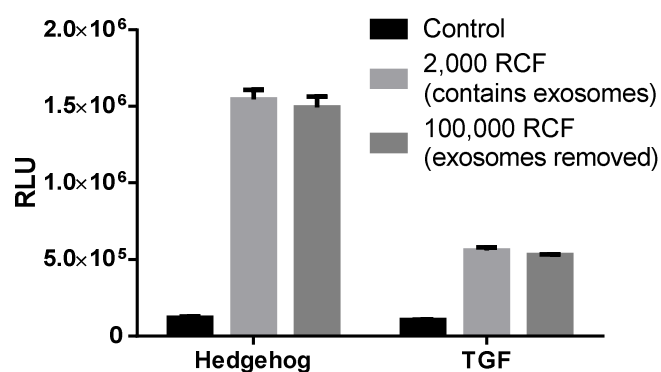


Figure 36. Hek293 reporter cells treated with exosome depleted, and 4X concentrated medium.

To further validate a lack of impact of exosomes on stimulation of the Hek293 Hedgehog signaling reporter cells, conditioned myeloid supernatants were processed either by low speed or by ultracentrifugation (100,000 RCF, relative centrifugal force). Ultracentrifugation removed cell debris

and all microparticles (including exosomes), yielding medium containing only soluble factors. Centrifugation at 2,000 RCF was done to remove cells and cell debris, but did not remove microparticles. Both preparations (after concentration to 8X, yielding 4X concentrated medium in the assay) showed strong induction of the Hek293-Hedgehog and -TGF reporters suggesting again that exosomes are not responsible for the

signaling events seen. Controls are untreated Hek293 reporter cells. Two experiments with three 96-wells per group.

Supernatants subjected to ultracentrifugation did not show any significant differences in activation experiments to the activation seen with non-exosome depleted supernatants. The results suggest that a soluble factor, probably a peptide, was the causal component.

4.3.4 Proteomics

To identify candidate soluble factors responsible for activation of the reporter lines, conditioned supernatants from lab polarized 2⁺MoPh and imDCs were analyzed proteomically in an initial set of experiments. Immediately after polarization, 2⁺MoPh and imDCs were cultured in the same serum-free assay medium for 46 hours. Supernatants were then harvested, proteolyzed with trypsin and their composition analyzed by mass spectrometry using a Q Exactive high field mass spectrometer by our collaboration partners at the Research Unit Protein Science, Helmholtz Zentrum München as detailed in 3.10. Out of the total 1807 identified components in the supernatants, 11 known growth factors, ligands, chemokines and cytokines were detected (see table 4). Importantly, ligands for the WNT or Hedgehog pathways were absent from the list, suggesting that a non-canonical mode of activation may be responsible for the pathway stimulation caused by 2⁺MoPh co-culture. Similarly, while the TGFB1 ligand was present, its protein level was elevated in the imDC sample as compared to the 2⁺MoPh sample and thus a stronger TGFβ/SMAD signal for imDC than 2⁺MoPh in co-culture experiments would have been expected. Two potential explanations for the contrary results seen *in-vitro*, are that there may be differences in either the processing of the latent TGFB1 protein, or there may be additional activation of TGFβ/SMAD signaling via cross-talk or non-canonical activation of the pathway.

A large number of surface proteins were also identified in the culture supernatants, this may result either from proteolytic cleavage from the cell surface, or by their presence on/in microbodies. Parallel experiments carried out using Mono-Mac-6 cells showed overlapping results with the 2⁺MoPh findings.

Based on these initial findings, direct stimulation experiments of HEK293 reporters were carried out using recombinant version of the candidates CXCL8 (IL-8), CCL2 (MCP-1) and IL18. Stimulation with these factors failed to activate the Hedgehog reporter cells (data not shown). MYDGF (short for myeloid derived growth factor), an

interesting candidate protein, was tested by its overexpression in a second, co-cultured cell line (using the inducible expression vector), but it was also found to have no discernible effect on Hedgehog pathway activation (data not shown).

Soluble Factor	Foldchange 2 ⁺ MoPh to imDC
CCL2	158
CXCL8	123
NCF4	12
IL18	7
MYDGF	2
TGFBI	-2
CXCL16	-2
IL16	-2
HDGF	-2
CXCL10	-14
CCL17	-521

Table 4. Growth factors, cytokines and chemokines identified via mass spectrometry.

4.3.5 Inhibitor studies were used to identify potential upstream signaling cascades

Since no causal factor could be readily identified proteomically, and to further characterize the nature of the signal cascade leading to activation of the relevant reporter lines, a series of small molecule inhibitors that target specific signaling cascades was employed. Since Hedgehog signaling showed the strongest activation across multiple experiments and myeloid cells, and cell lines, this reporter was chosen as a general read-out. The Hedgehog signaling pathway is known to have one canonical and at least two non-canonical branches [58, 61, 62]. Since no Hedgehog ligands were identified in the proteomics screen, a non-canonical activation was a potential explanation for the effects seen. In a first experiment, the GLI1/GLI2 inhibitor GANT61 was used in conjunction with concentrated Mono-Mac-6 supernatant. This control inhibitor specifically inhibits binding of the activated GLI1/2 transcription factor to DNA, thus further validating activation of the Hedgehog pathway [201].

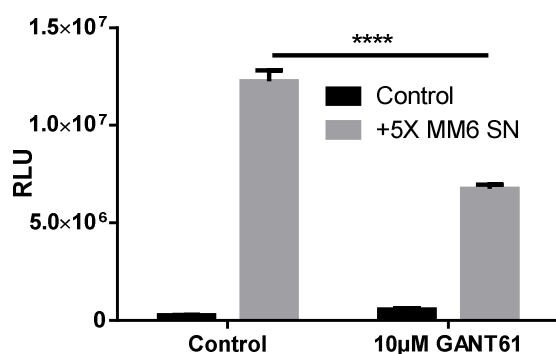


Figure 37. Hek293 Hedgehog reporter cells treated with GANT61. Hek293 Hedgehog signaling reporter cells were treated with or without conditioned Mono-Mac-6 supernatant (MM6 SN) and the GLI1/GLI2 specific DNA binding inhibitor GANT61. Treatment with GANT61 strongly decreased the activation seen with Mono-Mac-6 supernatant. Experiment

representative of three individual experiments, three 96-wells per treatment group.

The reporter activation seen with the Mono-Mac-6 supernatant was strongly reduced with GANT61 treatment. As Kinase signaling pathways are thought to be major contributing factors for the non-canonical Hedgehog signaling branches [63, 64], inhibitors for mTOR [202], ERK/MAPK and PI3K were then tested. Inhibition of ERK/MAPK with PD98059 [203] showed the strongest reduction of activity, with the PI3K [204] inhibitor Wortmannin [205] also showing significant reduction of the signal. These results suggest that a major component of the conditioned supernatants acts via stimulation of the MAPK / PI3K signaling network.

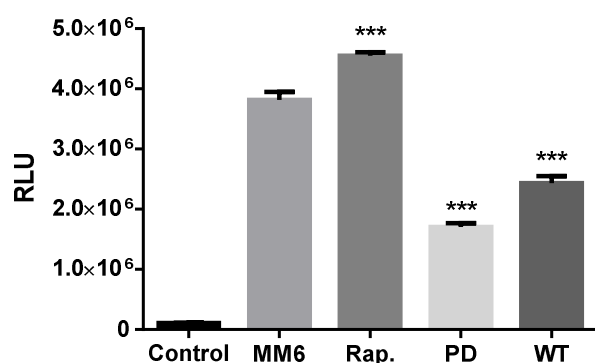


Figure 38. Hek293 Hedgehog reporter cells treated with Rapamycin, PD98059 or Wortmannin.

20,000 Hek293 Hedgehog signaling reporter cells were treated with or without 5X concentrated conditioned Mono-Mac-6 supernatant (MM6) and either the mTOR inhibitor Rapamycin (250nM), the MAPK/ERK inhibitor PD98059 (25µM) or the PI3K

inhibitor Wortmannin (200nM) for 48 hours in 96-well format. Treatment with PD98059 and Wortmannin strongly decreased the activation seen with Mono-Mac-6 supernatant, while Rapamycin slightly increased activation, possibly by modulating other signaling processes and resulting increased Hedgehog activity. Three 96-wells per treatment group, experiment representative of three individual experiments. All changes are significant with at least $p < 0.005$.

To assess whether a known non-conical Hedgehog activator, human epithelial growth factor (EGF) [117, 188], could also activate the reporter in this context, and whether this effect could be reduced by PD98059 or Wortmannin, an additional set of experiments was conducted.

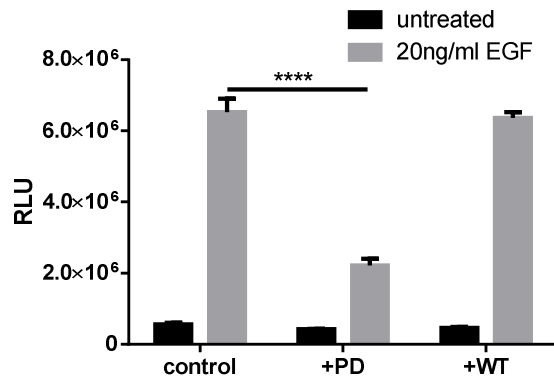


Figure 39. Hek293 Hedgehog reporter cells treated with rhEGF and PD98059 or Wortmannin.

Hek293 Hedgehog signaling reporter cells were treated with or without recombinant human EGF protein and the MAPK/ERK inhibitor PD98059 (25 μ M) or the PI3K inhibitor Wortmannin (200nM). Treatment with rhEGF strongly activated the Hedgehog reporter,

while treatment with PD98059, but not Wortmannin, strongly reduced the reporter activity. Three 96-wells per treatment group, experiment representative of two individual experiments.

As previously reported, EGF was able to strongly activate the HEK293 Hedgehog reporter cells, and thus demonstrated non-canonical Hedgehog activation. PD98059 was subsequently shown to reduce the EGF-mediated signal. More importantly, this assay also showed that Wortmannin could not reduce the activation seen analogous to the supernatant stimulation experiments, suggesting that there is another signal not provided by EGF-mediated signals that may be relevant for the 2⁺MoPh-mediated effects.

4.3.6 Can LXR activation modulate 2⁺MoPh and imDC activation patterns?

After the observation that co-culture with 2⁺MoPh and imDC cells could also activate the LXR reporter (see 4.3.2 and 6.4), modulation of myeloid cell activation patterns by targeted activation of LXR was studied. These studies were in part based on previous findings showing the importance of LXR signaling in the polarization and maturation of myeloid cell populations [183, 184]. In addition, increased LXR levels have been shown to suppress chronic damage in renal allograft and other disease models [185, 186], and their presence is also known to be important for regulation of renal sodium–phosphate transporters, as well as glucose and fatty acid homeostasis [206, 207].

As a first step, the functional range of the synthetic, non-steroidal LXR agonist GW3965 [208] was determined in the HEK293 LXR reporter cells. A titration experiment identified the function range of the agonist and showed that higher dosages of GW3965 appear toxic to the HEK293.

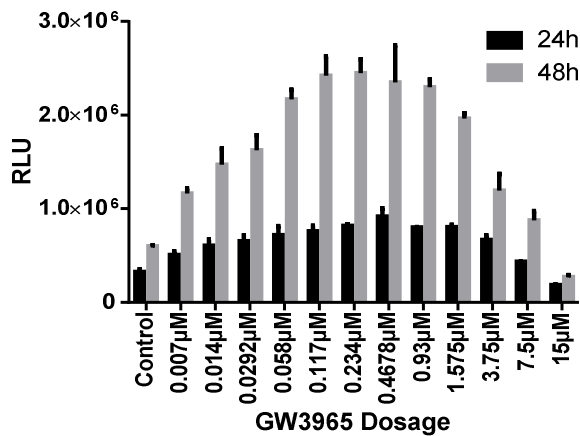


Figure 40. Stimulation of LXR reporter HEK293 cells with the synthetic LXR Agonist GW3965. To assess a functional range of GW3965 in HEK293 cells, stable transfected HEK293 LXR reporter cells were treated with varying doses of GW3965 for 48 hours after which reporter activity was assessed. Treatment with GW3965 activates the LXR nuclear receptors in a dosage dependent manner, with high doses being toxic to the cells. 3 wells per group, experiment representative of three individual experiments.

After determining an optimal concentration to use for LXR-based activation using GW3965, a variation of the co-culture experiments detailed in 4.3.2 was used to assess whether activation of LXR in polarized myeloid cells by GW3965 treatment would change their activation potential as measured with HEK293 reporter cell lines.

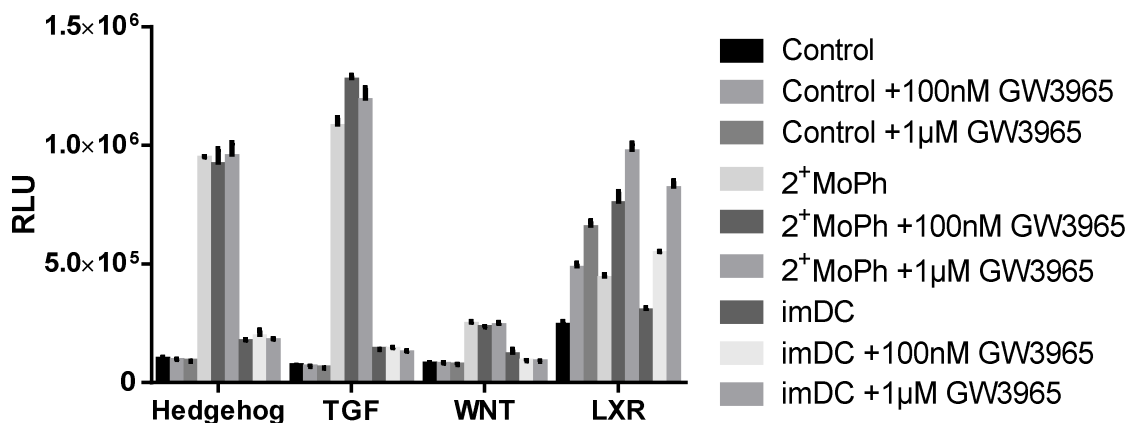


Figure 41. GW3965 Effect on primary cells: 20,000 reporter cells were co-cultured with 40,000 2⁺MoPh or imDC with and without GW3965. 100nM/1μM GW3965 was administered at the beginning of co-culture. Effects on LXR Reporter cells were assayed as an internal control for G3965 efficacy. GW3965 treatment had no effect on primary myeloid cell activation of HEK293 reporter cells. Three wells per treatment group, two experiments.

Since no differences could be detected with GW3965 treatment outside the HEK293 LXR control reporter cells, the treatment was deemed to have no effect on the secretion patterns of either fully polarized 2⁺MoPh or imDC. To determine whether the treatment with GW3965 could influence the pathway at an earlier point in myeloid polarization, 2⁺MoPh and imDCs were treated with 1μM GW3965 either at the

beginning of the polarization regimen or at the initiation of co-culture. In this experiment, the amount of 2⁺MoPh in the co-culture was reduced in order to enhance potential GW3965-mediated effects. No effect of GW3965 was observable (for additional characterization of LXR signaling see addendum 6.4).

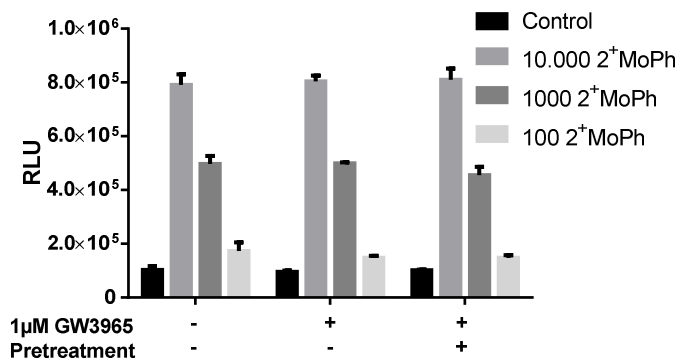


Figure 42. GW3965 Effect on diluted primary cells. 20,000 HEK293 reporter cells for Hedgehog were co-cultured with different amounts of 2⁺MoPh cells with and without GW3965. 1 μM GW3965 was administered either at the beginning of co-culture or prior, directly during polarization. GW3965 treatment had no effect on primary myeloid cell activation of HEK293 reporter cells. Three wells per treatment group, two experiments.

4.4 Bioinformatic analysis of pathway alterations associated with 2⁺MoPh in DN patient biopsies

Based on the results of the *in-vitro* studies detailed above, a set of the homeostatic pathways were experimentally validated in the experimental parenchymal cells to be activated by the presence of 2⁺MoPh cells. In addition, the data suggest that the effects occur via a MAPK-mediated non-canonical activation. To further expand our analysis to the DN patient data, we then sought to determine, if gene signatures representing the pathways identified in the *in-vitro* studies could be significantly correlated with the presence of 2⁺MoPh cells in human renal biopsy samples. To this end, the deconvolution signature that allowed the selective identification and quantification of 2⁺MoPh signals within complex transcriptomic data (detailed in 4.1.2) was applied. All subsequent analyses were based on transcriptomic data collected from the 17 microdissected DN biopsies and set of 30 LD control renal biopsies as described in 4.1.2.

4.4.1 Identification of co-regulated gene modules by weighted gene co-expression network analysis (WGCNA)

To determine the potential association of activated pathways identified *in-vitro* with the presence of 2⁺MoPh in patient biopsy samples, a detailed list of genes known to be associated with the four general homeostatic pathways identified in the *in-vitro* studies was first compiled. The sources for these gene lists included commercially available

pathway research tools, and pathway databases (Genomatix, <http://www.genomatix.de/>, literature-derived gene lists for RT-PCR arrays from Qiagen / SABiosciences, <http://www.sabiosciences.com/ArrayList.php>, and the Wikipathways platform <http://www.wikipathways.org/index.php/WikiPathways>). The list eventually comprised 773 genes previously established to be broadly associated with the WNT, Hedgehog, TGF β /SMAD and MAPK pathways. Hippo signaling genes were omitted from the final gene list due to the very low levels of activation in co-culture experiments (see also Addendum 6.5). LXR signaling was also omitted for the following analysis. Of the 773 genes, 680 were shown to be expressed in the tubulointerstitial compartment of the human kidney samples were studied. The goal was then to determine if changes in specific pathway signatures could significantly correlate with 2⁺MoPh deconvolution scores. As expected, the pathways exhibited diverse regulatory patterns for their individual component genes. Because of the potential for pathway crosstalk and evidence for non-canonical signaling, the genes were further grouped based on their expression patterns, irrespective of their classical association with a respective pathway. To this end, a weighted correlation network analysis (WGCNA) strategy was applied [163]. This bioinformatics tool was used to help identify clusters (also called modules) of highly co-regulated genes, which could then be used in place of individual genes for subsequent downstream correlation with the 2⁺MoPh deconvolution score. The general approach allowed us to focus on smaller groups of genes linked to the biology of specific pathways. Additionally, the WGCNA method was used to identify intramodular hub genes, allowing a measure of biological context in comparing the individual modules. In order to avoid potential bias in the analysis by adding a hierarchy, the individual modules were assigned an arbitrary color.

Module identifier	Hub Gene
black	HOXA5
blue	CAMK2A
brown	SNX4
green	GDF9
pink	UBE2L3
red	TCF7L2
turquoise	CDKN1A
yellow	RAC2
grey (remaining genes)	ROR1

Table 5. Modules identified by WGCNA. A pseudo-module was generated for unassigned genes; nine modules were identified using weighted correlation network analysis. The defining hub genes for each module are indicated in the table. Bold font indicates significant correlation with 2⁺MoPh

As detailed above, the correlation of the individual modules to the deconvolution scores from 4.1.2 was used as a screening criterion to discern which modules, and thus which pathway gene sets, changed transcriptomically with an increased 2⁺MoPh signature in the tubulointerstitial regions during DN disease progression (as evidenced with reduced eGFR in 4.1.2). A *p*-value based on the correlation of the genes with the individual samples was calculated to discern significant correlation. These studies were performed in collaboration with Ms. V. Nair, University of Michigan, Ann Arbor.

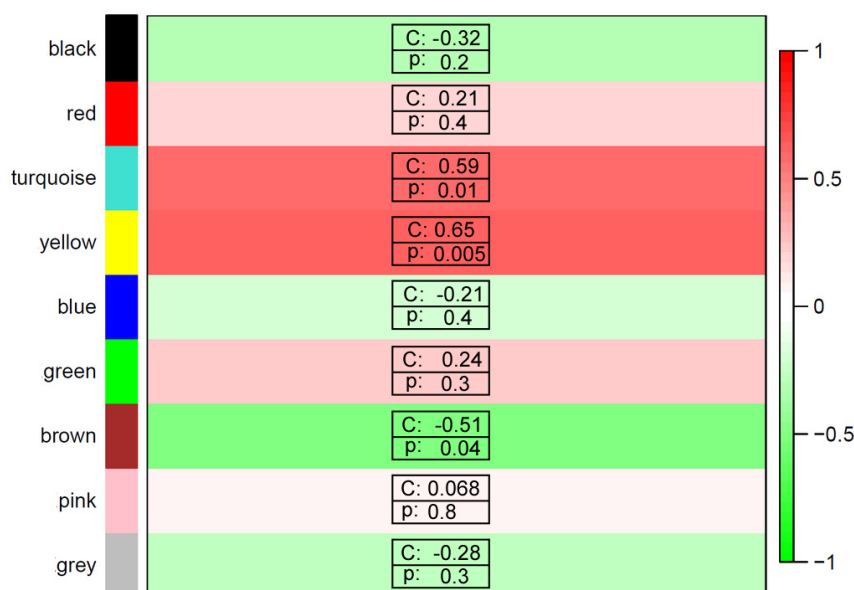


Figure 43. Correlation of modules identified by WGCNA to deconvolution score.

Expression profiles of modules across DN samples were correlated to the 2⁺MoPh deconvolution score calculated for the same samples to identify transcriptomic changes coinciding with increased 2⁺MoPh presence. Modules turquoise and yellow exhibited a significant

positive correlation, module brown exhibited a significant negative correlation. C: correlation coefficient, p: *p*-value, heat scale indicates correlation coefficient, with red being positive and green being negative.

The WGCNA strategy identified three significantly correlated modules: turquoise, yellow and brown. Turquoise and yellow exhibited positive correlation, indicating upregulated genes during DN, brown showed negative correlation indicating downregulation.

4.4.2 Genetic composition of modules

After filtering for significantly altered modules, the composition of the individual modules was studied in more detail. For each gene, an individual correlation coefficient to the deconvolution score was used as a measure of 2⁺MoPh presence, with a corresponding *p*-value calculated to allow for additional filtering. This filtering yielded 23 significant genes for module “brown”, 62 genes for module “turquoise” and 38 genes for module “yellow” (for a full list see the addendum). Through a literature

search, each gene was then assigned to functional or regulatory groups. The most highly represented groups per module can be found in table 6.

Module	Functional Group	Percentage in Module
"brown"	MAPK associated	52%
	WNT associated	13%
	Proteasome associated	9%
"turquoise"	MAPK associated	33%
	WNT associated	16%
	Proteasome associated	13%
	TGF β /SMAD associated	8%
	ECM/Fibrosis associated	6%
"yellow"	MAPK associated	39%
	Regulation of Cell Cycle	16%
	WNT associated	13%
	TGF β /SMAD associated	8%
	ECM/Fibrosis associated	8%

Table 6. Most highly represented functional groups per module. For each module, the genes with expression patterns significantly correlating with 2⁺MoPh presence as determined with the deconvolution analysis were considered. Genes were then grouped based on functional or regulatory context and percentages calculated in reference to the total number of genes in the corresponding module.

For the three modules, the MAPK associated group represented the largest component. The "brown" module was negatively correlated with 2⁺MoPh presence, while the "turquoise" and "yellow" modules were positively correlated. Similarly, WNT associated genes made up a large portion of all three modules. In contrast, proteasome, TGF β /SMAD or ECM/Fibrosis associated genes varied more between the modules. The "yellow" module is different from the other two modules due to its comparably large component of genes important for the regulation of the cell cycle, which underlies the control of cell proliferation.

4.4.3 Potential “high impact” pathway genes within modules

Within the function or pathway associated groups for each module, a number of well-characterized proteins associated with tissue homeostatic pathways were identified. This does not imply that genes not listed here (see addendum 6.1) do not play a role during DN, but many of these candidate genes are not well enough studied to provide a perspective on their potential to impact disease progression. For similar reasons, transcription factors that are not classically associated with a homeostatic pathway were omitted from this list as their regulation patterns are often highly context dependent and have rarely been exhaustively studied. For the sake of simplifying description of these “high impact” genes, the “turquoise” and “yellow” modules will be viewed together due to both of them being positively correlated to 2⁺MoPh presence at similar levels (and thus have a higher expression in comparison to control kidneys), while the “brown” module showed negative correlation (and thus downregulation in comparison to controls).

All changes are summarized in table 7. In the MAPK signaling network, the associated RTK ligands VEGFA, VEGFC and EGF showed altered expression, with VEGFA and EGF found to be downregulated and VEGFC upregulated [103]. The MAPK associated receptors RYK [209], MET [210], and the JAK/STAT co-receptor JAK1 [112] exhibited uniform upregulation and similar patterns could be found for the signal transducing MAP kinases MAP3K5, MAP3K8 [211] and STAT1, a pivotal transcription factor of the JAK/STAT branch [112]. MAP3K12 showed downregulation. The dimeric AP-1 transcription factor subunits that are also downstream of the MAPK network were upregulated, as evidenced by JUN, JUNB and FOS [212]. Finally, the MYC transcription factor was overrepresented while MYCN was downregulated [213].

In the WNT pathway, the WNT2B and WNT7A ligands were increased, while WNT8B was reduced [214]. All three ligands are considered canonical WNTs, and thus their presence leads to β -catenin stabilization. Complications in interpreting WNT ligand functions stem in part from the multitude of FZD ligands and their varying specificity for the individual ligands. In the DN setting, FZD2, FZD6, FZD7, FZD10 and FZDB were all upregulated and correlated with the 2⁺MoPh deconvolution signature [215]. Interestingly, the co-receptor LRP6 was reduced, while the signal transducing casein kinases were increased in expression. LRP6 is a component of the canonical pathway, but has also been shown to act in non-canonical contexts [190, 216, 217]. WNT/PCP

signaling interacts with JNK signaling, making the interplay of the two pathways in DN an interesting object to study [82].

In the TGF β /SMAD pathway, the TGFBR2 receptor was found to be upregulated with the deconvolution signature. In the BMP/SMAD pathway, the BMP2 ligand was significantly increased. TGF β target genes were also identified as being overrepresented in the samples. Matrix metalloproteinase-7 (MMP7) is associated with ECM turnover, the processing of growth factors, and has been reported to be upregulated in the context of renal fibrosing diseases [218, 219]. CTGF [220] and CYR61 [221] were also identified here, and are also known to be elevated during most fibrosing diseases, and implicated in wound healing programs.

Pathway	Gene name	Function	Regulation
MAPK	VEGFA	Ligand / growth factor	Down
	VEGFC	Ligand	Up
	EGF	Ligand	Down
	RYK	Receptor	Up
	MET	Receptor	Up
	JAK1	Co-receptor	Up
	STAT1	Signal transducer / transcription factor	Up
	MAP3K5	Signal transducer	Up
	MAP3K8	Signal transducer	Up
	MAP3K12	Signal transducer	Down
	JUN	AP-1 component, transcription factor	Up
	JUNB	AP-1 component, transcription factor	Up
	FOS	AP-1 component, transcription factor	Up
	MYC	Transcription factor	Up
	MYCN	Transcription factor	Down
	WNT	WNT2B	Ligand
WNT7A		Ligand	Up
WNT8B		Ligand	Down
FZD2		Receptor	Up
FZD6		Receptor	Up
FZD7		Receptor	Up
FZD10		Receptor	Up
FZDB		Receptor	Up
LRP6		Receptor	Down
CSNK1A1		Signal transducer	Up
CSNK1G3	Signal transducer	Up	

Pathway	Gene name	Function	Regulation
TGF β /SMAD	BMP2	Ligand	Up
	TGFBR2	Receptor	Up
	CTGF	TGF β target, wound healing and fibrosis	Up
	CYR61	TGF β target, wound healing and fibrosis	Up
	MMP7	TGF β target, ECM degradation	Up

Table 7. Dysregulated pathway genes correlating to 2⁺MoPh.

In addition to the alterations of core pathway genes, changes in the expression of gene ontological groups influenced by the homeostatic signaling pathways were observed. The upregulation of cyclins and cyclin dependent kinases suggests increased cell cycle activity and proliferation, potentially linked to the activation of wound healing programs [222, 223].

Increased ECM deposition, a hallmark of DN, was observed on the transcriptomic level with the increased expression of Galectin, Laminin, Fibronectin, Collagens and Versican [224]. The aforementioned TGF β associated markers MMP7, CTGF and CYR61 support this observation.

Finally, genes associated with the proteasome were upregulated, with five proteasome subunits found to be upregulated, and two subunits decreased. Additionally, the ubiquitination mediators Cullin1 and UBE2E1 were also upregulated [225]. These alterations are summarized in table 8.

Function	Gene	Description	Regulation
Cell cycle	CDKN1A	Cyclin dependent kinase inhibitor	Up
	CDK1	Cyclin dependent kinase	Up
	CCNB1	Cyclin B1	Up
	CCNB2	Cyclin B2	Up
	CCND2	Cyclin D2	Up
	CCND3	Cyclin D3	Up
ECM	LGALS3	Galectin 3	Up
	LAMC1	Laminin subunit gamma	Up
	FN1	Fibronectin	Up
	COL1A1	Collagen type I alpha 1 chain	Up
	COL1A2	Collagen type I alpha 2 chain	Up
	VCAN	Versican	Up

Function	Gene	Description	Regulation
Proteasome	PSMA2	Proteasome subunit alpha 2	Down
	PSMA4	Proteasome subunit alpha 4	Up
	PSMB8	Proteasome subunit beta 8	Up
	PSMB9	Proteasome subunit beta 9	Up
	PSMB10	Proteasome subunit beta 10	Up
	PSMC2	proteasome 26S subunit, ATPase	Down
	CUL1	Cullin 1,	Up
	UBE2E1	Ubiquitin conjugating enzyme	Up

Table 8. Pathway-associated genes correlating to 2⁺MoPh sorted by function.

5 Discussion

DN develops as a complication of diabetes [14, 15, 18, 21]. It is characterized by morphological changes in the kidney including a thickening of the glomerular basement membranes and the mesangium, glomerular sclerosis and progressive fibrosis of the interstitial region [22]. The fibrotic processes seen in most progressive chronic kidney diseases are thought to result in part from overly active wound healing programs leading to increased ECM deposition by fibroblasts and epithelial cells [29, 39]. An enhanced immune cell infiltrate, especially myeloid derived cells such as macrophages, DCs and other rMoPh, is associated with progressive DN [143, 146, 147, 150, 151]. The composition of the infiltrate may have direct effects on the parenchymal tissues.

Recently, the 2⁺MoPh cell type was described in normal kidney and shown to be increased in renal cell carcinoma and in examples of CKD [139, 151]. 2⁺MoPh expression patterns have been shown to be distinct from classical dendritic cells and to overlap with macrophage-associated genes. The renal 2⁺MoPh phenotype is thought to derive from invading monocytes that become conditioned by renal-associated signals, leading to the specific myeloid subtype [151]. A 2⁺MoPh-like phenotype can also be derived *in-vitro* through the treatment of peripheral blood monocytes with kidney epithelial, or renal cell carcinoma conditioned supernatants (Brech et al. submitted). Interestingly, 2⁺MoPh also express high levels of CCL2 (see 4.3.4), a chemokine ligand for the CCR2 receptor, suggesting that 2⁺MoPh may show a positive feedback, or amplification of myeloid infiltration.

Treatment with CCR2 antagonists could act by blocking the recruitment of 2⁺MoPh or related myeloid progenitors and thus impact the development of chronic damage. A series of preclinical DN studies have demonstrated the therapeutic efficacy of myeloid cell infiltration blockades via use of the CCR2 chemokine receptor antagonists RS504393, RO523444 and RS102895 [24, 226-229]. Treated kidneys in mouse models showed ameliorated albuminuria, renal dysfunction and less histological changes. Additionally, two recent clinical studies using the orally available CCR2 inhibitor CCX140-B [230] and the CCL2 inhibitor NOX-E36 [231] showed positive effects on urine albumin-to-creatinine ratio and slight reduction of HbA1c in diabetic nephropathy patients, even after cessation of treatment.

These general observations lead to our hypothesis that 2⁺MoPh may exert direct effects on the homeostatic pathways controlling tissue morphology in kidney parenchymal cells. If so, 2⁺MoPh would represent a key cell type in the progression of fibrosis leading to damage to the kidney fine structure, and ultimately resulting in nephron loss of function. Genes classically associated with fibrosis include CTGF and CYR61, downstream targets of the TGF β signaling pathway [34, 220, 221]. Similarly, members of the WNT and Hedgehog signaling pathways are strongly dysregulated during fibrotic renal disease progression [31, 37, 40]. To study the potential direct effect of 2⁺MoPh on kidney cells in the context of DN, a strategy combining bioinformatic analyses and *in-vitro* experiments was devised.

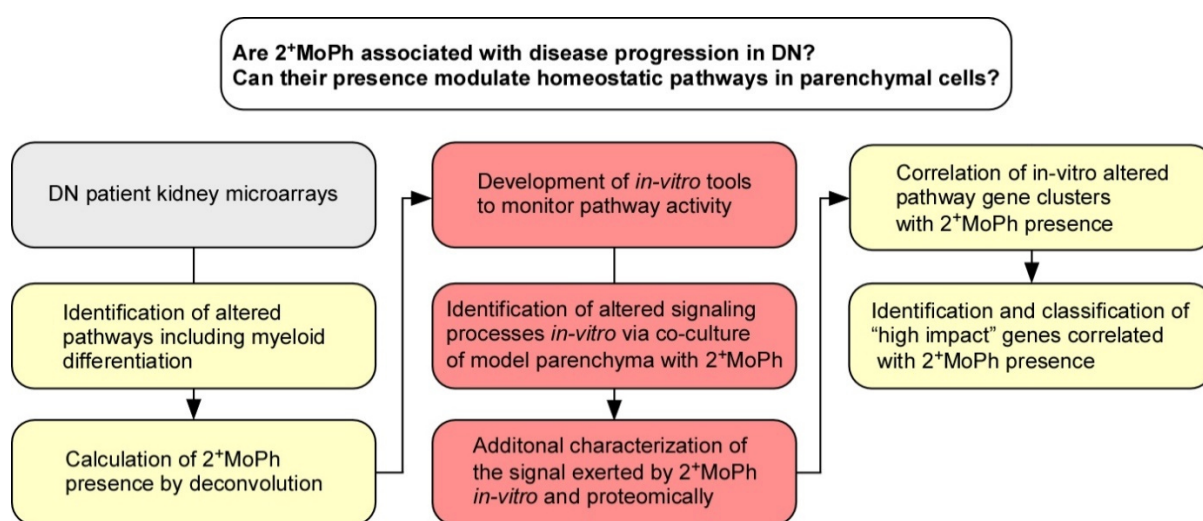


Figure 44. Experimental outline. Outline of the strategy applied for this study. (gray: pre-existing data, yellow: bioinformatic studies, red: *in-vitro* experiments.)

5.1 Initial transcriptomic findings

As a first step, a human microarray dataset generated from microdissected tubular interstitial samples taken from biopsies of DN patients, and control samples from living donor kidneys was transcriptomically analyzed [154]. Specifically, altered homeostatic pathways were identified in a non-biased approach to verify that the data set showed similar dysregulatory patterns as in previously published data [31, 35, 36, 156]. In a next step, the level of 2⁺MoPh transcripts in the human biopsy samples was estimated using a bioinformatics-based deconvolution strategy [162].

Deconvolution strategies allow a general calculation of the cellular composition of complex tissues based on gene profiles. 2⁺MoPh gene signatures were found to be significantly increased in the DN samples (see 4.1.2), as compared to the LD controls,

and in addition, the 2⁺MoPh gene signatures correlated negatively with glomerular filtration rate calculated for the patients at the time of biopsy demonstrating that the presence of 2⁺MoPh cells is strongly associated with progressive DN.

5.2 Development of a next generation vector system

To directly measure the potential effects of 2⁺MoPh cells on the activation of homeostatic pathways in experimental parenchymal cells, a vector platform and co-culture assay was developed. As designed, the vector system that lies behind the cell-based assay allows for the efficient generation of reporter and expression constructs, and active vector integration based on Sleeping Beauty transposon technology [165, 166]. The pSBTET.Reporter vector platform was used to facilitate pathway screening and titration strategies [168]. Based on the secreted *Gaussia* luciferase reporter gene, reporter measurements can be performed in a time course without cell lysis [181]. Previously described transcription factor binding sites/reporter elements were adapted to create the different reporter gene and vector backbones, and offered measurement of a dynamic range between unstimulated and stimulated samples (see 4.2 and addendum). Similarly, the Gateway cloning technology was used to allow the rapid generation of complex expression constructs in the pSBDEST vector [168]. The combination of reporter and expression vector families allowed the inducible expression of transgenes under the control of the CMV/TO promoter. The vectors were designed such that they can be integrated together or in series into the host cell. With a high degree of efficiency and flexibility, the vector platform should be easily adaptable to most cloning projects, and thus greatly expands our molecular toolkit [168].

5.3 2⁺MoPh *in-vitro* findings

In this doctoral work, stably engineered HEK293 reporter cells were used as model parenchyma-reporter cells that were then co-cultured with different myeloid cells including *in-vitro*-derived 2⁺MoPh. The results of the *in-vitro* reporter cell studies showed a direct activation of the MAPK, Hedgehog, TGF β and WNT pathways in HEK293 cells by co-incubation with the 2⁺MoPh cells, while Hippo signaling, which is associated with cell-cell contact, was largely unchanged.

While both imDC and 2⁺MoPh could activate MAPK, Hedgehog, TGF β and WNT pathways in the reporter cell lines, the strength of the activation varied significantly.

Hippo did not exhibit strong activation patterns, but standard cell culture on plastic surfaces may not be ideal setting to study this pathway [44, 88, 170]. Across all activated reporter cell lines, 2⁺MoPh showed a much higher activation than imDC. imDC essentially define conventional dendritic cells, while the 2⁺MoPh phenotype exhibits both DC and macrophage traits [139, 151, 196, 197].

Since myeloid development genes were also altered transcriptomically in the DN microarray dataset, a series of experiments targeting the myeloid differentiation pathway LXR were carried out [183-185, 206]. Treatment with the synthetic agonist GW3965 [208] efficiently activated the LXR reporter cells, but no differences in the secretion patterns for either imDC or 2⁺MoPh could be detected, even if GW3965 was added during polarization of the monocytes. While LXR signaling may still play important roles during myeloid development, it is probably not causal for the polarization to the 2⁺MoPh phenotype.

The precise nature of the signal exerted by 2⁺MoPh could not be determined in this study. The signal was shown to be soluble and probably protein/peptide based (exosome-based signals could be eliminated). While proteomic analysis of the conditioned supernatants identified candidate cytokines, recombinant versions of these candidates failed to replicate the activation seen. Thus, the central effector remains inconclusive. This may be due to technical reasons, or because a novel signaling protein/peptide is causal to the activation patterns exhibited.

5.3 Evidence implicating MAPK as pivotal for the homeostatic alterations caused by 2⁺MoPh presence

While the causal protein/peptide component underlying activation of the MAPK, Hedgehog, TGF β and WNT pathways in co-culture/supernatant studies with 2⁺MoPh could not be determined, inhibitor studies could be used to identify signaling components contributing to the effects seen.

Using the Hedgehog pathway reporter cells as a readout, with stimulation provided by myeloid derived serum-free supernatants, a panel of inhibitors targeting different signaling components of the mTOR [202], MAPK [103, 105] and PI3K [204] pathways was used to identify potential upstream signaling mechanisms. Treatment with the MAPK inhibitor PD98059 [203] and the PI3K inhibitor Wortmannin [205] led to a significant reduction in reporter signal. Wortmannin can exhibit some MAPK inhibition.

PD98059, by contrast, is specific for MEK (or MAP2K) and thus inhibits only MAPK associated signaling processes. Because EGF is a MAPK activating growth factor [232], an additional set of control experiments were performed which exhibited a similar activation of Hedgehog signaling and a reduction of signaling by treatment with PD98059. Interestingly, in this experiment, Wortmannin did not significantly alter the signal, suggesting that the signal exerted by myeloid cells may not be based on a single factor. The MAPK associated MAPK, JNK and JAK/STAT pathways were identified as contributing to activation of homeostatic signaling pathways in the co-culture experiments. While individual signaling pathways are generally still studied as somewhat distinct entities, their interaction (or cross-talk) suggests that viewing them in a larger “network” context may be a better approximation of biology involved in the processes being studied [233].

5.4 Identification of transcriptomically altered pathway components using the WGCNA method strongly hints at MAPK

After identifying 2⁺MoPh-driven alterations of the MAPK, Hedgehog, TGF β and WNT signaling network *in-vitro*, genes associated with these pathways were pooled for an in-depth study and validation using a WGCNA-based method [163]. The analysis was based on the same cDNA microarrays previously shown to have increased presence of 2⁺MoPh as calculated by deconvolution [162], and taken from patients showing decreased renal function as calculated by GFR MDRD [178]. The WGCNA approach led to the identification of co-regulated gene “modules” across this gene network identified in an unbiased manner, from a list of pathway associated genes. For each WGCNA derived gene cluster, a module eigengene, a summarization strategy representing the regulatory trends across the module was calculated. This module eigengene was then used for a correlation analysis with the 2⁺MoPh deconvolution score per sample. Clusters of genes that showed either significant positive or negative correlation with the calculated amount of 2⁺MoPh signals were selected for further study, and the remaining clusters discarded. Out of the three significantly correlated modules, two showed upregulation as compared to normal control samples, and one showed downregulation.

When analyzing the genes comprising each module, a strong MAPK-association component was identified in each module. These results were strongly supported by the results of the *in-vitro* MAPK inhibition studies, which showed strongly reduced

reporter activity. Together, the findings strongly suggest a potential clinical importance for MAPK based signaling processes underlying key pathophysiologic processes in the renal parenchyma as a consequence of enhanced myeloid (2⁺MoPh) infiltration.

Analysis of the individual, dysregulated and 2⁺MoPh correlated genes from the three most relevant modules identified a strong association with the pathophysiology of chronic fibrosis. Many of these genes represent core genes associated with specific pathways, or with phosphorylation-based signal transduction events of the relevant signaling cascade. In the MAPK network, the RTK-associated ligands VEGFA, VEGFC and EGF [103] were found to be significantly altered in steady state expression, and to correlate with changes in the deconvolution score. VEGFA and EGF were decreased, while VEGFC was increased. VEGFA is classically associated with angiogenesis [234], but can also serve as a chemotractant for myeloid cells [235]. VEGFC, by contrast, is involved in lymphangiogenesis (and chronic inflammation) [236, 237]. EGF plays a role in cellular proliferation, differentiation, and survival [49]. It was found to be reduced relative to the 2⁺MoPh signal. While the potential effects of these events are hard to predict, downregulation of EGF and VEGFA may occur as a compensation for the high activation levels of the MAPK network as indicated by the expression levels of most associated transcription factors. The MAPK associated receptors RYK [209], MET [210] and the JAK/STAT co-receptor JAK1 [110-112] were shown to be increased with deconvolution score. The function of the atypical receptor tyrosine kinase RYK is not fully understood, as it seems to lack kinase activity in its C-terminal domain. Since RYK is conserved across a number of species, it is likely to have an important albeit currently unknown function. MET (also known as HGFR) is a more classical RTK shown to activate MAPK, STAT and PI3K. JAK1 is a well-studied co-receptor in the JAK/STAT pathway and is linked to immunity, proliferation, differentiation, apoptosis. The signaling components MAP3K5, MAP3K8 [102] and STAT1 [110-112] were increased with 2⁺MoPh signals, while MAP3K12 [102] was decreased. MAP3K5, MAP3K8 and MAP3K12 are all upstream kinases that interact with different downstream MAP2Ks, and thus, the consequences of their dysregulation are hard to predict, but are likely significant, as the signals transmitted by them are amplified through the signaling cascade [106]. STAT1 is the target of JAK1, and can serve as a transcription factor, but it also directly interacts with other MAPKs and JNKs [112]. Finally, dramatic changes in the activity of the MAPK network were also evident

based on the strongly upregulated transcription factors JUN, JUNB and FOS. These are subunits of the dimeric AP-1 transcription factor. AP-1 is pivotal in mediating signals linked to cell growth and regeneration, differentiation, and apoptosis [212]. MYC was found to be increased, while MYCN was decreased in the progressive DN biopsy samples. The MYC family is a downstream target of WNT and helps control cell proliferation, growth, differentiation and apoptosis [213, 238]. The MYC family has also been shown to upregulate the cyclins, which are also increased in DN [239]. MYCN is less well studied, but has been shown to be highly important in the development of various cancers [240, 241]. Its functions in the kidney however are not well understood.

Under the current paradigm, that disease progression in DN results in part from failed or overly active regenerative processes [18-20], the potential impact of MAPK activated programs represents a novel potential pathophysiologic mechanism. Regeneration, differentiation, proliferation, and apoptosis, are all required to restore tissue in the context of damage [242]. However, the precise control over these processes may be lost in the context of excessive MAPK signaling leading to progressive tissue fibrosis and damage. In addition to the Hedgehog pathway [63], MAPK signaling has also been shown to influence both TGF β and WNT signaling [71, 120, 121], pathways associated with the progressive damage seen in DN samples.

MAPK driven alteration of WNT signaling has been suggested to mediate changes in the expression of β -catenin and provides additional levels of modulation [243]. In the present study, canonical WNT2B and WNT7A ligands (downstream Hedgehog targets) were found to be increased with deconvolution score, while WNT8B was decreased [214]. No clear function has thus far been described for WNT2B. Mouse deletion mutants for WNT2B are viable, and it is implicated in some cancers [244]. For WNT7A the potential ramifications are also not clear. While WNT7B has been associated with renal repair [245], no parallel role has been identified for WNT7A. WNT7A has been shown to be important for angiogenesis of the forebrain [246] and has been implicated in cancers [247]. WNT7A is thought to also signal via the non-canonical WNT/PCP pathway [248]. Similar to WNT7A, WNT8B is present during neurogenesis [249]. The dynamics of the Frizzled receptors and ligand binding are also very complex [215], however the Frizzled receptors are important signaling molecules and required for WNT ligand-mediated signaling. FZD2, FZD6, FZD7,

FZD10 and FZDB were all upregulated in the context of the 2⁺MoPh presence, supporting the observation of an increased activity of WNT signaling during progressive DN. Interestingly, LRP6, which has been shown to be required for canonical WNT signaling but also acts in non-canonical ways [190, 216, 217] was reduced.

Finally, in the TGF β /SMAD pathway, TGFBR2 and BMP2 showed altered expression [194]. In addition, expression of the well-characterized fibrosis-associated TGF β related target genes MMP7 [218, 219], CTGF [220] and CYR61 [221] correlated with the deconvolution signature. Other direct links to fibrosis-related biology were also shown to correlate with the presence of 2⁺MoPh cells in the DN biopsy samples. An increased level of expression of genes directly linked to the genesis of ECM (galectin, laminin, fibronectin, collagens and versican) [224] was identified in the DN samples. Cell proliferation is thought to be increased in ongoing damage to kidney tissues, and can be evidenced here by alteration in the expression of cyclin and cyclin dependent kinase expression patterns [222, 223]. Finally, proteasome associated genes were also shown to be modulated, possibly as a response to the alterations to cell cycle. The ubiquitin/proteasome pathway plays an important role in the activation of MAPK derived signals during the detection of bacterial LPS and subsequent induction of cytokine production [250-252]. Additionally, the protease inhibitor camostat mesilate has proven effective in reducing kidney damage following the sterile unilateral ureteral obstruction disease model in rats [253]. These observations suggest protease inhibitors as a potential avenue in DN treatment.

5.5 Working model

The presence of 2⁺MoPh in the DN transcriptomic data, as evidenced by the 2⁺MoPh deconvolution score, was correlated with a decrease in eGFR (MDRD) [178], suggesting that factors produced by 2⁺MoPh cells may play a role in driving renal fibrosis. A direct effect of 2⁺MoPh cells on the activation of a series of homeostatic pathways in experimental parenchyma was validated. The relevant signals from the 2⁺MoPh cells were not direct cell-cell contact dependent, as they could be mimicked using 2⁺MoPh supernatant. Taken together, the results further suggest that increasing levels of 2⁺MoPh may directly activate homeostatic pathways linked to progressive tissue damage in the renal tubulointerstitial regions.

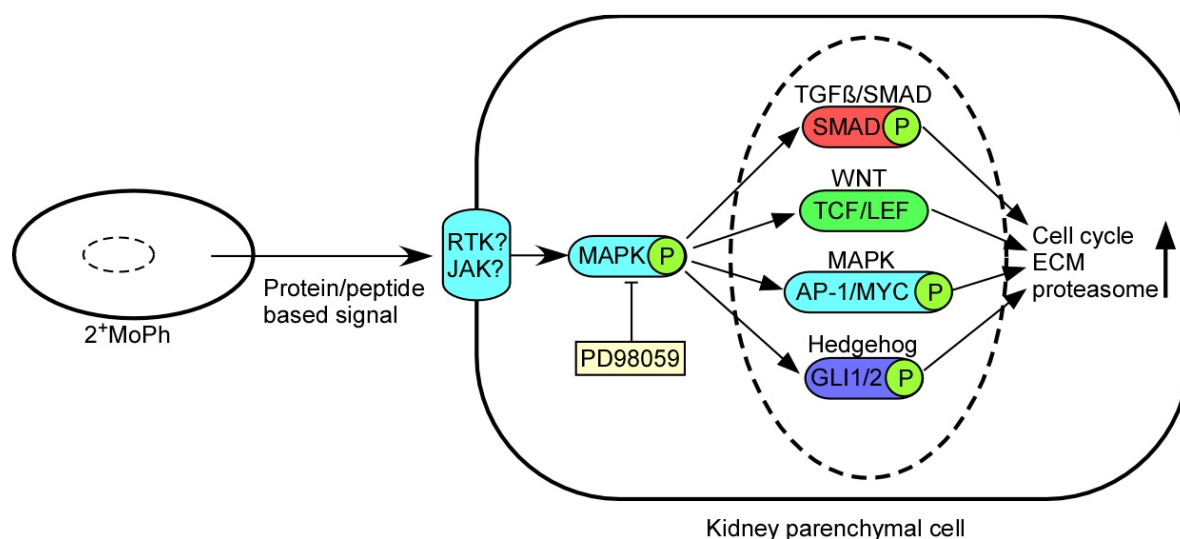


Figure 45. Current interpretation of the observations presented here. Increasing presence of 2⁺MoPh caused by metabolic changes in diabetes leads to increased secretion of growth factors that cause the activation of MAPK signaling in the kidney parenchyma via a receptor, potentially an RTK. Activation of MAPK signaling leads to secondary activation of TGFβ, WNT and Hedgehog signaling. As a consequence, cell cycle genes, ECM production and proteasome activity are dysregulated, contributing to kidney damage as the disease progresses.

Based on the findings discussed here, we propose the following model. Due to the tissue stress situation caused by diabetes, an enhanced recruitment of myeloid cells into the tubular interstitium of the kidney leads to increased levels of the macrophage like 2⁺MoPh phenotype. This renal myeloid phenotype in turn secretes growth factors that can directly influence kidney parenchyma, causing the activation of an RTK or JAK-like receptor, leading to phosphorylation and activation of a MAPK associated signaling pathway. MAPK signaling then causes activation of additional homeostatic pathways (Hedgehog, WNT, SMAD) either by phosphorylation of their components, or direct interaction of the MAPK linked AP-1 or MYC transcription factors with pathway specific TFs. The potential signals mediating the activation of these pathways were shown to be soluble, not associated with exosomes, and to be probably protein/peptide based. Harvested supernatants were analyzed using proteomic platforms yielding potential candidate factors.

As a consequence, a homeostatic shift towards fibrosis, cell cycle alterations and proteasome activation occurs, contributing to disruptions of the kidney fine structure and gradual loss of function. The amount of 2⁺MoPh increases during disease progression, potentially exacerbated by a feedback mechanism caused by the high expression levels of the myeloid cell chemotractor CCL2 found in 2⁺MoPh.

Potential treatment strategies to target this biology include a blockade of CCR2 signaling to reduce the influx of myeloid infiltrates into the kidney, and targeting the proteasome to reduce signals leading to the activation of MAPK signaling processes. Identification of the pivotal signaling molecules could allow for more specific clinical intervention to suppress damaging changes to the kidney fine structure.

6 Addendum

6.1 Supplemental tables

6.1.1 Full list of dysregulated pathways from 4.1.1

Pathway	Genomatix Pathway id	p-value	Obs	Exp
IMMUNE	PW_IMMUNE_HOMO_SAPIENS	4.54E-18	93	35.9
INFLAMMATORY	PW_INFLAMMATORY_HOMO_SAPIENS	3.33E-14	80	32.7
MATRIX METALLOPROTEINASE	PW_MMP_HOMO_SAPIENS	3.24E-10	51	19.9
INTEGRIN	PW_INTEGRIN_HOMO_SAPIENS	4.11E-10	46	17.0
CHEMOKINE (C C MOTIF) LIGAND 2	PW_CCL2_HOMO_SAPIENS	6.50E-10	30	8.4
TOLL LIKE RECEPTOR	PW_TOLL_HOMO_SAPIENS	2.71E-09	46	18.0
ANGIOGENESIS	PW_ANGIOGENESIS_HOMO_SAPIENS	2.66E-08	47	19.9
TUMOR NECROSIS FACTOR (TNF SUPERFAMILY, MEMBER 2)	PW_TNF_HOMO_SAPIENS	2.82E-07	46	20.8
INTERLEUKIN 6 (INTERFERON, BETA 2)	PW_IL6_HOMO_SAPIENS	4.11E-07	36	14.6
ZETA CHAIN (TCR) ASSOCIATED PROTEIN KINASE 70KDA	PW_ZAP_70_HOMO_SAPIENS	7.28E-07	22	6.8
THROMBOSPONDIN 1	PW_THBS1_HOMO_SAPIENS	9.15E-07	17	4.4
NF KAPPA B	PW_NFKB_HOMO_SAPIENS	9.24E-07	64	34.5
T CELL RECEPTOR CD3 COMPLEX	PW_CD3_HOMO_SAPIENS	9.35E-07	24	8.0
INTERLEUKIN 18 (INTERFERON GAMMA INDUCING FACTOR)	PW_IL18_HOMO_SAPIENS	1.72E-06	19	5.6
CD2	PW_CD2_HOMO_SAPIENS	2.70E-06	17	4.7
LYMPHOCYTE SPECIFIC PROTEIN TYROSINE KINASE	PW_LCK_HOMO_SAPIENS	4.97E-06	22	7.6
CHEMOKINE (C C MOTIF) RECEPTOR 2	PW_CCR2_HOMO_SAPIENS	8.04E-06	14	3.6
CADHERIN 1, TYPE 1, E CADHERIN (EPITHELIAL)	PW_CDH1_HOMO_SAPIENS	8.40E-06	30	12.7
V YES 1 YAMAGUCHI SARCOMA VIRAL RELATED ONCOGENE HOMOLOG LCK/YES RELATED NOVEL PROTEIN TYROSINE KINASE	PW_LYN_HOMO_SAPIENS	1.31E-05	24	9.2
PTK2B PROTEIN TYROSINE KINASE 2 BETA	PW_PTK2B_HOMO_SAPIENS	1.72E-05	21	7.6
PROTEIN TYROSINE PHOSPHATASE, RECEPTOR TYPE	PW_PTPR_HOMO_SAPIENS	1.80E-05	25	10.0

Pathway	Genomatix Pathway id	p-value	Obs	Exp
CD36 MOLECULE (THROMBOSPONDIN RECEPTOR)	PW_CD36_HOMO_SAPIENS	2.29E-05	18	6.0
VASCULAR ENDOTHELIAL GROWTH FACTOR	PW_VEGF_HOMO_SAPIENS	2.66E-05	35	16. 8
CHEMOKINE (C C MOTIF) RECEPTOR 7	PW_CCR7_HOMO_SAPIENS	2.88E-05	14	4.0
CD19	PW_CD19_HOMO_SAPIENS	5.10E-05	14	4.2
ATP BINDING CASSETTE, SUB FAMILY B (MDR/TAP)	PW_ABCB_HOMO_SAPIENS	5.25E-05	22	8.8
MYELOID DIFFERENTIATION PRIMARY RESPONSE GENE (88)	PW_MYD88_HOMO_SAPIENS	6.46E-05	24	10. 1
SNAIL FAMILY ZINC FINGER 1	PW_SNAIL_HOMO_SAPIENS	6.60E-05	25	10. 8
NUCLEOTIDE OLIGOMERIZATION DOMAIN/CASPASE RECRUITMENT DOMAIN PROTEIN FAMILY	PW_NOD_HOMO_SAPIENS	9.24E-05	22	9.1
CLASSICAL COMPLEMENT	PW_CLASSICAL_COMPLEMENT_HO MO_SAPIENS	1.01E-04	12	3.4
INTERLEUKIN 1	PW_IL1_HOMO_SAPIENS	1.28E-04	31	15. 3
FOCAL ADHESION KINASE 1	PW_FAK_HOMO_SAPIENS	1.56E-04	34	17. 6
HEPATOCTYTE GROWTH FACTOR RECEPTOR	PW_HGF_HOMO_SAPIENS	1.59E-04	23	10. 1
TISSUE INHIBITOR OF METALLOPROTEINASE	PW_TIMP_HOMO_SAPIENS	1.62E-04	17	6.3
MOTHERS AGAINST DPP HOMOLOG	PW_SMAD_HOMO_SAPIENS	1.87E-04	49	29. 0
JANUS KINASE	PW_JAK_HOMO_SAPIENS	1.99E-04	30	15. 0
NITRIC OXIDE	PW_NITRIC_OXIDE_HOMO_SAPIENS	2.27E-04	25	11. 6
B CELL RECEPTOR	PW_BCR_HOMO_SAPIENS	3.04E-04	24	11. 2
COAGULATION FACTOR II (THROMBIN) RECEPTOR	PW_F2R_HOMO_SAPIENS	3.13E-04	15	5.5
PLATELET/ENDOTHELIAL CELL ADHESION MOLECULE 1 (CD31)	PW_PECAM1_HOMO_SAPIENS	3.58E-04	12	3.9
LYMPHOTOXIN ALPHA (TNF SUPERFAMILY, MEMBER 1)	PW_LTA_HOMO_SAPIENS	3.92E-04	9	2.4
SPLEEN TYROSINE KINASE	PW_SYK_HOMO_SAPIENS	4.86E-04	23	10. 9
RIBONUCLEASE L	PW_RNASEL_HOMO_SAPIENS	6.55E-04	8	2.0
SPHINGOMYELIN PHOSPHODIESTERASE 1, ACID LYOSOMAL	PW_SMPD1_HOMO_SAPIENS	6.55E-04	8	2.0
TOLL LIKE RECEPTOR ADAPTOR MOLECULE 1 (TICAM1)	PW_TRIF_HOMO_SAPIENS	7.86E-04	14	5.4

Pathway	Genomatix Pathway id	p-value	Obs	Exp
INTERLEUKIN 10	PW_IL10_HOMO_SAPIENS	8.71E-04	23	11.3
B CELL TRANSLOCATION GENE (BTG/TOB FAMILY)	PW_BTG_HOMO_SAPIENS	9.00E-04	10	3.1
ALTERNATIVE COMPLEMENT	PW_ALTERNATIVE_COMPLEMENT_HOMO_SAPIENS	9.00E-04	10	3.1
CCAAT/ENHANCER BINDING PROTEIN (C/EBP), ALPHA	PW_CEBPA_HOMO_SAPIENS	1.07E-03	15	6.1
T CELL RECEPTOR	PW_TCR_HOMO_SAPIENS	1.08E-03	30	16.5
GUANINE NUCLEOTIDE EXCHANGE FACTOR VAV	PW_VAV_HOMO_SAPIENS	1.17E-03	20	9.5
DOUBLE STRANDED RNA DEPENDENT PROTEIN KINASE/EUKARYOTIC INITIATION FACTOR 2ALPHA	PW_PKR_HOMO_SAPIENS	1.49E-03	15	6.3
INTERLEUKIN 3 (COLONY STIMULATING FACTOR, MULTIPLE)	PW_IL3_HOMO_SAPIENS	1.51E-03	16	7.0
SIGNAL TRANSDUCER AND ACTIVATOR OF TRANSCRIPTION	PW_STAT_HOMO_SAPIENS	1.66E-03	41	25.5
LOW DENSITY LIPOPROTEIN RECEPTOR RELATED PROTEIN	PW_LRP_HOMO_SAPIENS	1.74E-03	23	11.9
PHOSPHOLIPASE C	PW_PLC_HOMO_SAPIENS	1.95E-03	26	14.2
CYCLIC ADP RIBOSE HYDROLASE (CD38)	PW_CD38_HOMO_SAPIENS	2.32E-03	11	4.1
TYROSINE PROTEIN KINASE SRC	PW_SRC_HOMO_SAPIENS	2.37E-03	38	23.6
STRESS	PW_STRESS_HOMO_SAPIENS	2.38E-03	37	22.8
COLONY STIMULATING FACTOR 1	PW_CSF1_HOMO_SAPIENS	3.02E-03	14	6.1
INTERLEUKIN 4	PW_IL4_HOMO_SAPIENS	3.03E-03	19	9.5
CAVEOLIN 1	PW_CAVEOLIN_HOMO_SAPIENS	3.21E-03	16	7.5
PARATHYROID HORMONE	PW_PTH_HOMO_SAPIENS	3.30E-03	15	6.9
PHOSPHOLIPASE A2	PW_PLA2_HOMO_SAPIENS	3.30E-03	15	6.9
INTERLEUKIN 12	PW_IL12_HOMO_SAPIENS	3.36E-03	17	8.2
CADHERIN 5, TYPE 2 (VASCULAR ENDOTHELIUM)	PW_CDH5_HOMO_SAPIENS	3.39E-03	11	4.3
VERY LOW DENSITY LIPOPROTEIN RECEPTOR	PW_VLDLR_HOMO_SAPIENS	3.94E-03	7	2.1
CALCIUM	PW_CALCIIUM_HOMO_SAPIENS	4.10E-03	59	41.8
INTEGRIN LINKED KINASE	PW_ILK_HOMO_SAPIENS	4.32E-03	15	7.1
CHEMOKINE (C X C MOTIF) RECEPTOR 4	PW_CXCR4_HOMO_SAPIENS	4.91E-03	16	7.8
TGF BETA	PW_TGFBR_HOMO_SAPIENS	5.15E-03	67	49.1

Pathway	Genomatix Pathway id	p-value	Obs	Exp
CCAAT/ENHANCER BINDING PROTEIN (C/EBP), BETA	PW_CEBPB_HOMO_SAPIENS	5.33E-03	16	7.9
NITRIC OXIDE SYNTHASE	PW_NOS_HOMO_SAPIENS	5.42E-03	20	10.8
BETA CATENIN	PW_BETA CATENIN_HOMO_SAPIENS	5.75E-03	56	39.9
F BOX AND WD REPEAT DOMAIN CONTAINING 7	PW_FBXW7_HOMO_SAPIENS	5.77E-03	10	4.0
ADIPOQ	PW_ADIPONECTIN_HOMO_SAPIENS	6.01E-03	13	6.0
NUCLEAR RECEPTOR SUBFAMILY 0, GROUP B, MEMBER 2	PW_NR0B2_HOMO_SAPIENS	7.74E-03	9	3.5
NUCLEAR RECEPTOR SUBFAMILY 4, GROUP A, MEMBER 3	PW_NR4A3_HOMO_SAPIENS	7.99E-03	5	1.3
PEROXISOME PROLIFERATOR ACTIVATED RECEPTOR DELTA	PW_PPARD_HOMO_SAPIENS	8.13E-03	10	4.2
GLYCOGEN SYNTHASE KINASE	PW_GSK_HOMO_SAPIENS	8.18E-03	31	19.7
TYROSINE PROTEIN KINASE FYN	PW_FYN_HOMO_SAPIENS	8.28E-03	21	12.0
CD40 LIGAND	PW_CD40_HOMO_SAPIENS	9.09E-03	11	4.9
INTERFERON (ALPHA, BETA AND OMEGA) RECEPTOR	PW_IFNAR_HOMO_SAPIENS	9.82E-03	9	3.7

Table 9. Full GeneRanker results, supplemental to 4.1.1. Obs. = number of observed genes, Exp. = number of expected genes.

6.1.2 Full gene list from 4.4.3

Geneset	Gene / Module color	Annotation
.14-3-3/HIPPO	YWHAH	tyrosine 3-monooxygenase/tryptophan 5-monooxygenase activation protein eta(YWHAH)
.14-3-3/HIPPO	YWHAZ	tyrosine 3-monooxygenase/tryptophan 5-monooxygenase activation protein zeta(YWHAZ)
?	TBL1XR1	transducin β like 1 X-linked receptor 1(TBL1XR1)
?	AP2B1	adaptor related protein complex 2 β 1 subunit(AP2B1)
?	NRCAM	neuronal cell adhesion molecule(NRCAM)
?	EDN1	endothelin 1(EDN1)
?	PPP2R5B	protein phosphatase 2 regulatory subunit B' β (PPP2R5B)
?	IKBKB	inhibitor of kappa light polypeptide gene enhancer in B-cells, kinase β (IKBKB)
?	CCL4	C-C motif chemokine ligand 4(CCL4)
?	SP3	Sp3 transcription factor(SP3)
cell cycle	CDKN1A	cyclin dependent kinase inhibitor 1A(CDKN1A)
cell cycle	CDK1	cyclin dependent kinase 1(CDK1)
cell cycle	CCND3	cyclin D3(CCND3)
cell cycle	CCNB1	cyclin B1(CCNB1)
cell cycle	CCND2	cyclin D2(CCND2)
cell cycle	CCNB2	cyclin B2(CCNB2)
cell cycle	STIL	SCL/TAL1 interrupting locus(STIL)
cell cycle?	TFDP2	transcription factor Dp-2(TFDP2)
Fibrotic gene	PITX2	paired like homeodomain 2(PITX2)
Fibrotic gene	LGALS3	galectin 3(LGALS3)
Fibrotic gene	CEBPB	CCAAT/enhancer binding protein β (CEBPB)
Fibrotic gene	LAMC1	laminin subunit gamma 1(LAMC1)
Fibrotic gene	FN1	fibronectin 1(FN1)
Fibrotic gene	COL1A2	collagen type I alpha 2 chain(COL1A2)
Fibrotic gene	COL1A1	collagen type I alpha 1 chain(COL1A1)
Fibrotic gene	VCAN	versican(VCAN)
Hippo? Regulates RUNX	CBFB	core-binding factor β subunit(CBFB)
inflammatory	PROC	protein C, inactivator of coagulation factors Va and VIIIa(PROC)
inflammatory	SPP1	secreted phosphoprotein 1(SPP1)
inflammatory	LYN	LYN proto-oncogene, Src family tyrosine kinase(LYN)
inflammatory	ITK	IL2 inducible T-cell kinase(ITK)
kidney TF	HNF1A	HNF1 homeobox A(HNF1A)
MAPK	CAMK2G	calcium/calmodulin dependent protein kinase II gamma(CAMK2G)

Geneset	Gene / Module color	Annotation
MAPK	MAP3K12	mitogen-activated protein kinase kinase kinase 12(MAP3K12)
MAPK	EGF	epidermal growth factor(EGF)
MAPK	MYCN	v-myc avian myelocytomatosis viral oncogene neuroblastoma derived homolog(MYCN)
MAPK	RAF1	Raf-1 proto-oncogene, serine/threonine kinase(RAF1)
MAPK	VEGFA	vascular endothelial growth factor A(VEGFA)
MAPK	LRPAP1	LDL receptor related protein associated protein 1(LRPAP1)
MAPK	GRB2	growth factor receptor bound protein 2(GRB2)
MAPK	SNX4	sorting nexin 4(SNX4)
MAPK	RAC3	ras-related C3 botulinum toxin substrate 3 (rho family, small GTP binding protein Rac3)(RAC3)
MAPK	RHOA	ras homolog family member A(RHOA)
MAPK	EGR1	early growth response 1(EGR1)
MAPK	ETS2	ETS proto-oncogene 2, transcription factor(ETS2)
MAPK	STAT1	signal transducer and activator of transcription 1(STAT1)
MAPK	MYC	v-myc avian myelocytomatosis viral oncogene homolog(MYC)
MAPK	UBE2I	ubiquitin conjugating enzyme E2 I(UBE2I)
MAPK	JAK1	Janus kinase 1(JAK1)
MAPK	VEGFC	vascular endothelial growth factor C(VEGFC)
MAPK	CALM2	calmodulin 2(CALM2)
MAPK	GNAS	GNAS complex locus(GNAS)
MAPK	FOS	Fos proto-oncogene, AP-1 transcription factor subunit(FOS)
MAPK	JUNB	JunB proto-oncogene, AP-1 transcription factor subunit(JUNB)
MAPK	FHL2	four and a half LIM domains 2(FHL2)
MAPK	JUN	Jun proto-oncogene, AP-1 transcription factor subunit(JUN)
MAPK	MET	MET proto-oncogene, receptor tyrosine kinase(MET)
MAPK	ARF5	ADP ribosylation factor 5(ARF5)
MAPK	TRRAP	transformation/transcription domain associated protein(TRRAP)
MAPK	SHC1	SHC adaptor protein 1(SHC1)
MAPK	RAC2	ras-related C3 botulinum toxin substrate 2 (rho family, small GTP binding protein Rac2)(RAC2)
MAPK	ARHGEF6	Rac/Cdc42 guanine nucleotide exchange factor 6(ARHGEF6)
MAPK	RYK	receptor-like tyrosine kinase(RYK)
MAPK	CXCL8	C-X-C motif chemokine ligand 8(CXCL8)

Geneset	Gene / Module color	Annotation
MAPK	TIAM1	T-cell lymphoma invasion and metastasis 1(TIAM1)
MAPK	FGR	FGR proto-oncogene, Src family tyrosine kinase(FGR)
MAPK	DAPP1	dual adaptor of phosphotyrosine and 3-phosphoinositides 1(DAPP1)
MAPK	HCK	HCK proto-oncogene, Src family tyrosine kinase(HCK)
MAPK	MAP3K8	mitogen-activated protein kinase kinase kinase 8(MAP3K8)
MAPK	MEF2C	myocyte enhancer factor 2C(MEF2C)
MAPK	ARRB1	arrestin β 1(ARRB1)
MAPK	MAP3K5	mitogen-activated protein kinase kinase kinase 5(MAP3K5)
MAPK	LCK	LCK proto-oncogene, Src family tyrosine kinase(LCK)
MAPK	EFNB2	ephrin B2(EFNB2)
MAPK associated	AKT1	AKT serine/threonine kinase 1(AKT1)
MAPK, among others	TP53	tumor protein p53(TP53)
MAPK/EGF	CELSR1	cadherin EGF LAG seven-pass G-type receptor 1(CELSR1)
MAPK/PI3K family member	PRKDC	protein kinase, DNA-activated, catalytic polypeptide(PRKDC)
MAPK/TGF β	PTEN	phosphatase and tensin homolog(PTEN)
MAPK?	CALM1	calmodulin 1(CALM1)
MTOR	MTOR	mechanistic target of rapamycin(MTOR)
MTOR	FKBP1A	FK506 binding protein 1A(FKBP1A)
Notch	MAML1	mastermind like transcriptional coactivator 1(MAML1)
nuclear importer	KPNA2	karyopherin subunit alpha 2(KPNA2)
Proteasome	PSMC2	proteasome 26S subunit, ATPase 2(PSMC2)
proteasome	PSMA2	proteasome subunit alpha 2(PSMA2)
proteasome	PSMB9	proteasome subunit β 9(PSMB9)
proteasome	PSMB8	proteasome subunit β 8(PSMB8)
proteasome	UBE2D1	ubiquitin conjugating enzyme E2 D1(UBE2D1)
proteasome	CUL1	cullin 1(CUL1)
proteasome	PSMB10	proteasome subunit β 10(PSMB10)
proteasome	PSMA4	proteasome subunit alpha 4(PSMA4)
proteasome	RBX1	ring-box 1(RBX1)
proteasome	HSPA5	heat shock protein family A (Hsp70) member 5(HSPA5)
proteasome	UBE2E1	ubiquitin conjugating enzyme E2 E1(UBE2E1)

Geneset	Gene / Module color	Annotation
regulation of transcription	HDAC6	histone deacetylase 6(HDAC6)
regulation of transcription	RBBP7	RB binding protein 7, chromatin remodeling factor(RBBP7)
MAPK target/TGF β	GJA1	gap junction protein alpha 1(GJA1)
TGF β	TGFBR2	transforming growth factor β receptor 2(TGFBR2)
TGF β	MMP7	matrix metalloproteinase 7(MMP7)
TGF β	ENG	endoglin(ENG)
TGF β	ZEB1	zinc finger E-box binding homeobox 1(ZEB1)
TGF β /BMP	BMP2	bone morphogenetic protein 2(BMP2)
TGF β /HIPPO	CTGF	connective tissue growth factor(CTGF)
TGF β /HIPPO	CYR61	cysteine rich angiogenic inducer 61(CYR61)
WNT	WNT8B	Wnt family member 8B(WNT8B)
WNT	LRP6	LDL receptor related protein 6(LRP6)
WNT	FZD7	frizzled class receptor 7(FZD7)
WNT	CSNK1A1	casein kinase 1 alpha 1(CSNK1A1)
WNT	CSNK1G3	casein kinase 1 gamma 3(CSNK1G3)
WNT	CDH1	cadherin 1(CDH1)
WNT	MACF1	microtubule-actin crosslinking factor 1(MACF1)
WNT	FZD6	frizzled class receptor 6(FZD6)
WNT	TLE1	transducin like enhancer of split 1(TLE1)
WNT	WNT7A	Wnt family member 7A(WNT7A)
WNT	FZD10	frizzled class receptor 10(FZD10)
WNT	WNT2B	Wnt family member 2B(WNT2B)
WNT	FRZB	frizzled-related protein(FRZB)
WNT	FZD2	frizzled class receptor 2(FZD2)
WNT target	CD44	CD44 molecule (Indian blood group)(CD44)
WNT/Hedgehog	VDR	vitamin D (1,25- dihydroxyvitamin D3) receptor(VDR)
WNT/Hedgehog	GPC4	glypican 4(GPC4)
WNT	MDFIC	MyoD family inhibitor domain containing(MDFIC)

Table 10. Full list of dysregulated and 2⁺MoPh correlated genes, supplemental to 4.4.3

6.2 Proof of principle and validation of reporter tools

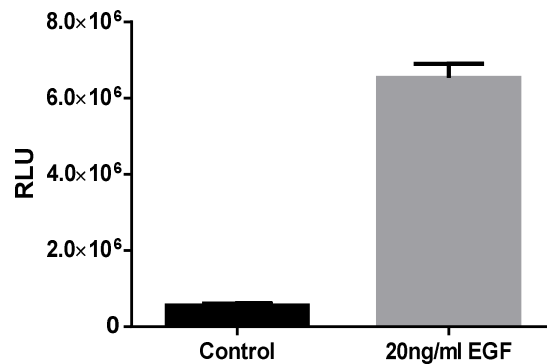


Figure 46. Stimulation of Hedgehog reporter HEK293 cells with recombinant human EGF protein. To assess activity of the GLI reporter cassette, stable transfected HEK293 cells were treated with 20ng/ml EGF for 48 hours after which reporter activity was assessed. Treatment with EGF strongly activates the GLI transcription factors.

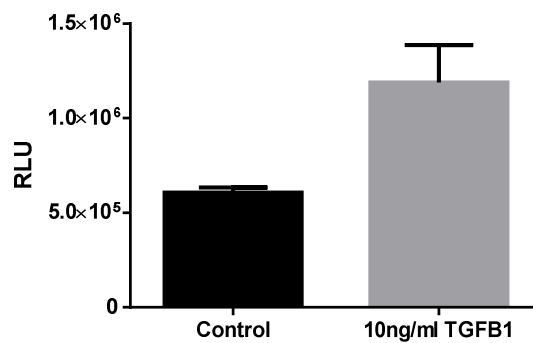


Figure 47. Stimulation of TGFβ/SMAD reporter HEK293 cells with recombinant human TGFB1 protein. To assess activity of the TGFβ/SMAD reporter cassette, stable transfected HEK293 cells were treated with 10ng/ml TGFB1 for 48 hours after which reporter activity was assessed. Treatment with TGFB1 strongly activates the SMAD transcription factors.

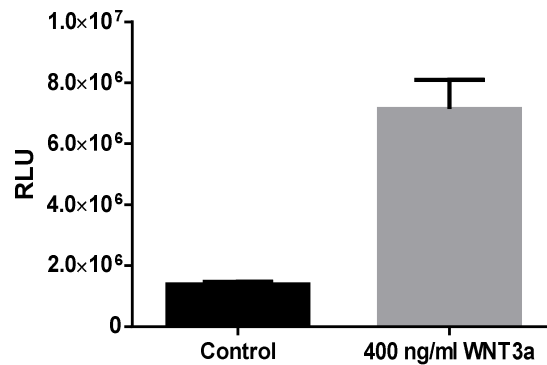


Figure 48. Stimulation of canonical WNT reporter HEK293 cells with recombinant human WNT3A protein. To assess activity of the TCF/LEF reporter cassette, stable transfected HEK293 cells were treated with 400ng/ml WNT3A for 48 hours after which reporter activity was assessed. Treatment with WNT3A strongly activates the TCF/LEF transcription factors.

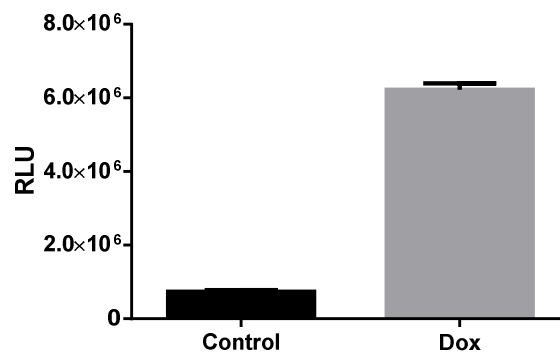


Figure 49. Canonical WNT reporter TCF7 overexpression: Stable Hek293 WNT reporter cells were transfected with a Doxycycline-inducible TCF7 overexpression construct. Overexpression of TCF7 leads to greatly induced WNT Reporter activity.

6.3 Flow cytometric characterization of myeloid cell lines

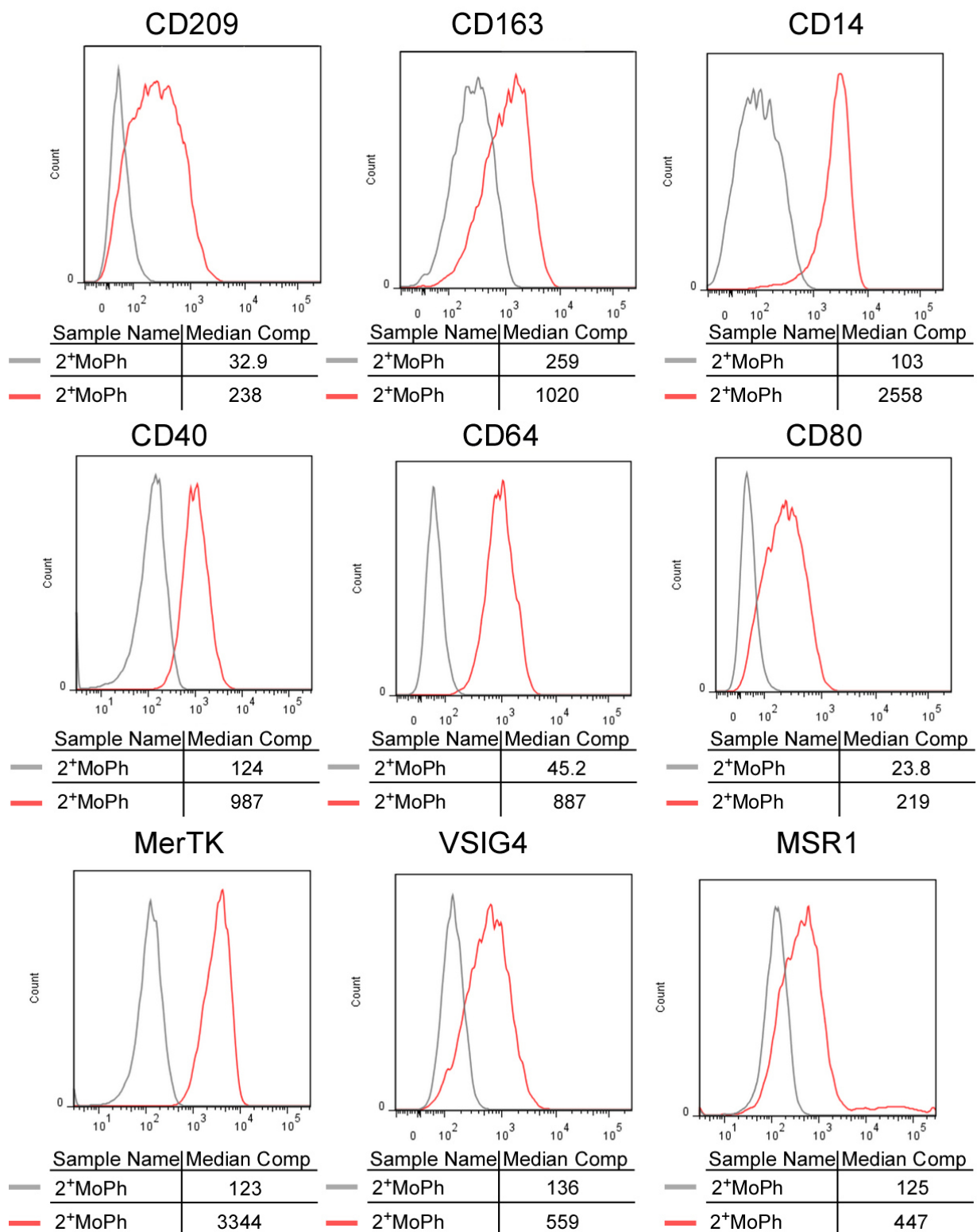


Figure 50. Flow cytometric characterization of 2⁺MoPh cells

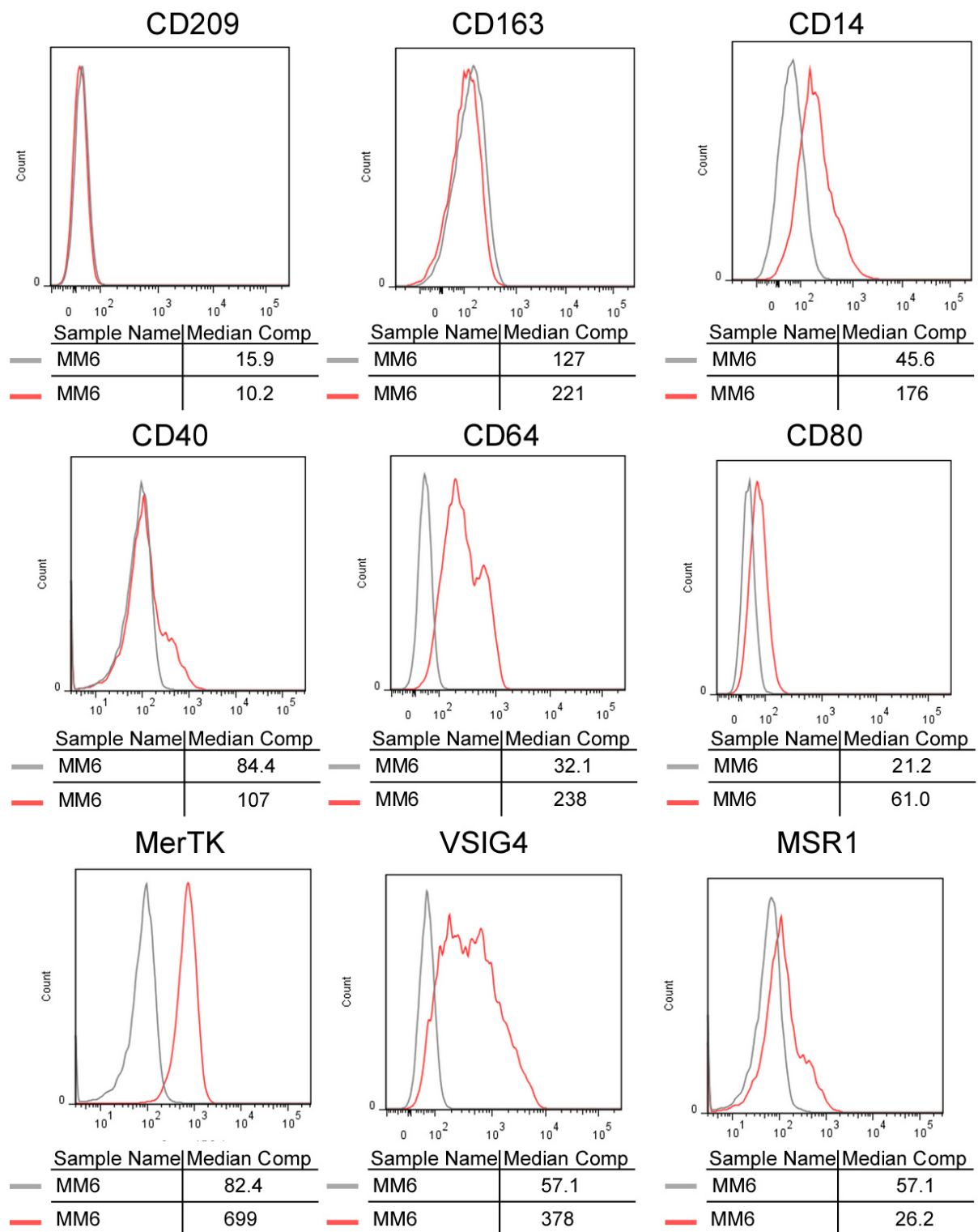


Figure 51. Flow cytometric characterization of Mono-Mac-6 (MM6) cells

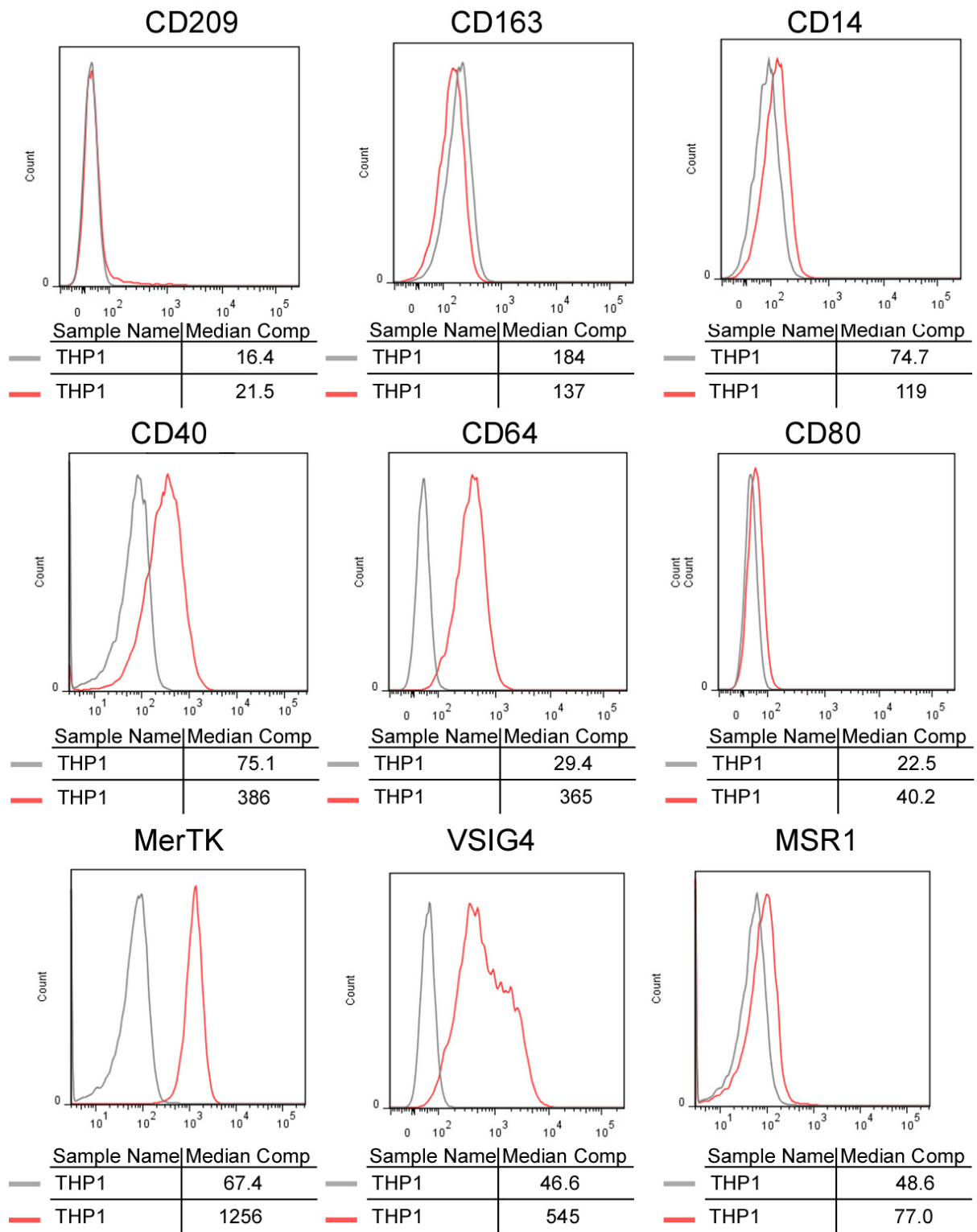


Figure 52. Flow cytometric characterization of THP1 cells

6.3.1 AP-1 reporter titration with Mono-Mac-6 cells

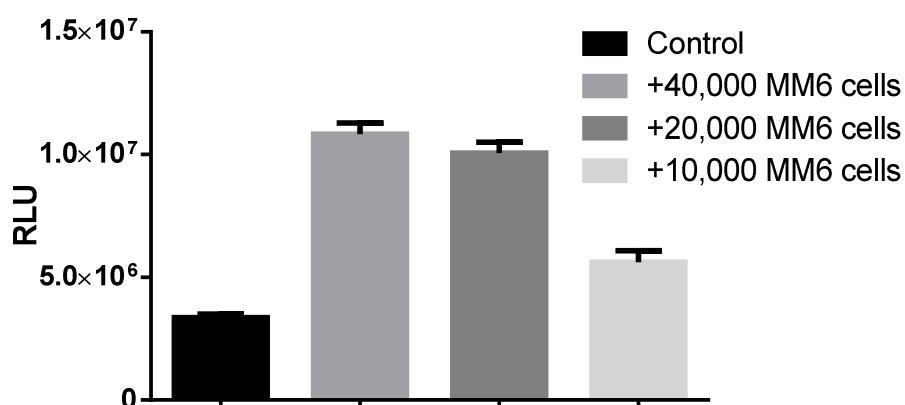


Figure 53. Hek293 AP-1 reporter, Mono-Mac-6 Co-culture

HEK293 cells were co-incubated for 48 with either 40,000, 20,000 or 10,000 or Mono-Mac-6 cells. After 48 hours Luciferase activity was measured. A strong and dose dependent activation of the reporter construct could be seen.

6.4 Additional characterization of LXR signaling

The Liver X Receptor (LXR) family of nuclear receptor has been implicated in myeloid regulation and activation and was thus an interesting target [183, 185]. Additionally we had seen that HEK293 LXR reporter cells get activated to a significant degree during the co-culture experiments with 2⁺MoPh and imDC cells. To better understand the underlying mechanisms, a number of LXR modulation experiments were done using the synthetic, non-steroidal LXR ligand GW3965 [208] and engineered reporter / LXR expression cells.

6.4.1 Elucidation of the modulatory effect of LXR Signaling on homeostatic signaling pathways

As an important tool for crosstalk studies, HEK293 cells carrying a reporter construct and an inducible NR1H2 (LXR β) or NR1H3 (LXR α) expression construct were generated. LXR reporter cells with NR1H2 / NR1H3 served as an important internal control, to prove the bioactivity of the LXR constructs. These cells were stimulated with Doxycycline, to activate expression of the transgene, and/or the synthetic LXR agonist GW3965 to activate LXR activity in a highly specific manner. Since the cells carry the

reporter for LXR activity the effects of both GW3965 and the expression of the transgene could be directly detected.

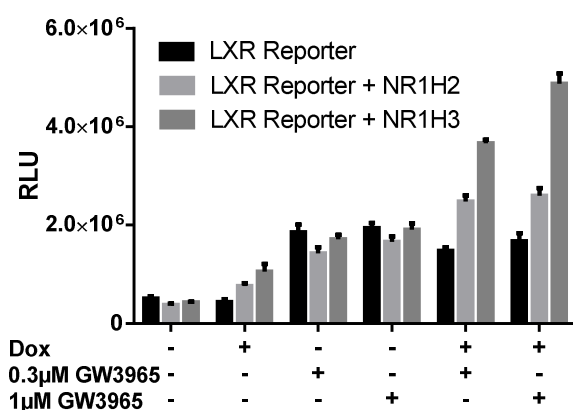


Figure 54. Inducible LXR overexpression and treatment with GW3965. Stable Hek293 LXR Reporter cells were transfected with Doxycycline inducible LXR alpha and beta (NR1H3, NR1H2) overexpression constructs. Upon induction for 48 hours, the cells showed more LXR activity due to overexpression. Stimulation with only GW3965 for the same time frame lead to increased activity, same as cells carrying only the reporter. Combined treatment with Doxycycline and GW3965 showed additive effects. 4 wells per group, single experiment.

The experiment shows that the generated LXR expression constructs are bioactive and have an additive effect with GW3965 treatment. Additionally the LXR antagonist GSK2033 was used to inhibit LXR signaling.

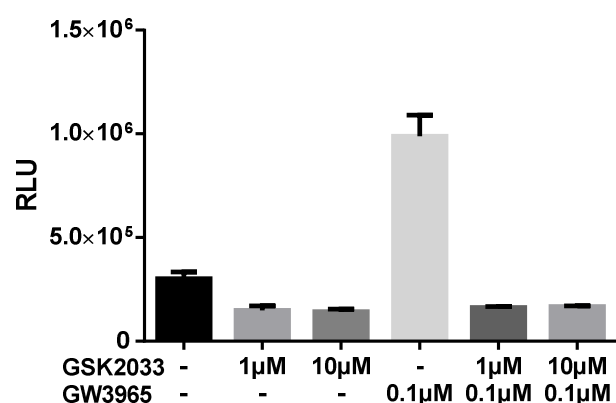


Figure 55. Effects of the LXR antagonist GSK2033 on LXR reporter cells. 20,000 Hek293 LXR reporter cells were treated with GSK2033, GW3965 or both for 48 hours. GSK2033 greatly reduced reporter activity. 3 wells per treatment group, experiment representative of 2 individual experiments.

6.4.2 Crosstalk between LXR and other pathways

To assess the effects LXR signaling can have on other pathways, HEK293 reporter cells for other 2⁺MoPh and imDC modulated pathways were stimulated with GW3965 to activate LXR signaling.

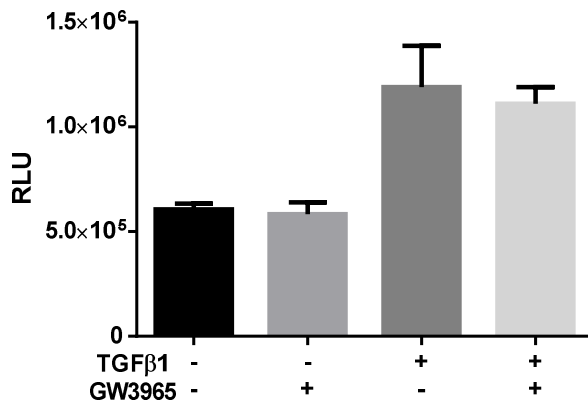


Figure 56. Hek293 TGFβ reporter cells stimulation with recombinant TGFB1 and GW3965. Hek cells stably transfected with a TGFβ reporter plasmid were treated with either 10ng/ml TGFB1 alone or TGFB1 + 0.3μM GW3965 for 48hours. GW3965 had no impact on activation. 3 wells per group, experiment representative of two individual experiments.

TGFβ signaling was not modulated by addition of GW3965, independent on whether that pathway was activated by adding recombinant human TGFβ or not.

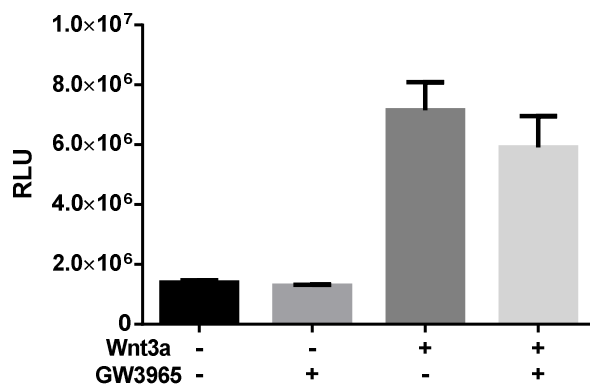


Figure 57. Hek293 WNT reporter cells stimulation with recombinant Wnt3a and GW3965. Hek cells stably transfected with a WNT reporter plasmid were treated with either 400ng/ml WNT3A or WNT3A + 0.3μM GW3965 for 48 hours. GW3965 had limited impact on activation. 3 wells per group, experiment representative of two individual experiments.

Similarly, GW3965 treatment did not impact the activation of the WNT reporter cells with recombinant human WNT3A protein.

As there is no known 'simple' activation method for the Hippo pathway, cells were seeded out dilute (analogous to 6.5) with or without added GW3965. No differences in Hippo activation state could be detected with GW3965.

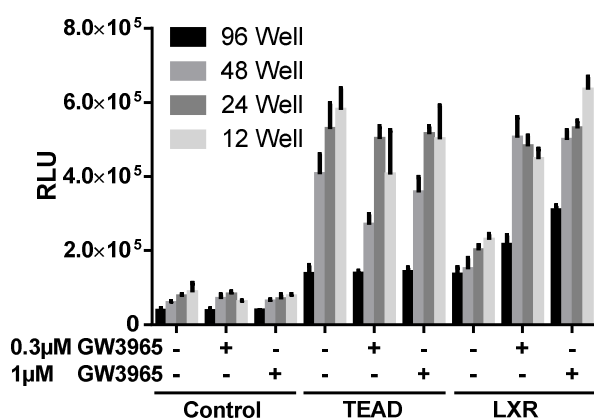


Figure 58. Impact of GW3965 on the Hippo Pathway. 60,000 Hek TEAD or LXR reporter cells were seeded out in various well sizes for 48 hours. The Hippo Pathway activity is strongly regulated by cell density and greatly activated by seeding in subconfluent cell numbers. LXR activation, via GW3965, does not modulate this activation, but activates the LXR reporter. Control cells carrying an empty pseudo-reporter construct

were included to control for cytotoxic effects. 3 wells per group, experiment representative of two individual experiments.

In a next set of experiments, the effect of GW3965 was to be 'magnified' by engineering the same reporter cells with inducible NR1H2 / NR1H3 expression constructs. The idea was that the reporter cells potentially had too low expression levels of NR1H2 / NR1H3 to detect the usually comparably weak crosstalk effects.

TGFβ/SMAD reporter cells were transfected with either inducible NR1H2 or inducible NR1H3 overexpression constructs and after selection, seeded out and (pre-)treated with either Doxycycline, GW3965 or recombinant human TGFB1 protein.

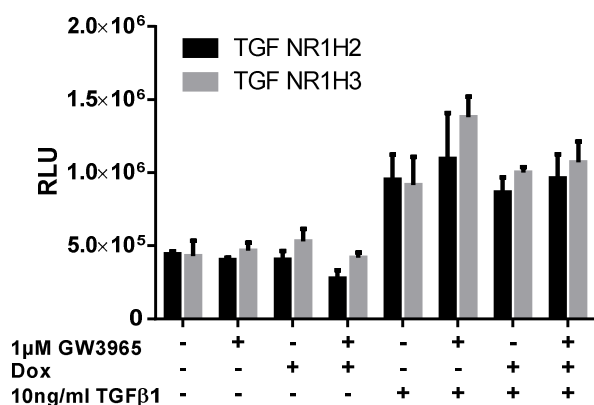


Figure 59. LXR overexpression and stimulation in Hek293 TGFβ reporter cells. Stable Hek293 TGFβ/SMAD Reporter cells were transfected with Doxycycline inducible LXR alpha and beta overexpression constructs. Cells were prestimulated (or not, as control) with Doxycycline for 24 hours, then stimulated with TGFB1 or TGFB1 + 1 μM GW. Overexpression of LXRalpha and beta did not change the effects of

GW3965. 3 wells per group, experiment representative of two individual experiments.

Unfortunately, no significant effects could be detected with added overexpression of NR1H2 or NR1H3. A parallel experiment was done for the WNT reporter cells. WNT reporter cells were transfected with inducible NR1H2 / NR1H3 expression constructs and treated with Doxycycline, recombinant WNT3A and/or GW3965.

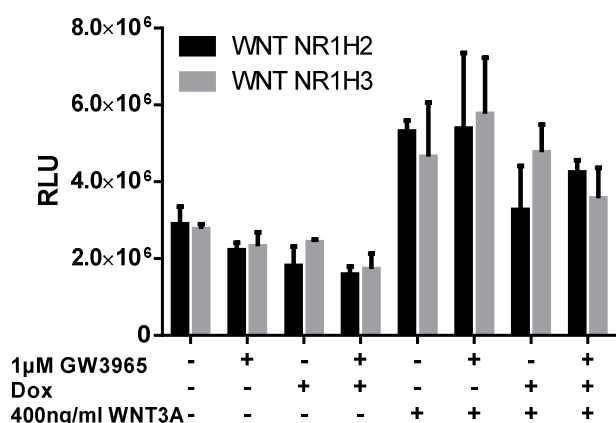


Figure 60. LXR overexpression and stimulation in Hek293 WNT reporter cells. Stable Hek293 WNT Reporter cells were transfected with Doxycycline inducible LXR alpha and beta overexpression constructs. Cells were prestimulated (or not, as control) with Doxycycline for 24 hours, then stimulated with WNT3A or TGFB1 + 1 μM GW. Overexpression of LXRalpha and beta did not change the effects of GW3965. 3 wells per group, experiment representative of

two individual experiments.

The same as for TGFβ/SMAD signaling, no modulation of WNT with doxycycline or GW3965 could be observed. Finally, a third experiment with Hippo reporter cells was done in a similar way. HIPPO reporter cells were transfected with inducible NR1H2 / NR1H3 expression constructs and treated with Doxycycline and/or GW3965 while seeding the same amount of cells in differently sized culture wells.

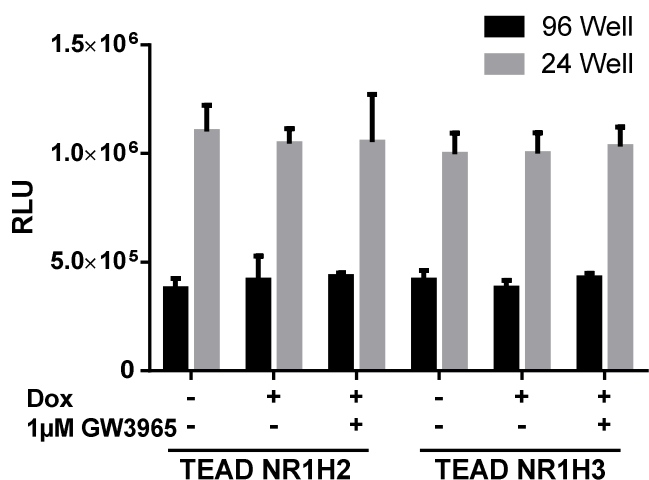


Figure 61. LXR overexpression in Hek293 Hippo Reporter cells. To assess whether an increased dose of NR1H2/H3 expression would lead to modulated Hippo Pathway activity, TEAD reporter cells were transfected with inducible NR1H2/H3 reporter plasmids. Cells were seeded either confluent or diluted and treated with Doxycycline or Doxycycline and GW3965. See next section for particulars on this biology. 4 wells per group, experiment representative of two individual experiments.

Hippo signaling, like TGFβ and canonical WNT signaling was not modulated by GW3965 stimulation.

After ascertaining that the canonical pathways in the reporter cells were not regulated by GW3965 treatment or NR1H2 / NR1H3 overexpression, LXR modulation in myeloid cells was studied.

6.4.3 GW3965 effects on myeloid cell lines

To establish the regulatory effect of GW3965 on myeloid cell lines, experiments using Mono-Mac-6 cells were done. The very first step was to verify that GW3965 used at the same concentrations used for HEK293 cells was not toxic to Mono-Mac-6 cells and by inference 2⁺MoPh and imDCs. As Mono-Mac-6 cells proliferate in cell culture conditions, cell number along with trypan blue staining of dead cells was used to assess toxicity.

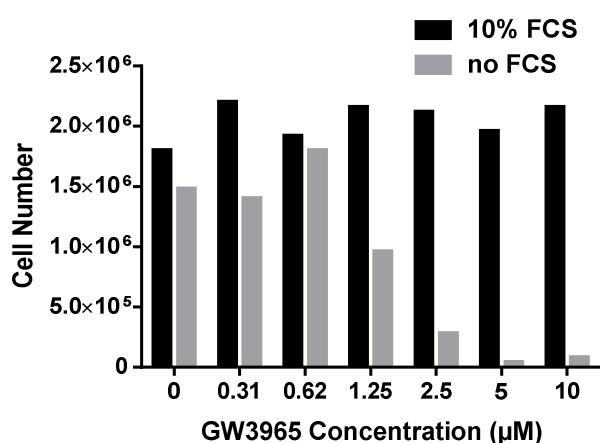


Figure 62. Toxicity of GW3965 on Mono-Mac-6 cells. Mono-Mac-6 cells were cultured either in medium with 10% FCS, or in serum-free medium. GW3965 in the range used was toxic only to cells cultured without FCS. Assessment of viability was done after 48 hours with Trypan-blue staining. Single experiment, two 12wells per treatment group.

The assay showed that concentrations up to 10 µM of GW3965 were not toxic in culture conditions containing serum, in serum free cultures toxicity started at around 1 µM GW3965. Since all previous experiments had been carried out using 1 µM GW3965 and with serum, this would not pose a problem for co-culture studies.

To measure whether GW3965 would regulate the expression of NR1H3 as previously described, qPCR was done on Mono-Mac-6 cells treated with GW3965.

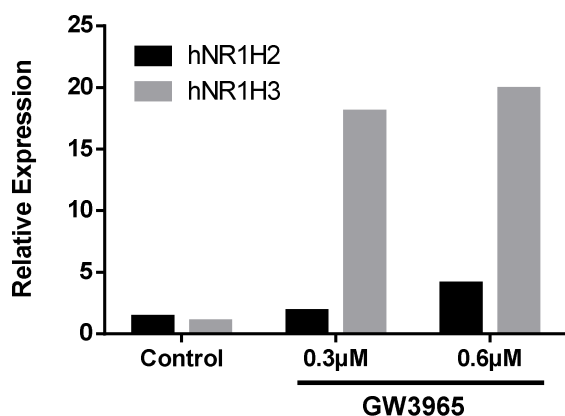


Figure 63. Effect of GW3965 on LXR. Mono-Mac-6 cells were treated with GW3965 for 24 hours, cells were then lysed and qPCR performed. NR1H3 (LXRalpha) is upregulated upon GW3965 treatment. NR1H2 (LXRbeta) is slightly upregulated, but overall remains at comparably low levels. Summary data for 2 wells per treatment group, single experiment.

To test the effect pre-treatment with GW3965 has on myeloid cells, the Mono-Mac-6 model cell line was once again chosen. Mono-Mac-6 cells were pre-treated with serial dilutions of GW3965 for 18 hours, then washed and put into co-culture with HEK293 reporter cell lines. After further 48 hours, reporter activity was measured.

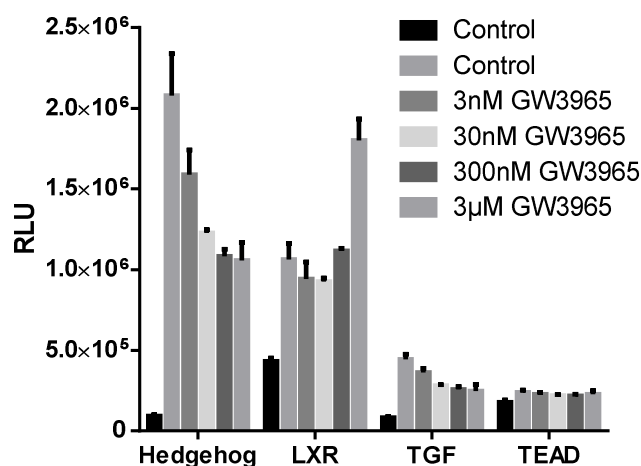


Figure 64. Co-Incubation of Hek293 reporter cells with GW3965 pre-treated Mono-Mac-6 cells. treatment of Mono-Mac-6 cells with GW3965 could modulate the activation Mono-Mac-6 cells confer to Hek reporter cell lines. Mono-Mac-6 cells were treated for 18hours with various concentrations of GW3965 in 10% FCS containing media, afterwards washed with PBS and then cultured in GW3965 free medium together with Hek293 reporter cell lines. Measurements were done after 48h

co-culture. Hedgehog and TGFβ/SMAD signaling were inhibited by presence of GW3965, LXR reporter cells were activated due to GW3965 presence. There was no effect on the Hippo reporter. Three wells per treatment group, experiment representative of two individual experiments.

While LXR activity was increased in a dosage dependent manner, which serves as an internal control, Hedgehog and TGFβ/SMAD signaling were reduced. Hippo was unchanged. To rule out the possibility that GW3965 treatment modulated the reporter cells (except for the LXR reporter line) a parallel experiment was carried out using Mono-Mac-6 conditioned medium concentrated 5X with added GW3965.

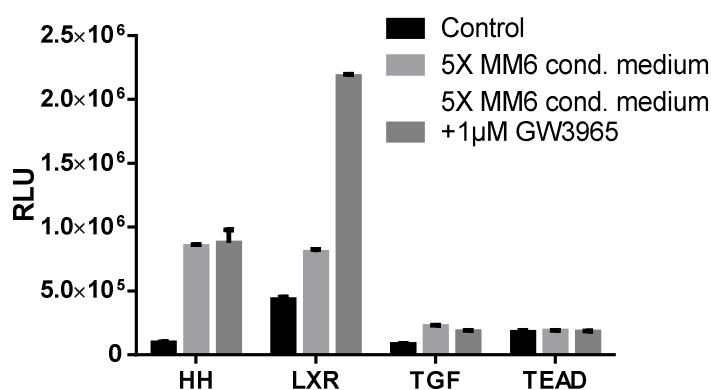


Figure 65. Effect of GW3965 on Hek293 reporter cells under Mono-Mac-6 conditioned media stimulation. To verify that GW3965 does not directly inhibit the Hek293 reporter cells, cells were treated for 48h with either Mono-Mac-6 conditioned medium or the same conditioned medium with added GW3965. GW3965 treatment lead to no difference in signal except for the LXR reporter which can be directly activated with GW3965.

LXR reporter cells serve as internal control for LXR activation and are strongly activated. Three wells per treatment group, experiment representative of two individual experiments.

As expected, GW3965 only modulated the LXR reporter line in addition to the effect seen by addition of Mono-Mac-6 conditioned medium. This shows that any effects witnessed with GW3965 pre-treated Mono-Mac-6 cells occur due to modulation of the Mono-Mac-6 cells, not the parenchymal model HEK293 cells.

6.5 Additional characterization of Hippo signaling

6.5.1 Do the transcriptional co-activators YAP1 and TAZ (WWTR1) modulate the Hedgehog, TGF β , WNT signaling network?

The homeostatic signaling pathways at work in renal development and that coordinately regulate complex processes during wound repair and chronic tissue damage, can be shown to be linked together through crosstalk suggesting that the pathways are really part of a larger regulatory network that drives the specific biologic process [155]. Hippo signaling is an important mediator of responses linked to contact inhibition, cell-cell contact, mechanical cues and certain extracellular factors [88, 89, 99, 170]. As Hippo signaling has been described to crosstalk with TGF β and canonical WNT signaling [96], two pathways strongly modulated by co-incubation with 2⁺MoPh and to a lesser degree imDC cells, the question arose whether Hippo signaling could act as a major contributing factor in the activation state of the regulatory network formed by these pathways. To elucidate the importance of YAP1 and TAZ, the transcriptional co-activators central to the Hippo pathway, first the dynamics of Hippo signaling in HEK293 cells were characterized and then the effects of YAP1 and TAZ overexpression on other pathways studied. The presence of nuclear YAP1 and TAZ in damaged kidney was first established by microscopy.

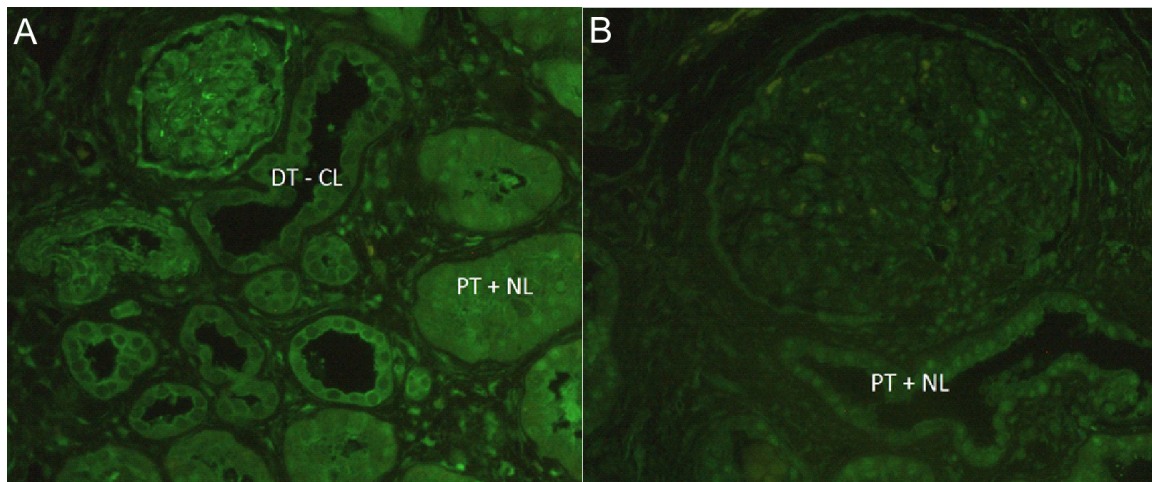


Figure 66. Kidney sections stained for YAP1 or TAZ. For both YAP1 and TAZ nuclear localization can be observed in proximal tubules. Distal tubules exhibit cytoplasmic localization of YAP1/TAZ. (DT = Distal tubulus, PT = Proximal Tubulus, CL=Cytoplasmic Localization, NL= Nuclear Localization)

A first step in establishing activity of the Hippo Reporter construct was to find a way to ensure Hippo activation/deactivation in a previously described manner. To verify the

function of the Hippo/TEAD reporter a simple stimulation experiment is problematic since this pathway is mainly activated by cell-cell contact and mechanical signals. To mimic differences in cell density in a tissue, cells were seeded out diluted, largely depriving them of cell-cell contact and the resulting signals. Practically this was done by seeding the same amount of cells with the same amount of medium in cell culture dishes of varying size.

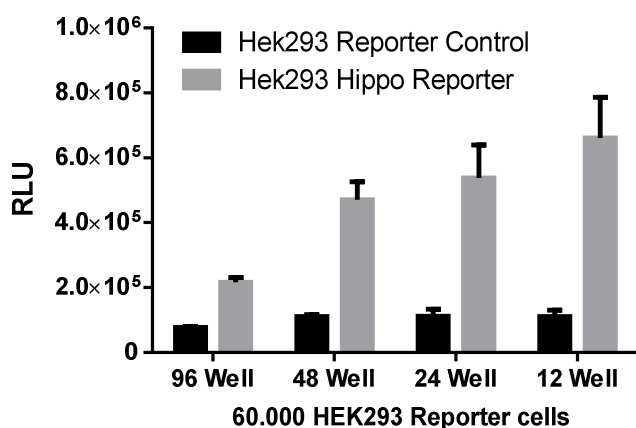


Figure 67. HIPPO/TEAD reporter activity and dilute seeding. Hippo signaling activity increases with reduced cell-cell contact, so seeding 60,000 TEAD reporter cells in larger surface areas for 24 hours increases reporter activity. As a control, a stable cell line carrying an inert reporter element was used. Activity of the control cells does not increase with dilute seeding. Three wells per treatment group, experiment representative of two individual experiments.

Originally the hope was to use one of a few previously described lipid compounds to activate Hippo signaling *in-vitro*. To that end, lysophosphatidic acid (LPA), which had been shown to activate Hippo signaling in MCF10A cells, was used [98]. Since the function of the reporter plasmids had already been ascertained by dilute seeding experiments (see 4.2.6), treatment with LPA and parallel dilute seeding was chosen to contrast stimulation and dilute seeding and potentially magnify the effects of stimulation with LPA.

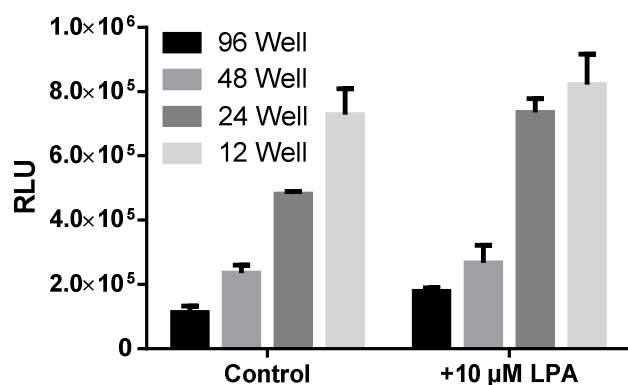


Figure 68. Stimulation of Hek293 TEAD reporter cells with LPA. Hek293 TEAD Reporter cells were treated with LPA (Lysophosphatidic Acid) for 24h with or without decreased cell-cell contact. The general effects of LPA on the TEAD reporter were weak, but measurable. Three wells per treatment group, experiment representative of two individual experiments.

In addition to establishing the Hippo reporter element, inducible overexpression constructs for wildtype and constitutively active mutant versions of YAP1 and TAZ

were generated and tested for bioactivity. In a first experiment, HEK293 Hippo reporter cells were transfected with YAP1 or TAZ constitutively active mutant variants in a Doxycycline inducible manner.

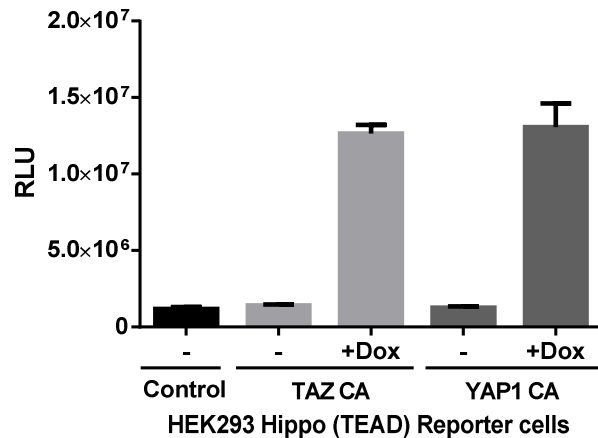


Figure 69. YAP1 / TAZ overexpression in Hippo reporter cells: Stable Hek293 TEAD reporter cells were transfected with Doxycycline-inducible YAP1 / TAZ (WWTR1) overexpression constructs and cultured with or without Doxycycline for 48 hours. Over-expression of YAP1 / TAZ leads to greatly induced TEAD Reporter activity. In this experiment constitutively active (CA) mutant variants of YAP1 and TAZ were used. Three wells per treatment

group, experiment representative of two individual experiments.

While there was an increased signal with LPA treatment, this effect was too weak to be considered for cross-talk studies, where the changes in signal are expected to be much weaker than for the actually targeted Hippo associated TEAD transcription factors. As an additional control for the activating properties of LPA on the Hippo pathway and it's feasibility as an activating agent for cross talk studies HEK293 TEAD reporter cells were engineered with inducible overexpression constructs for Wildtype YAP1 or TAZ(WWTR1) and then stimulated with LPA.

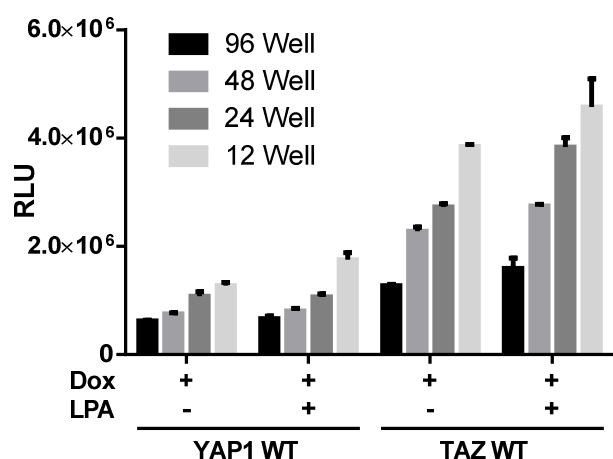


Figure 70. LPA effect on overexpression of wildtype YAP1/TAZ. Hek293 Hippo reporter cells were engineered with inducible overexpression constructs for wildtype YAP1 or TAZ (WWTR1) and stimulated with LPA and or Doxycycline for 48 hours to induce expression of the transgene. While there was a slight increase in reporter activity with added LPA, the differences were too weak to use LPA as a stimulating reagent, even with overexpressed YAP1 /

TAZ(WWTR1). Three wells per treatment group, experiment representative of two individual experiments.

Same as in the Hippo reporter-only Hek293 cells, there was some activating effect of LPA, but this effect was deemed too small for crosstalk studies. In addition to better characterize the reporter, HEK293 cells carrying the inducible YAP1 or TAZ(WWTR1) wildtype expression cassette were seeded dilute (as in fig 67) but with or without induction of the transgene.

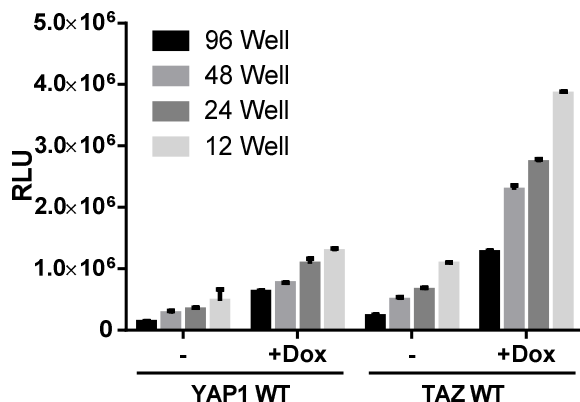


Figure 71. Overexpression of wildtype YAP1/TAZ and effect on dilute seeding. Stable Hek293 TEAD reporter cells were transfected with Doxycyclin-inducible wildtype YAP1/TAZ overexpression constructs and seeded out in varying well sizes. Upon induction the activity of the reporter constructs increased greatly and dependent on the dilution. TAZ overexpression showed stronger activation

potential than YAP1 overexpression. Three wells per treatment group, experiment representative of two individual experiments.

Dilute seeding showed a strong additive effect with overexpression of YAP1 or TAZ(WWTR1), with the TAZ effects being stronger.

Another potential activation mechanism of the Hippo pathway besides dilute seeding, stimulation with lipid compounds like LPA and overexpression of YAP1 and TAZ is the cultivation of the cells on soft substrates to modulate mechanotransduction which will in turn regulate activity of YAP1 and TAZ [44, 88, 170]. To assess the viability of this approach Hippo reporter cells were seeded out on 2.5% Collagen1 gels. This much softer surface was then contrasted to standard plastic surfaces from routine cell culture plates.

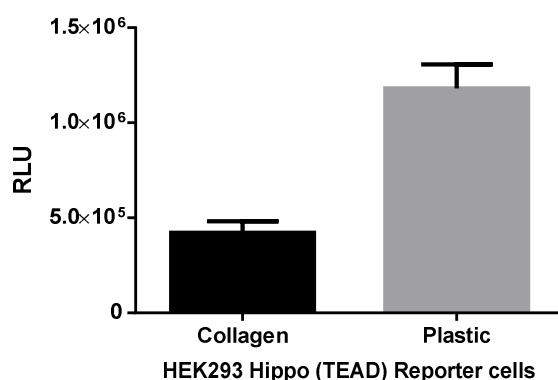


Figure 72. Hippo reporter cells on soft substrates. Hippo reporter cells were plated on soft substrate (2.5% Collagen1 Gel). Cells on soft substrate proliferate less and give less TEAD/Hippo signal. Three wells per treatment group, experiment representative of two individual experiments.

Growth on collagen strongly reduced the activity of the Hippo reporter in contrast to growth on the hard plastic surfaces. Additionally, there was less cell proliferation observable on the soft surface.

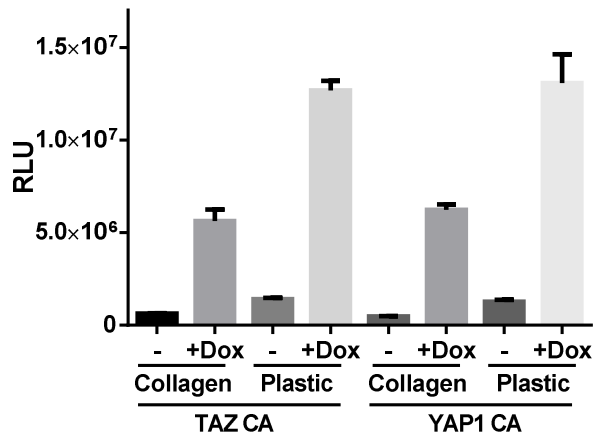


Figure 73. Overexpression of YAP1/TAZ and growth on soft substrates. Hippo reporter cells transfected with inducible YAP1/TAZ constitutively active mutant overexpression constructs were plated on soft substrate (2,5% Collagen1 Gel) and stimulated with Doxycycline. Overexpression of YAP1/TAZ does not restore proliferation to the levels seen on plastic. Three wells per treatment group, experiment representative of two individual experiments.

To see whether the same effect would be observable with overexpressed and constitutively active mutant variants of YAP1 and TAZ(WWTR1) or the effect could be rescued, Hippo reporter cells with inducible expression cassettes for these activate variants were generated and seeded the same way as in fig 67 but with or without added Doxycycline. YAP1 and TAZ overexpression could not rescue the phenotype and growth on soft substrates still caused reduced proliferation, while the reporter constructs were strongly activated with YAP1 and TAZ overexpression. This showed that cultivation on soft in comparison to hard surfaces would introduce experimental artifacts and thus would be a very problematic read-out of YAP1 and TAZ effect on other pathways.

Having assessed these multiple avenues of Hippo activation, the best strategy to assess crosstalk proved to be direct overexpression of constitutively active YAP1 and TAZ(WWTR1) in reporters for other pathways. Overexpression lines of YAP1 / TAZ(WWTR1) were established for the TGF β /SMAD, canonical WNT and the Hedgehog reporter. Each line was seeded out and treated with Doxycycline for 48 hours or not.

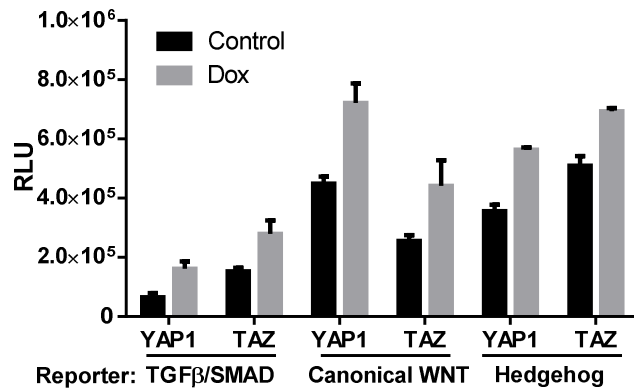


Figure 74. YAP1 / TAZ Overexpression in Hek293 TGFβ, WNT and Hedgehog reporter cells. Stable Hek293 TGFβ, WNT or Hedgehog reporter cells were transfected with Doxycycline - inducible YAP1 / TAZ(WWTR1) constitutively active mutant constructs and treated with Doxycycline or not. Upon Doxycycline treatment the activity of the reporters was increased, though not to the same extent as with

myeloid cell co-culture. Three wells per treatment group, single experiment for each pathway.

Overexpression of YAP1 and TAZ(WWTR1) activated each pathway to a small but significant degree, and much less than the effects of co-culture with myeloid cells or cell lines. This shows that while Hippo signaling may be a contribution factor for the effects exhibited by co-culture with myeloid cells, it most certainly is not the key modulating component. So the nature of the myeloid signal had to be further determined.

7 References

1. Thomas, R., A. Kalso, and J.R. Sedor, *Chronic Kidney Disease and Its Complications*. Primary care, 2008. **35**(2): p. 329-vii.
2. Rahman, M. and M.C. Smith, *Chronic renal insufficiency: a diagnostic and therapeutic approach*. Arch Intern Med, 1998. **158**(16): p. 1743-52.
3. Eknoyan, G., et al., *The burden of kidney disease: improving global outcomes*. Kidney Int, 2004. **66**(4): p. 1310-4.
4. Tonelli, M., et al., *Chronic kidney disease and mortality risk: a systematic review*. J Am Soc Nephrol, 2006. **17**(7): p. 2034-47.
5. Eckardt, K.U. and B.L. Kasiske, *Kidney disease: improving global outcomes*. Nat Rev Nephrol, 2009. **5**(11): p. 650-7.
6. Heidenheim, A.P., M.P. Kooistra, and R.M. Lindsay, *Quality of life*. Contrib Nephrol, 2004. **145**: p. 99-105.
7. de Francisco, A.L. and C. Pinera, *Challenges and future of renal replacement therapy*. Hemodial Int, 2006. **10 Suppl 1**: p. S19-23.
8. Weiner, D.E., *Causes and consequences of chronic kidney disease: implications for managed health care*. J Manag Care Pharm, 2007. **13**(3 Suppl): p. S1-9.
9. Webb, S. and G. Dobb, *ARF, ATN or AKI? It's now acute kidney injury*. Anaesth Intensive Care, 2007. **35**(6): p. 843-4.
10. Makris, K. and L. Spanou, *Acute Kidney Injury: Diagnostic Approaches and Controversies*. Clin Biochem Rev, 2016. **37**(4): p. 153-175.
11. Reid, J., et al., *A literature review of end-stage renal disease and cachexia: understanding experience to inform evidence-based healthcare*. J Ren Care, 2013. **39**(1): p. 47-51.
12. Martinez-Castelao, A., et al., *Consensus document for the detection and management of chronic kidney disease*. Nefrologia, 2014. **34**(2): p. 243-62.
13. U. Frei, H.-J.S.-H. *Nierenersatztherapie in Deutschland. Jahresberichte 1995 bis 2005/2006*.; Available from: <http://www.bundesverband-niere.de/bundesverband/quasi-niere/jahresberichte.html>.
14. Gross, J.L., et al., *Diabetic nephropathy: diagnosis, prevention, and treatment*. Diabetes Care, 2005. **28**(1): p. 164-76.
15. Lim, A., *Diabetic nephropathy - complications and treatment*. Int J Nephrol Renovasc Dis, 2014. **7**: p. 361-81.
16. Schena, F.P. and L. Gesualdo, *Pathogenetic mechanisms of diabetic nephropathy*. J Am Soc Nephrol, 2005. **16 Suppl 1**: p. S30-3.
17. Kanwar, Y.S., et al., *A glimpse of various pathogenetic mechanisms of diabetic nephropathy*. Annu Rev Pathol, 2011. **6**: p. 395-423.
18. Cao, Z. and M.E. Cooper, *Pathogenesis of diabetic nephropathy*. J Diabetes Investig, 2011. **2**(4): p. 243-7.
19. Navarro-Gonzalez, J.F. and C. Mora-Fernandez, *The role of inflammatory cytokines in diabetic nephropathy*. J Am Soc Nephrol, 2008. **19**(3): p. 433-42.
20. Hickey, F.B. and F. Martin, *Diabetic kidney disease and immune modulation*. Curr Opin Pharmacol, 2013. **13**(4): p. 602-12.
21. Tervaert, T.W., et al., *Pathologic classification of diabetic nephropathy*. J Am Soc Nephrol, 2010. **21**(4): p. 556-63.
22. Vivian, E. and C. Mannebach, *Therapeutic approaches to slowing the progression of diabetic nephropathy - is less best?* Drugs Context, 2013. **2013**: p. 212249.

23. Wang, Y., et al., *Common drugs for stabilization of renal function in the progression of diabetic nephropathy and their relations with hypertension therapy*. *Curr Diabetes Rev*, 2017.
24. Braga, T.T., et al., *CCR2 contributes to the recruitment of monocytes and leads to kidney inflammation and fibrosis development*. *Inflammopharmacology*, 2017.
25. Fornoni, A., et al., *Role of inflammation in diabetic nephropathy*. *Curr Diabetes Rev*, 2008. **4**(1): p. 10-7.
26. Imig, J.D. and M.J. Ryan, *Immune and inflammatory role in renal disease*. *Compr Physiol*, 2013. **3**(2): p. 957-76.
27. Cao, Q., D.C. Harris, and Y. Wang, *Macrophages in kidney injury, inflammation, and fibrosis*. *Physiology (Bethesda)*, 2015. **30**(3): p. 183-94.
28. Pulkkinen, K., S. Murugan, and S. Vainio, *Wnt signaling in kidney development and disease*. *Organogenesis*, 2008. **4**(2): p. 55-9.
29. Chen, S., B. Jim, and F.N. Ziyadeh, *Diabetic nephropathy and transforming growth factor-beta: transforming our view of glomerulosclerosis and fibrosis build-up*. *Semin Nephrol*, 2003. **23**(6): p. 532-43.
30. Walsh, D.W., et al., *Co-regulation of Gremlin and Notch signalling in diabetic nephropathy*. *Biochim Biophys Acta*, 2008. **1782**(1): p. 10-21.
31. Edeling, M., et al., *Developmental signalling pathways in renal fibrosis: the roles of Notch, Wnt and Hedgehog*. *Nat Rev Nephrol*, 2016. **12**(7): p. 426-39.
32. Woroniecka, K.I., et al., *Transcriptome analysis of human diabetic kidney disease*. *Diabetes*, 2011. **60**(9): p. 2354-69.
33. Conserva, F., L. Gesualdo, and M. Papale, *A Systems Biology Overview on Human Diabetic Nephropathy: From Genetic Susceptibility to Post-Transcriptional and Post-Translational Modifications*. *J Diabetes Res*, 2016. **2016**: p. 7934504.
34. Brennan, E.P., et al., *Next-generation sequencing identifies TGF-beta1-associated gene expression profiles in renal epithelial cells reiterated in human diabetic nephropathy*. *Biochim Biophys Acta*, 2012. **1822**(4): p. 589-99.
35. Martini, S., et al., *Integrative biology identifies shared transcriptional networks in CKD*. *J Am Soc Nephrol*, 2014. **25**(11): p. 2559-72.
36. Cohen, C.D., et al., *Improved elucidation of biological processes linked to diabetic nephropathy by single probe-based microarray data analysis*. *PLoS One*, 2008. **3**(8): p. e2937.
37. Nelson, P.J., C. von Toerne, and H.J. Grone, *Wnt-signaling pathways in progressive renal fibrosis*. *Expert Opin Ther Targets*, 2011. **15**(9): p. 1073-83.
38. Song, L., et al., *Crosstalk between Wnt/beta-catenin and Hedgehog/Gli signaling pathways in colon cancer and implications for therapy*. *Cancer Biol Ther*, 2015. **16**(1): p. 1-7.
39. Kramann, R., et al., *Matrix Producing Cells in Chronic Kidney Disease: Origin, Regulation, and Activation*. *Curr Pathobiol Rep*, 2013. **1**(4).
40. Zhou, D., R.J. Tan, and Y. Liu, *Sonic hedgehog signaling in kidney fibrosis: a master communicator*. *Sci China Life Sci*, 2016. **59**(9): p. 920-9.
41. Whisenant, T.C., et al., *Computational prediction and experimental verification of new MAP kinase docking sites and substrates including Gli transcription factors*. *PLoS Comput Biol*, 2010. **6**(8).
42. Ma, F.Y., et al., *A pathogenic role for c-Jun amino-terminal kinase signaling in renal fibrosis and tubular cell apoptosis*. *J Am Soc Nephrol*, 2007. **18**(2): p. 472-84.

43. Seo, E., et al., *The Hippo-Salvador signaling pathway regulates renal tubulointerstitial fibrosis*. *Sci Rep*, 2016. **6**: p. 31931.
44. Liu, F., et al., *Mechanosignaling through YAP and TAZ drives fibroblast activation and fibrosis*. *Am J Physiol Lung Cell Mol Physiol*, 2015. **308**(4): p. L344-57.
45. Schenk, P.W. and B.E. Snear-Jagalska, *Signal perception and transduction: the role of protein kinases*. *Biochimica et Biophysica Acta (BBA) - Molecular Cell Research*, 1999. **1449**(1): p. 1-24.
46. Barolo, S. and J.W. Posakony, *Three habits of highly effective signaling pathways: principles of transcriptional control by developmental cell signaling*. *Genes Dev*, 2002. **16**(10): p. 1167-81.
47. Tang, D., et al., *PAMPs and DAMPs: signal 0s that spur autophagy and immunity*. *Immunol Rev*, 2012. **249**(1): p. 158-75.
48. Lopez, A.F., et al., *Molecular basis of cytokine receptor activation*. *IUBMB Life*, 2010. **62**(7): p. 509-18.
49. Herbst, R.S., *Review of epidermal growth factor receptor biology*. *Int J Radiat Oncol Biol Phys*, 2004. **59**(2 Suppl): p. 21-6.
50. !!! INVALID CITATION !!! {}.
51. Nusslein-Volhard, C. and E. Wieschaus, *Mutations affecting segment number and polarity in Drosophila*. *Nature*, 1980. **287**(5785): p. 795-801.
52. Ingham, P.W., Y. Nakano, and C. Seger, *Mechanisms and functions of Hedgehog signalling across the metazoa*. *Nat Rev Genet*, 2011. **12**(6): p. 393-406.
53. Kasai, K., *GLI1, a master regulator of the hallmark of pancreatic cancer*. *Pathol Int*, 2016. **66**(12): p. 653-660.
54. Gan, G.N. and A. Jimeno, *Emerging from their burrow: Hedgehog pathway inhibitors for cancer*. *Expert Opin Investig Drugs*, 2016. **25**(10): p. 1153-66.
55. Ruiz i Altaba, A., *Hedgehog signaling and the Gli code in stem cells, cancer, and metastases*. *Sci Signal*, 2011. **4**(200): p. pt9.
56. Wang, S. and Z. Dong, *Primary cilia and kidney injury: current research status and future perspectives*. *Am J Physiol Renal Physiol*, 2013. **305**(8): p. F1085-98.
57. Winyard, P. and D. Jenkins, *Putative roles of cilia in polycystic kidney disease*. *Biochim Biophys Acta*, 2011. **1812**(10): p. 1256-62.
58. Jenkins, D., *Hedgehog signalling: emerging evidence for non-canonical pathways*. *Cell Signal*, 2009. **21**(7): p. 1023-34.
59. Lauth, M. and R. Toftgard, *Non-canonical activation of GLI transcription factors: implications for targeted anti-cancer therapy*. *Cell Cycle*, 2007. **6**(20): p. 2458-63.
60. Guo, X. and X.F. Wang, *Signaling cross-talk between TGF-beta/BMP and other pathways*. *Cell Res*, 2009. **19**(1): p. 71-88.
61. Teperino, R., et al., *Canonical and non-canonical Hedgehog signalling and the control of metabolism*. *Semin Cell Dev Biol*, 2014. **33**: p. 81-92.
62. Brennan, D., et al., *Noncanonical Hedgehog signaling*. *Vitam Horm*, 2012. **88**: p. 55-72.
63. Seto, M., et al., *Regulation of the hedgehog signaling by the mitogen-activated protein kinase cascade in gastric cancer*. *Mol Carcinog*, 2009. **48**(8): p. 703-12.
64. Riobo, N.A., et al., *Phosphoinositide 3-kinase and Akt are essential for Sonic Hedgehog signaling*. *Proc Natl Acad Sci U S A*, 2006. **103**(12): p. 4505-10.

65. Kern, D., et al., *Hedgehog/GLI and PI3K signaling in the initiation and maintenance of chronic lymphocytic leukemia*. *Oncogene*, 2015. **34**(42): p. 5341-51.
66. Wrana, J.L., et al., *TGF beta signals through a heteromeric protein kinase receptor complex*. *Cell*, 1992. **71**(6): p. 1003-14.
67. Vega, G., S. Alarcon, and R. San Martin, *The cellular and signalling alterations conducted by TGF-beta contributing to renal fibrosis*. *Cytokine*, 2016. **88**: p. 115-125.
68. Carthy, J.M., *TGFbeta Signalling and the Control of Myofibroblast Differentiation: Implications for Chronic Inflammatory Disorders*. *J Cell Physiol*, 2017.
69. Feng, X.H. and R. Derynck, *Specificity and versatility in tgf-beta signaling through Smads*. *Annu Rev Cell Dev Biol*, 2005. **21**: p. 659-93.
70. Heldin, C.H., K. Miyazono, and P. ten Dijke, *TGF-beta signalling from cell membrane to nucleus through SMAD proteins*. *Nature*, 1997. **390**(6659): p. 465-71.
71. Zhang, Y.E., *Non-Smad Signaling Pathways of the TGF-beta Family*. *Cold Spring Harb Perspect Biol*, 2017. **9**(2).
72. Liu, Q., et al., *A crosstalk between the Smad and JNK signaling in the TGF-beta-induced epithelial-mesenchymal transition in rat peritoneal mesothelial cells*. *PLoS One*, 2012. **7**(2): p. e32009.
73. Moustakas, A. and C.H. Heldin, *Non-Smad TGF-beta signals*. *J Cell Sci*, 2005. **118**(Pt 16): p. 3573-84.
74. Yamashita, M., et al., *TRAF6 mediates Smad-independent activation of JNK and p38 by TGF-beta*. *Mol Cell*, 2008. **31**(6): p. 918-24.
75. Nusse, R., et al., *Mode of proviral activation of a putative mammary oncogene (int-1) on mouse chromosome 15*. *Nature*, 1984. **307**(5947): p. 131-6.
76. Nusse, R. and H.E. Varmus, *Wnt genes*. *Cell*, 1992. **69**(7): p. 1073-87.
77. Logan, C.Y. and R. Nusse, *The Wnt signaling pathway in development and disease*. *Annu Rev Cell Dev Biol*, 2004. **20**: p. 781-810.
78. MacDonald, B.T., K. Tamai, and X. He, *Wnt/beta-catenin signaling: components, mechanisms, and diseases*. *Dev Cell*, 2009. **17**(1): p. 9-26.
79. Gonzalez-Sancho, J.M., et al., *Wnt proteins induce dishevelled phosphorylation via an LRP5/6- independent mechanism, irrespective of their ability to stabilize beta-catenin*. *Mol Cell Biol*, 2004. **24**(11): p. 4757-68.
80. Li, C., et al., *Non-canonical WNT signalling in the lung*. *J Biochem*, 2015. **158**(5): p. 355-65.
81. De, A., *Wnt/Ca2+ signaling pathway: a brief overview*. *Acta Biochim Biophys Sin (Shanghai)*, 2011. **43**(10): p. 745-56.
82. Kestler, H.A. and M. Kuhl, *From individual Wnt pathways towards a Wnt signalling network*. *Philos Trans R Soc Lond B Biol Sci*, 2008. **363**(1495): p. 1333-47.
83. Gao, B., *Wnt regulation of planar cell polarity (PCP)*. *Curr Top Dev Biol*, 2012. **101**: p. 263-95.
84. Mlodzik, M., *Planar cell polarization: do the same mechanisms regulate *Drosophila* tissue polarity and vertebrate gastrulation?* *Trends in Genetics*. **18**(11): p. 564-571.
85. Saucedo, L.J. and B.A. Edgar, *Filling out the Hippo pathway*. *Nat Rev Mol Cell Biol*, 2007. **8**(8): p. 613-21.
86. Bae, J.S., S.M. Kim, and H. Lee, *The Hippo signaling pathway provides novel anti-cancer drug targets*. *Oncotarget*, 2016.

87. Juan, W.C. and W. Hong, *Targeting the Hippo Signaling Pathway for Tissue Regeneration and Cancer Therapy*. Genes (Basel), 2016. **7**(9).
88. Dupont, S., *Role of YAP/TAZ in cell-matrix adhesion-mediated signalling and mechanotransduction*. Exp Cell Res, 2016. **343**(1): p. 42-53.
89. Halder, G. and R.L. Johnson, *Hippo signaling: growth control and beyond*. Development, 2011. **138**(1): p. 9-22.
90. Wennmann, D.O., et al., *Evolutionary and molecular facts link the WWC protein family to Hippo signaling*. Mol Biol Evol, 2014. **31**(7): p. 1710-23.
91. Angus, L., et al., *Willin/FRMD6 expression activates the Hippo signaling pathway kinases in mammals and antagonizes oncogenic YAP*. Oncogene, 2012. **31**(2): p. 238-50.
92. Katoh, M., *Function and cancer genomics of FAT family genes (review)*. Int J Oncol, 2012. **41**(6): p. 1913-8.
93. Reginensi, A., et al., *A critical role for NF2 and the Hippo pathway in branching morphogenesis*. Nat Commun, 2016. **7**: p. 12309.
94. Hong, W. and K.L. Guan, *The YAP and TAZ transcription co-activators: key downstream effectors of the mammalian Hippo pathway*. Semin Cell Dev Biol, 2012. **23**(7): p. 785-93.
95. Grannas, K., et al., *Crosstalk between Hippo and TGFbeta: Subcellular Localization of YAP/TAZ/Smad Complexes*. J Mol Biol, 2015. **427**(21): p. 3407-15.
96. Piersma, B., R.A. Bank, and M. Boersema, *Signaling in Fibrosis: TGF-beta, WNT, and YAP/TAZ Converge*. Front Med (Lausanne), 2015. **2**: p. 59.
97. Kim, M. and E.H. Jho, *Cross-talk between Wnt/beta-catenin and Hippo signaling pathways: a brief review*. BMB Rep, 2014. **47**(10): p. 540-5.
98. Yu, F.X., et al., *Regulation of the Hippo-YAP pathway by G-protein-coupled receptor signaling*. Cell, 2012. **150**(4): p. 780-91.
99. Meng, Z., T. Moroishi, and K.L. Guan, *Mechanisms of Hippo pathway regulation*. Genes Dev, 2016. **30**(1): p. 1-17.
100. Fan, R., N.G. Kim, and B.M. Gumbiner, *Regulation of Hippo pathway by mitogenic growth factors via phosphoinositide 3-kinase and phosphoinositide-dependent kinase-1*. Proc Natl Acad Sci U S A, 2013. **110**(7): p. 2569-74.
101. Sun, G. and K.D. Irvine, *Ajuba family proteins link JNK to Hippo signaling*. Sci Signal, 2013. **6**(292): p. ra81.
102. Cargnello, M. and P.P. Roux, *Activation and function of the MAPKs and their substrates, the MAPK-activated protein kinases*. Microbiol Mol Biol Rev, 2011. **75**(1): p. 50-83.
103. Katz, M., I. Amit, and Y. Yarden, *Regulation of MAPKs by growth factors and receptor tyrosine kinases*. Biochim Biophys Acta, 2007. **1773**(8): p. 1161-76.
104. Zhou, Y.Y., et al., *MAPK/JNK signaling: A potential autophagy regulation pathway*. Biosci Rep, 2015.
105. Chen, R.E. and J. Thorner, *Function and regulation in MAPK signaling pathways: lessons learned from the yeast Saccharomyces cerevisiae*. Biochim Biophys Acta, 2007. **1773**(8): p. 1311-40.
106. Mayawala, K., C.A. Gelmi, and J.S. Edwards, *MAPK cascade possesses decoupled controllability of signal amplification and duration*. Biophys J, 2004. **87**(5): p. L01-2.
107. Roskoski, R., Jr., *ERK1/2 MAP kinases: structure, function, and regulation*. Pharmacol Res, 2012. **66**(2): p. 105-43.

108. Johnson, G.L. and K. Nakamura, *The c-jun kinase/stress-activated pathway: regulation, function and role in human disease*. *Biochim Biophys Acta*, 2007. **1773**(8): p. 1341-8.
109. Vial, E., E. Sahai, and C.J. Marshall, *ERK-MAPK signaling coordinately regulates activity of Rac1 and RhoA for tumor cell motility*. *Cancer Cell*, 2003. **4**(1): p. 67-79.
110. O'Shea, J.J., et al., *The JAK-STAT pathway: impact on human disease and therapeutic intervention*. *Annu Rev Med*, 2015. **66**: p. 311-28.
111. Villarino, A.V., et al., *Mechanisms of Jak/STAT signaling in immunity and disease*. *J Immunol*, 2015. **194**(1): p. 21-7.
112. Rawlings, J.S., K.M. Rosler, and D.A. Harrison, *The JAK/STAT signaling pathway*. *J Cell Sci*, 2004. **117**(Pt 8): p. 1281-3.
113. Phizicky, E.M. and S. Fields, *Protein-protein interactions: methods for detection and analysis*. *Microbiol Rev*, 1995. **59**(1): p. 94-123.
114. Kolch, W., et al., *The dynamic control of signal transduction networks in cancer cells*. *Nat Rev Cancer*, 2015. **15**(9): p. 515-27.
115. Logue, J.S. and D.K. Morrison, *Complexity in the signaling network: insights from the use of targeted inhibitors in cancer therapy*. *Genes Dev*, 2012. **26**(7): p. 641-50.
116. Chen, H., et al., *Context-dependent signaling defines roles of BMP9 and BMP10 in embryonic and postnatal development*. *Proc Natl Acad Sci U S A*, 2013. **110**(29): p. 11887-92.
117. Aberger, F. and I.A.A. Ruiz, *Context-dependent signal integration by the GLI code: the oncogenic load, pathways, modifiers and implications for cancer therapy*. *Semin Cell Dev Biol*, 2014. **33**: p. 93-104.
118. Cselenyi, C.S. and E. Lee, *Context-dependent activation or inhibition of Wnt-beta-catenin signaling by Kremen*. *Sci Signal*, 2008. **1**(8): p. pe10.
119. Fey, D., et al., *Crosstalk and signaling switches in mitogen-activated protein kinase cascades*. *Front Physiol*, 2012. **3**: p. 355.
120. Cheruku, H.R., et al., *Transforming growth factor- β , MAPK and Wnt signaling interactions in colorectal cancer*. *EuPA Open Proteomics*, 2015. **8**: p. 104-115.
121. Bikkavilli, R.K. and C.C. Malbon, *Mitogen-activated protein kinases and Wnt/beta-catenin signaling: Molecular conversations among signaling pathways*. *Commun Integr Biol*, 2009. **2**(1): p. 46-9.
122. Zhang, Y.E., *Non-Smad pathways in TGF-beta signaling*. *Cell Res*, 2009. **19**(1): p. 128-39.
123. Reddy, B.V. and K.D. Irvine, *Regulation of Hippo signaling by EGFR-MAPK signaling through Ajuba family proteins*. *Dev Cell*, 2013. **24**(5): p. 459-71.
124. Attisano, L. and J.L. Wrana, *Signal integration in TGF-beta, WNT, and Hippo pathways*. *F1000Prime Rep*, 2013. **5**: p. 17.
125. Chaplin, D.D., *1. Overview of the human immune response*. *J Allergy Clin Immunol*, 2006. **117**(2 Suppl Mini-Primer): p. S430-5.
126. Chaplin, D.D., *Overview of the immune response*. *J Allergy Clin Immunol*, 2010. **125**(2 Suppl 2): p. S3-23.
127. Turvey, S.E. and D.H. Broide, *Innate immunity*. *J Allergy Clin Immunol*, 2010. **125**(2 Suppl 2): p. S24-32.
128. Kumar, H., T. Kawai, and S. Akira, *Pathogen recognition by the innate immune system*. *Int Rev Immunol*, 2011. **30**(1): p. 16-34.
129. Litman, G.W., J.P. Rast, and S.D. Fugmann, *The origins of vertebrate adaptive immunity*. *Nat Rev Immunol*, 2010. **10**(8): p. 543-53.

130. Boehm, T. and J.B. Swann, *Origin and evolution of adaptive immunity*. *Annu Rev Anim Biosci*, 2014. **2**: p. 259-83.
131. Boehm, T., *Design principles of adaptive immune systems*. *Nat Rev Immunol*, 2011. **11**(5): p. 307-17.
132. Dempsey, P.W., S.A. Vaidya, and G. Cheng, *The art of war: Innate and adaptive immune responses*. *Cell Mol Life Sci*, 2003. **60**(12): p. 2604-21.
133. Reiner, S.L., *Decision making during the conception and career of CD4+ T cells*. *Nat Rev Immunol*, 2009. **9**(2): p. 81-2.
134. Zhang, N. and M.J. Bevan, *CD8(+) T cells: foot soldiers of the immune system*. *Immunity*, 2011. **35**(2): p. 161-8.
135. Pieper, K., B. Grimbacher, and H. Eibel, *B-cell biology and development*. *J Allergy Clin Immunol*, 2013. **131**(4): p. 959-71.
136. Farber, D.L., et al., *Immunological memory: lessons from the past and a look to the future*. *Nat Rev Immunol*, 2016. **16**(2): p. 124-8.
137. Weisheit, C.K., D.R. Engel, and C. Kurts, *Dendritic Cells and Macrophages: Sentinels in the Kidney*. *Clin J Am Soc Nephrol*, 2015. **10**(10): p. 1841-51.
138. Kurts, C., et al., *The immune system and kidney disease: basic concepts and clinical implications*. *Nat Rev Immunol*, 2013. **13**(10): p. 738-53.
139. Segerer, S., et al., *Compartment specific expression of dendritic cell markers in human glomerulonephritis*. *Kidney Int*, 2008. **74**(1): p. 37-46.
140. Rabinovitch, M., *Professional and non-professional phagocytes: an introduction*. *Trends in Cell Biology*. **5**(3): p. 85-87.
141. Duffield, J.S., *Macrophages and immunologic inflammation of the kidney*. *Semin Nephrol*, 2010. **30**(3): p. 234-54.
142. Murray, P.J. and T.A. Wynn, *Protective and pathogenic functions of macrophage subsets*. *Nat Rev Immunol*, 2011. **11**(11): p. 723-37.
143. Lech, M. and H.J. Anders, *Macrophages and fibrosis: How resident and infiltrating mononuclear phagocytes orchestrate all phases of tissue injury and repair*. *Biochim Biophys Acta*, 2013. **1832**(7): p. 989-97.
144. Hochheiser, K., A. Tittel, and C. Kurts, *Kidney dendritic cells in acute and chronic renal disease*. *Int J Exp Pathol*, 2011. **92**(3): p. 193-201.
145. Rogers, N.M., et al., *Dendritic cells and macrophages in the kidney: a spectrum of good and evil*. *Nat Rev Nephrol*, 2014. **10**(11): p. 625-43.
146. Lindenmeyer, M., et al., *Dendritic cells in experimental renal inflammation--Part I*. *Nephron Exp Nephrol*, 2011. **119**(4): p. e83-90.
147. Noessner, E., et al., *Dendritic cells in human renal inflammation--Part II*. *Nephron Exp Nephrol*, 2011. **119**(4): p. e91-8.
148. Hume, D.A., *Macrophages as APC and the dendritic cell myth*. *J Immunol*, 2008. **181**(9): p. 5829-35.
149. Geissmann, F., et al., *Unravelling mononuclear phagocyte heterogeneity*. *Nat Rev Immunol*, 2010. **10**(6): p. 453-60.
150. Nelson, P.J., et al., *The renal mononuclear phagocytic system*. *J Am Soc Nephrol*, 2012. **23**(2): p. 194-203.
151. Figel, A.M., et al., *Human renal cell carcinoma induces a dendritic cell subset that uses T-cell crosstalk for tumor-permissive milieu alterations*. *Am J Pathol*, 2011. **179**(1): p. 436-51.
152. Rock, K.L., et al., *The sterile inflammatory response*. *Annu Rev Immunol*, 2010. **28**: p. 321-42.
153. Lee, S.B. and R. Kalluri, *Mechanistic connection between inflammation and fibrosis*. *Kidney Int Suppl*, 2010(119): p. S22-6.

154. Cohen, C.D. and M. Kretzler, [*Gene expression analyses of kidney biopsies: the European renal cDNA bank--Kroner-Fresenius biopsy bank*]. *Pathologie*, 2009. **30**(2): p. 101-4.
155. Moll, A.G., et al., *Transcript-specific expression profiles derived from sequence-based analysis of standard microarrays*. *PLoS One*, 2009. **4**(3): p. e4702.
156. Ju, W., et al., *Renal gene and protein expression signatures for prediction of kidney disease progression*. *Am J Pathol*, 2009. **174**(6): p. 2073-85.
157. Irizarry, R.A., et al., *Exploration, normalization, and summaries of high density oligonucleotide array probe level data*. *Biostatistics*, 2003. **4**(2): p. 249-64.
158. Dai, M., et al., *Evolving gene/transcript definitions significantly alter the interpretation of GeneChip data*. *Nucleic Acids Res*, 2005. **33**(20): p. e175.
159. Johnson, W.E., C. Li, and A. Rabinovic, *Adjusting batch effects in microarray expression data using empirical Bayes methods*. *Biostatistics*, 2007. **8**(1): p. 118-27.
160. Reich, M., et al., *GenePattern 2.0*. *Nat Genet*, 2006. **38**(5): p. 500-1.
161. Frisch, M., et al., *LitInspector: literature and signal transduction pathway mining in PubMed abstracts*. *Nucleic Acids Res*, 2009. **37**(Web Server issue): p. W135-40.
162. Abbas, A.R., et al., *Deconvolution of blood microarray data identifies cellular activation patterns in systemic lupus erythematosus*. *PLoS One*, 2009. **4**(7): p. e6098.
163. Langfelder, P. and S. Horvath, *WGCNA: an R package for weighted correlation network analysis*. *BMC Bioinformatics*, 2008. **9**: p. 559.
164. Ramos, J.L., et al., *The TetR family of transcriptional repressors*. *Microbiol Mol Biol Rev*, 2005. **69**(2): p. 326-56.
165. Ivics, Z., et al., *Molecular reconstruction of Sleeping Beauty, a Tc1-like transposon from fish, and its transposition in human cells*. *Cell*, 1997. **91**(4): p. 501-10.
166. Mates, L., et al., *Molecular evolution of a novel hyperactive Sleeping Beauty transposase enables robust stable gene transfer in vertebrates*. *Nat Genet*, 2009. **41**(6): p. 753-61.
167. Baus, J., et al., *Hyperactive transposase mutants of the Sleeping Beauty transposon*. *Mol Ther*, 2005. **12**(6): p. 1148-56.
168. Jackel, C., et al., *A vector platform for the rapid and efficient engineering of stable complex transgenes*. *Sci Rep*, 2016. **6**: p. 34365.
169. Vasanwala, F.H., et al., *Repression of AP-1 function: a mechanism for the regulation of Blimp-1 expression and B lymphocyte differentiation by the B cell lymphoma-6 protooncogene*. *J Immunol*, 2002. **169**(4): p. 1922-9.
170. Dupont, S., et al., *Role of YAP/TAZ in mechanotransduction*. *Nature*, 2011. **474**(7350): p. 179-83.
171. Kolben, T., et al., *Dissecting the impact of Frizzled receptors in Wnt/beta-catenin signaling of human mesenchymal stem cells*. *Biol Chem*, 2012. **393**(12): p. 1433-47.
172. Schmid, H., et al., *Validation of endogenous controls for gene expression analysis in microdissected human renal biopsies*. *Kidney Int*, 2003. **64**(1): p. 356-60.
173. Pfaffl, M.W., *A new mathematical model for relative quantification in real-time RT-PCR*. *Nucleic Acids Res*, 2001. **29**(9): p. e45.
174. Wisniewski, J.R., et al., *Universal sample preparation method for proteome analysis*. *Nat Methods*, 2009. **6**(5): p. 359-62.

175. Grosche, A., et al., *The Proteome of Native Adult Muller Glial Cells From Murine Retina*. Mol Cell Proteomics, 2016. **15**(2): p. 462-80.
176. Maroz, N. and R. Simman, *Wound Healing in Patients With Impaired Kidney Function*. J Am Coll Clin Wound Spec, 2013. **5**(1): p. 2-7.
177. Eming, S.A., P. Martin, and M. Tomic-Canic, *Wound repair and regeneration: mechanisms, signaling, and translation*. Sci Transl Med, 2014. **6**(265): p. 265sr6.
178. Klahr, S., et al., *The effects of dietary protein restriction and blood-pressure control on the progression of chronic renal disease. Modification of Diet in Renal Disease Study Group*. N Engl J Med, 1994. **330**(13): p. 877-84.
179. Barczyk, M., S. Carracedo, and D. Gullberg, *Integrins*. Cell Tissue Res, 2010. **339**(1): p. 269-80.
180. Katzen, F., *Gateway((R)) recombinational cloning: a biological operating system*. Expert Opin Drug Discov, 2007. **2**(4): p. 571-89.
181. Tannous, B.A., et al., *Codon-optimized Gaussia luciferase cDNA for mammalian gene expression in culture and in vivo*. Mol Ther, 2005. **11**(3): p. 435-43.
182. Boor, P. and J. Floege, *Chronic kidney disease growth factors in renal fibrosis*. Clin Exp Pharmacol Physiol, 2011. **38**(7): p. 441-50.
183. Geyeregger, R., et al., *Liver X receptors regulate dendritic cell phenotype and function through blocked induction of the actin-bundling protein fascin*. Blood, 2007. **109**(10): p. 4288-95.
184. Sanchez, P.V., et al., *Induced differentiation of acute myeloid leukemia cells by activation of retinoid X and liver X receptors*. Leukemia, 2014. **28**(4): p. 749-60.
185. Kiss, E., et al., *Suppression of chronic damage in renal allografts by Liver X receptor (LXR) activation relevant contribution of macrophage LXRA*. Am J Pathol, 2011. **179**(1): p. 92-103.
186. Kiss, E., et al., *Lipid droplet accumulation is associated with an increase in hyperglycemia-induced renal damage: prevention by liver X receptors*. Am J Pathol, 2013. **182**(3): p. 727-41.
187. Cheo, D.L., et al., *Concerted assembly and cloning of multiple DNA segments using in vitro site-specific recombination: functional analysis of multi-segment expression clones*. Genome Res, 2004. **14**(10b): p. 2111-20.
188. Mangelberger, D., et al., *Cooperative Hedgehog-EGFR signaling*. Front Biosci (Landmark Ed), 2012. **17**: p. 90-9.
189. Abnaof, K., et al., *TGF-beta stimulation in human and murine cells reveals commonly affected biological processes and pathways at transcription level*. BMC Syst Biol, 2014. **8**: p. 55.
190. Grumolato, L., et al., *Canonical and noncanonical Wnts use a common mechanism to activate completely unrelated coreceptors*. Genes Dev, 2010. **24**(22): p. 2517-30.
191. Hillen, W. and C. Berens, *Mechanisms underlying expression of Tn10 encoded tetracycline resistance*. Annu Rev Microbiol, 1994. **48**: p. 345-69.
192. Villavicencio, E.H., D.O. Walterhouse, and P.M. Iannaccone, *The sonic hedgehog-patched-gli pathway in human development and disease*. Am J Hum Genet, 2000. **67**(5): p. 1047-54.
193. Cadigan, K.M. and M.L. Waterman, *TCF/LEFs and Wnt signaling in the nucleus*. Cold Spring Harb Perspect Biol, 2012. **4**(11).
194. Moustakas, A., S. Souchelnytskyi, and C.H. Heldin, *Smad regulation in TGF-beta signal transduction*. J Cell Sci, 2001. **114**(Pt 24): p. 4359-69.

195. Regl, G., et al., *Human GLI2 and GLI1 are part of a positive feedback mechanism in Basal Cell Carcinoma*. *Oncogene*, 2002. **21**(36): p. 5529-39.
196. Mantovani, A., et al., *The chemokine system in diverse forms of macrophage activation and polarization*. *Trends Immunol*, 2004. **25**(12): p. 677-86.
197. Ziegler-Heitbrock, L., et al., *Nomenclature of monocytes and dendritic cells in blood*. *Blood*, 2010. **116**(16): p. e74-80.
198. Ziegler-Heitbrock, H.W., et al., *Establishment of a human cell line (Mono Mac 6) with characteristics of mature monocytes*. *Int J Cancer*, 1988. **41**(3): p. 456-61.
199. Tsuchiya, S., et al., *Establishment and characterization of a human acute monocytic leukemia cell line (THP-1)*. *Int J Cancer*, 1980. **26**(2): p. 171-6.
200. Thery, C., L. Zitvogel, and S. Amigorena, *Exosomes: composition, biogenesis and function*. *Nat Rev Immunol*, 2002. **2**(8): p. 569-79.
201. Agyeman, A., et al., *Mode and specificity of binding of the small molecule GANT61 to GLI determines inhibition of GLI-DNA binding*. *Oncotarget*, 2014. **5**(12): p. 4492-503.
202. Zarogoulidis, P., et al., *mTOR pathway: A current, up-to-date mini-review (Review)*. *Oncol Lett*, 2014. **8**(6): p. 2367-2370.
203. Di Paola, R., et al., *PD98059, a specific MAP kinase inhibitor, attenuates multiple organ dysfunction syndrome/failure (MODS) induced by zymosan in mice*. *Pharmacol Res*, 2010. **61**(2): p. 175-87.
204. Vanhaesebroeck, B., L. Stephens, and P. Hawkins, *PI3K signalling: the path to discovery and understanding*. *Nat Rev Mol Cell Biol*, 2012. **13**(3): p. 195-203.
205. Park, Y.C., et al., *Wortmannin, a specific inhibitor of phosphatidylinositol-3-kinase, enhances LPS-induced NO production from murine peritoneal macrophages*. *Biochem Biophys Res Commun*, 1997. **240**(3): p. 692-6.
206. Baranowski, M., *Biological role of liver X receptors*. *J Physiol Pharmacol*, 2008. **59 Suppl 7**: p. 31-55.
207. Caldas, Y.A., et al., *Liver X receptor-activating ligands modulate renal and intestinal sodium-phosphate transporters*. *Kidney Int*, 2011. **80**(5): p. 535-44.
208. Wang, Y.Y., et al., *Liver X receptor agonist GW3965 dose-dependently regulates lps-mediated liver injury and modulates posttranscriptional TNF-alpha production and p38 mitogen-activated protein kinase activation in liver macrophages*. *Shock*, 2009. **32**(5): p. 548-53.
209. Katso, R.M., R.B. Russell, and T.S. Ganesan, *Functional analysis of H-Ryk, an atypical member of the receptor tyrosine kinase family*. *Mol Cell Biol*, 1999. **19**(9): p. 6427-40.
210. Organ, S.L. and M.S. Tsao, *An overview of the c-MET signaling pathway*. *Ther Adv Med Oncol*, 2011. **3**(1 Suppl): p. S7-s19.
211. Arthur, J.S. and S.C. Ley, *Mitogen-activated protein kinases in innate immunity*. *Nat Rev Immunol*, 2013. **13**(9): p. 679-92.
212. Sanchez, A.P. and K. Sharma, *Transcription factors in the pathogenesis of diabetic nephropathy*. *Expert Rev Mol Med*, 2009. **11**: p. e13.
213. Gnanaprakasam, J.N. and R. Wang, *MYC in Regulating Immunity: Metabolism and Beyond*. *Genes (Basel)*, 2017. **8**(3).
214. Miller, J.R., *The Wnts*. *Genome Biol*, 2002. **3**(1): p. Reviews3001.
215. Dijksterhuis, J.P., J. Petersen, and G. Schulte, *WNT/Frizzled signalling: receptor-ligand selectivity with focus on FZD-G protein signalling and its physiological relevance: IUPHAR Review 3*. *Br J Pharmacol*, 2014. **171**(5): p. 1195-209.

216. Cselenyi, C.S., et al., *LRP6 transduces a canonical Wnt signal independently of Axin degradation by inhibiting GSK3's phosphorylation of beta-catenin*. Proc Natl Acad Sci U S A, 2008. **105**(23): p. 8032-7.
217. Gray, J.D., et al., *LRP6 exerts non-canonical effects on Wnt signaling during neural tube closure*. Hum Mol Genet, 2013. **22**(21): p. 4267-81.
218. Fanjul-Fernandez, M., et al., *Matrix metalloproteinases: evolution, gene regulation and functional analysis in mouse models*. Biochim Biophys Acta, 2010. **1803**(1): p. 3-19.
219. Ke, B., et al., *Matrix Metalloproteinases-7 and Kidney Fibrosis*. Front Physiol, 2017. **8**: p. 21.
220. Grotendorst, G.R., *Connective tissue growth factor: a mediator of TGF-beta action on fibroblasts*. Cytokine Growth Factor Rev, 1997. **8**(3): p. 171-9.
221. Bartholin, L., et al., *The human Cyr61 gene is a transcriptional target of transforming growth factor beta in cancer cells*. Cancer Lett, 2007. **246**(1-2): p. 230-6.
222. Suryadinata, R., M. Sadowski, and B. Sarcevic, *Control of cell cycle progression by phosphorylation of cyclin-dependent kinase (CDK) substrates*. Biosci Rep, 2010. **30**(4): p. 243-55.
223. Lim, S. and P. Kaldis, *Cdks, cyclins and CKIs: roles beyond cell cycle regulation*. Development, 2013. **140**(15): p. 3079-93.
224. Karsdal, M.A., et al., *Extracellular matrix remodeling: the common denominator in connective tissue diseases. Possibilities for evaluation and current understanding of the matrix as more than a passive architecture, but a key player in tissue failure*. Assay Drug Dev Technol, 2013. **11**(2): p. 70-92.
225. Debigare, R. and S.R. Price, *Proteolysis, the ubiquitin-proteasome system, and renal diseases*. Am J Physiol Renal Physiol, 2003. **285**(1): p. F1-8.
226. Kang, Y.S., et al., *CCR2 antagonism improves insulin resistance, lipid metabolism, and diabetic nephropathy in type 2 diabetic mice*. Kidney Int, 2010. **78**(9): p. 883-94.
227. Awad, A.S., et al., *Monocyte/macrophage chemokine receptor CCR2 mediates diabetic renal injury*. Am J Physiol Renal Physiol, 2011. **301**(6): p. F1358-66.
228. Sayyed, S.G., et al., *An orally active chemokine receptor CCR2 antagonist prevents glomerulosclerosis and renal failure in type 2 diabetes*. Kidney Int, 2011. **80**(1): p. 68-78.
229. Seok, S.J., et al., *Blockade of CCL2/CCR2 signalling ameliorates diabetic nephropathy in db/db mice*. Nephrol Dial Transplant, 2013. **28**(7): p. 1700-10.
230. de Zeeuw, D., et al., *The effect of CCR2 inhibitor CCX140-B on residual albuminuria in patients with type 2 diabetes and nephropathy: a randomised trial*. Lancet Diabetes Endocrinol, 2015. **3**(9): p. 687-96.
231. Menne, J., et al., *C-C motif-ligand 2 inhibition with emapticap pegol (NOX-E36) in type 2 diabetic patients with albuminuria*. Nephrol Dial Transplant, 2016.
232. Gao, J., J. Li, and L. Ma, *Regulation of EGF-induced ERK/MAPK activation and EGFR internalization by G protein-coupled receptor kinase 2*. Acta Biochim Biophys Sin (Shanghai), 2005. **37**(8): p. 525-31.
233. Vert, G. and J. Chory, *Crosstalk in cellular signaling: background noise or the real thing?* Dev Cell, 2011. **21**(6): p. 985-91.
234. Takahashi, S., *Vascular endothelial growth factor (VEGF), VEGF receptors and their inhibitors for antiangiogenic tumor therapy*. Biol Pharm Bull, 2011. **34**(12): p. 1785-8.

235. Avraham-Davidi, I., et al., *On-site education of VEGF-recruited monocytes improves their performance as angiogenic and arteriogenic accessory cells.* J Exp Med, 2013. **210**(12): p. 2611-25.
236. Onimaru, M., et al., *VEGF-C regulates lymphangiogenesis and capillary stability by regulation of PDGF-B.* Am J Physiol Heart Circ Physiol, 2009. **297**(5): p. H1685-96.
237. Nihei, M., et al., *Chronic inflammation, lymphangiogenesis, and effect of an anti-VEGFR therapy in a mouse model and in human patients with aspiration pneumonia.* J Pathol, 2015. **235**(4): p. 632-45.
238. Wilkins, J.A. and O.J. Sansom, *C-Myc is a critical mediator of the phenotypes of Apc loss in the intestine.* Cancer Res, 2008. **68**(13): p. 4963-6.
239. Mateyak, M.K., A.J. Obaya, and J.M. Sedivy, *c-Myc regulates cyclin D-Cdk4 and -Cdk6 activity but affects cell cycle progression at multiple independent points.* Mol Cell Biol, 1999. **19**(7): p. 4672-83.
240. Huang, M. and W.A. Weiss, *Neuroblastoma and MYCN.* Cold Spring Harb Perspect Med, 2013. **3**(10): p. a014415.
241. Beltran, H., *The N-myc Oncogene: Maximizing its Targets, Regulation, and Therapeutic Potential.* Mol Cancer Res, 2014. **12**(6): p. 815-22.
242. Rinkevich, Y., et al., *In vivo clonal analysis reveals lineage-restricted progenitor characteristics in mammalian kidney development, maintenance, and regeneration.* Cell Rep, 2014. **7**(4): p. 1270-83.
243. Zhang, Y., T. Pizzute, and M. Pei, *A review of crosstalk between MAPK and Wnt signals and its impact on cartilage regeneration.* Cell Tissue Res, 2014. **358**(3): p. 633-49.
244. Katoh, M., *Differential regulation of WNT2 and WNT2B expression in human cancer.* Int J Mol Med, 2001. **8**(6): p. 657-60.
245. Lin, S.L., et al., *Macrophage Wnt7b is critical for kidney repair and regeneration.* Proc Natl Acad Sci U S A, 2010. **107**(9): p. 4194-9.
246. Fernando, C.V., et al., *Diverse roles for Wnt7a in ventral midbrain neurogenesis and dopaminergic axon morphogenesis.* Stem Cells Dev, 2014. **23**(17): p. 1991-2003.
247. Yoshioka, S., et al., *WNT7A regulates tumor growth and progression in ovarian cancer through the WNT/beta-catenin pathway.* Mol Cancer Res, 2012. **10**(3): p. 469-82.
248. Le Grand, F., et al., *Wnt7a activates the planar cell polarity pathway to drive the symmetric expansion of satellite stem cells.* Cell Stem Cell, 2009. **4**(6): p. 535-47.
249. Lee, J.E., et al., *Canonical Wnt signaling through Lef1 is required for hypothalamic neurogenesis.* Development, 2006. **133**(22): p. 4451-61.
250. Kim, E.K. and E.J. Choi, *Pathological roles of MAPK signaling pathways in human diseases.* Biochim Biophys Acta, 2010. **1802**(4): p. 396-405.
251. Lin, Y.W., S.M. Chuang, and J.L. Yang, *ERK1/2 achieves sustained activation by stimulating MAPK phosphatase-1 degradation via the ubiquitin-proteasome pathway.* J Biol Chem, 2003. **278**(24): p. 21534-41.
252. Wiegand, C., et al., *Protease and pro-inflammatory cytokine concentrations are elevated in chronic compared to acute wounds and can be modulated by collagen type I in vitro.* Arch Dermatol Res, 2010. **302**(6): p. 419-28.
253. Morinaga, J., et al., *The antifibrotic effect of a serine protease inhibitor in the kidney.* Am J Physiol Renal Physiol, 2013. **305**(2): p. F173-81.

8 Acknowledgements

I would like to thank

Prof. Dr. Peter Nelson, for mentoring me, granting liberties, but also nudging in the right direction where required

Prof. Dr. Hermann-Josef Gröne, for providing scientific insight and support of the project

Prof. Dr. Elfriede Nößner and Dr. Dorothee Brech, for making large parts of the project possible and being supportive and open for ideas all around

PD Dr. Bruno Luckow, for always being open for scientific or technical questions and providing important advice along the way

Kathie Witte, for making administrative processes that much more bearable

The technical staff, for organizing everything so greatly and being of great help, especially Moni who I could always count on if I needed help.

The medical students in the lab, for helping with so much along the way as well as sharing methods and ideas

My family, for always supporting me along the way and making my studies possible in the first place

My friends, for always being there for me

Kasia, for so many small and big things that listing them would fill at least one more thesis.

Eidesstattliche Versicherung

Carsten Jäckel

Ich erkläre hiermit an Eides statt, dass ich die vorliegende Dissertation mit dem Thema:

Modulation of the renal homeostatic milieu by mononuclear phagocytes in diabetic nephropathy

selbständig verfasst, mich außer der angegebenen keiner weiteren Hilfsmittel bedient und alle Erkenntnisse, die aus dem Schrifttum ganz oder annähernd übernommen sind, als solche kenntlich gemacht und nach ihrer Herkunft unter Bezeichnung der Fundstelle einzeln nachgewiesen habe.

Ich erkläre des Weiteren, dass die hier vorgelegte Dissertation nicht in gleicher oder in ähnlicher Form bei einer anderen Stelle zur Erlangung eines akademischen Grades eingereicht wurde.

Neufahrn, den 21.11.2017

Carsten Jäckel